SPATIOTEMPORAL CONTROL OF ACTIN CYTOSKELETAL MACHINERY IN CELLS: MULTIVALENCY MEDIATED PROTEIN CLUSTERING AT THE PLASMA MEMBRANE AND OPTOGENETIC TOOL DEVELOPMENT

APPROVED BY SUPERVISORY COMMITTEE

Michael K. Rosen, Ph.D.

Kate Luby-Phelps, Ph.D.

Hongtao Yu, Ph.D.

Steven Altschuler, Ph.D.

This thesis is dedicated to my family

SPATIOTEMPORAL CONTROL OF ACTIN CYTOSKELETAL MACHINERY IN CELLS: MULTIVALENCY MEDIATED PROTEIN CLUSTERING AT THE PLASMA MEMBRANE AND OPTOGENETIC TOOL DEVELOPMENT

by

SOYEON KIM

DISSERTATION

Presented to the Faculty of the Graduate School of Biomedical Sciences

The University of Texas Southwestern Medical Center at Dallas

In Partial Fulfillment of the Requirements

For the Degree of

DOCTOR OF PHILOSOPHY

The University of Texas Southwestern Medical Center at Dallas

Dallas, Texas

August, 2015

ACKNOWLEDGEMENT

I would like to give my sincere gratitude to all the people who have helped and inspired me during my graduate study.

First, I want to express the deepest appreciation to my advisor, Dr. Michael Rosen, for his continuous support of my doctoral research. When I was a first year student searching for rotation labs, one professor recommended the Rosen lab, saying, 'Mike is one of the true scientists I know.' Throughout my doctoral training, I became realize what those words really meant. Every discussion I had with him encouraged me to clear my thoughts about positive data and not to neglect any negative data. His enthusiasm for science has always reminded me how fun the biology could be if I think about deeper questions and creative approaches. Without his support and words of encouragement this dissertation would not have been possible.

I sincerely appreciate my committee member Dr. Kate Luby-Phelps, Dr. Hongtao Yu, and Dr. Steven Altschuler for their generous support and numerous advices. They have always provided so much inspiration in my projects. In addition, I would like to express my gratitude for tremendous help from Dr. Kate Luby-Phelps and Abhijit Bugde at the Live Cell Imaging Core Facility. I am also very thankful to be a student in the Cell and Molecular Biology Program where energetic discussions about diverse topics broadened my view.

I would like to thank all past and current members of the Rosen Lab for all stimulating discussions, for all the fun we had with late night experiments and for introducing great restaurants in Dallas. In particular, I appreciate Dr. Pilong Li, Dr. Hui-chun Cheng, Dr. Xiaolan Yao and Dr. Shae Padrick who helped me through rotation and early

stage of my training. Their passion about science always restored my energy and challenged me to try harder on my work. I would like to thank to the oligomerization subgroup, Dr. Pilong Li, Dr. Hui-chun Cheng, Dr. Sudeep Banjade, Dr. Jonathon Ditlev, Salman Banani, Yuan Lin, and Dr. Chi Pak for their valuable input on the nephrin project and to Dr. Xiaolan Yao and Junko Umetani for their help on the optogenetics project. I also thank Dr. Hui-chun Cheng, Dr. Bingke Yu, and Dr. Xiaolan Yao for being such great friends in whom I could always confide whenever I had difficulties.

Finally, it would be a great pleasure to express my appreciation to my family for all of their love and support throughout my doctoral studies. I would like to thank my father, Byunguk Kim, who has taught me that happiness resides on doing what you love and loving what you do. I also would like to thank my mother, Kongmi Sin, who has been always there for me, showing tremendous devotion to the family. And my sister, Mijeong Kim, you are a little bit of my childhood who shares all the laughers and tears, my dearest friend and the most special person I know. Thank you for making my life so wonderful.

SPATIOTEMPORAL CONTROL OF ACTIN CYTOSKELETAL MACHINERY IN CELLS: MULTIVALENCY MEDIATED PROTEIN CLUSTERING AT THE PLASMA MEMBRANE AND OPTOGENETIC TOOL DEVELOPMENT

Publication No. _____

Soyeon Kim

The University of Texas Southwestern Medical Center at Dallas, Graduation Year

Supervising Professor: Michael Rosen, Ph.D.

Precise regulation of actin cytoskeleton dynamics is crucial for numerous cellular processes. My thesis work has demonstrated two different mechanisms that cells use to achieve spatiotemporal control of actin assembly – multivalency mediated phase separation and subcellular activation of actin polymerization machinery.

The plasma membrane of the living cell is believed to function as a dynamic platform for signal transduction, rather than existing simply as a static barrier between intracellular and extracellular environments. Moreover the membrane is organized into distinct lipid and protein microdomains. Recent work has shown the importance of protein assembly at the membrane in the formation of these domains. However, the mechanisms by which proteins organize at the membrane are largely unknown. Here I demonstrate that multivalent interactions among proteins in the Nephrin/Nck/N-WASP actin-regulatory pathway can drive clustering of the components at the plasma membrane in cells. Generation of the micron-sized domains is dependent on the phosphorylation-mediated interaction between the transmembrane protein, Nephrin, and its effectors, Nck and N-WASP, in the cytoplasm. These structures are dynamic and associated with increased actin polymerization activity, suggesting the importance of clustering in local rearrangements of the cytoskeleton. My studies suggest that multivalent interactions between the signaling proteins can, in general, contribute to spatiotemporal regulation of cellular processes by clustering of molecules at the plasma membrane.

Precise spatiotemporal regulation of protein activity is a key feature of cellular signaling pathways. While contemporary tools in biology have limited control in space and time, recent developments in optogenetics have demonstrated that light can be used as a general tool to investigate protein function *in vivo*. Many optogenetic tools, however, indirectly regulate protein activity by modulating expression level or cellular localization. Other optogenetic tools with direct control of protein activity have limited applications. Here I demonstrate a method based on fragment complementation that can be generally applicable

to a protein of interest based on the light-dependent interaction of Phytochrome B (PhyB) and phytochrome interacting factor 3 (Pif3). My method allows subcellular control of protein function via light-induced reconstitution of a split protein. In particular, I show that light-dependent activation of SopE, a bacterial GEF protein, induces membrane ruffling in a living cell. Furthermore, as an application to inter-molecular regulation between two different molecules, I induced light-mediated interactions between Rho-GTPase Cdc42 and its effector Wiskott-Aldrich Syndrome Protein (WASp) to promote filopodia formation in HeLa cells. Using these optogenetic tools, I demonstrate a general method that can be used to study a broad range of proteins and protein-protein interactions.

TABLE OF CONTENTS

PRIOR PUBLICATIONS

Kim S, Rosen MK (2015) Multivalency mediated protein clustering at the plasma membrane. *In preparation*

Kim S, Rosen MK (2015) Optogenetic tool development based on fragment complementation. *In preparation*

Li P, Banjade S, Cheng HC, **Kim S**, Chen B, Guo L, Llaguno M, Hollingsworth JV, King DS, Banani SF, Russo PS, Jiang QX, Nixon BT, Rosen MK (2012) Phase transitions in the assembly of multivalent signaling proteins. *Nature* **483:** 336-340

Padrick SB, Cheng HC, Ismail AM, Panchal SC, Doolittle LK, **Kim S**, Skehan BM, Umetani J, Brautigam CA, Leong JM, Rosen MK (2008) Hierarchical regulation of WASP/WAVE proteins. *Mol Cell* **32:** 426-438

Song SJ, Song MS, Kim SJ, **Kim SY**, Kwon SH, Kim JG, Calvisi DF, Kang D, Lim DS (2009) Aurora A regulates prometaphase progression by inhibiting the ability of RASSF1A to suppress APC-Cdc20 activity. *Cancer Res* **69:** 2314-2323

Song MS, Song SJ, **Kim SY**, Oh HJ, Lim DS (2008) The tumour suppressor RASSF1A promotes MDM2 self-ubiquitination by disrupting the MDM2-DAXX-HAUSP complex. *EMBO J* **27:** 1863-1874

LIST OF FIGURES

LIST OF TABLES

LIST OF ABBREVIATIONS

l_{em}	Emission wavelength
l_{ex}	Excitation wavelength
$^{\circ}$ C	Degrees Celsius
A.U.	Arbitrary units
AJ	adherens junctions
Anx	annexin
ARF1	ADP-ribosylation factor 1
Arp2/3	Actin related protein 2/3
B	Basic
C	Central
Cdc42	Cell division cycle 42
ChR2	chanelrhodopsin-2
CIB1	calcium and integrin-binding protein 1
CRIB	Cdc42- and Rac-interactive binding
CRY2	cryptochrome 2
DD	death domains
Duf	Dumbfounded
EC	extracellular immunoglobulin-fold
Eph	Erythropoietin-producing hepatocellular receptor
ER	endoplasmic reticulum

F-actin	Filamentous actin
FA	focal adhesions
FKBP	FK506 binding protein
FRAP	fluorescence recovery after photobleaching
FRB	FKBP12-rapamycin-binding
FRET	fluorescence resonance energy transfer
FUS	fused in sarcoma
G-actin	Globular or monomeric actin
Gal3	galectin-3
GBD	GTPase binding domain
GDP	Guanosine diphosphate
GEF	Guanine nucleotide exchange factor
Gln1	glutamine synthetase
GPI	glycosylphosphatidylinositol
GPI-AP	GPI-anchored protein
GSL	glycospingolipid
GTP	Guanosine triphosphate
GUV	giant unilamellar vesicles
HSN	hermaphrodite-specific neurons
Ig	immunoglobulin
Ig-CAM	immunoglobulin cell adhesion molecules
IgSF	immunoglobulin superfamily

IL-2	interleukin 2
K_D	Equilibrium dissociation constant
kDa	Kilo-dalton
LAD	light activated heterodimerization
LatB	Latrunculin B
LBD	ligand binding domain
LC	low complexity
L_D	Liquid disordered
L_O	Liquid ordered
LOV2	light oxygen voltage 2
MbCD	methyl-beta-cyclodextrin
mg	milligram
MIM	Missing In Metastasis protein
min	minute
mM	micromolar
mol	mole
ms	millisecond
Nck	non-catalytic regions of tyrosine kinase adaptor protein
NFAT	nuclear factor of activated T cells
nm	nanometer
nM	nanomolar
Pak1	p21 protein (Cdc42/Rac)-activated kinase 1

PDGF	platelet-derived growth factor
PH	pleckstrin homology
PhyB	phytochrome B
PI3K	Phosphatidylinostol 3-kinase
Pif	phytochrome interacting factor
PIP2	Phosphatidylinostol 4,5-biphosphate
PIP3	phosphatidylinositol 3,4,5-triphosphate
PRM	Proline rich motif
PS	phosphatidylserine
PX	phox
Rac	receptor-aenylate cyclase protein
RBD	receptor binding domain
Rho	Ras homology
SAM	sterile-alpha motif
SFK	Src family kinases
SH2	Src homology 2
SH3	Src homology 3
Sns	Sticks and stones
SOCE	store-operated calcium entry
SopE	salmonella outer protein E
STIM1	stromal interacting molecule 1
STORM	stochastic optical reconstruction microscopy

TCR	T cell receptor
TIRFM	total internal reflection fluorescence microscope
WASP	Wiskott-Aldrich Syndrome Protein
WH2	Wiskott-Aldrich Homology 2
WT	wild type

Chapter 1

Introduction I

The organization of the plasma membrane into biochemically distinct compartments is essential to transmitting signals between the cytoplasm and extracellular environment. Such spatially isolated domains can be functionally characterized by their protein and lipid composition (Astro & de Curtis, 2015; Day & Kenworthy, 2009; Edidin, 2003; Grecco et al, 2011). For example, numerous receptors involved in cell growth, neuronal signaling, and cell adhesion are often reported to cluster and form oligomers upon binding to external ligands (Grecco et al, 2011; Groves & Kuriyan, 2010; Honerkamp-Smith et al, 2009; Kusumi et al, 2011). However, these micron-sized receptor clusters have been observed with little explanation as to what biophysical mechanism or mechanisms regulate their formation.

Lipid-mediated protein clustering at the plasma membrane

Much of the effort to understand receptor cluster formation has focused on the role of lipids in regulating cluster formation. Membrane lipids undergo phase transitions between liquid ordered (L_O) and disordered (L_D) phases by interactions between sterols and saturated acyl chains (Lingwood & Simons, 2010). Liquid ordered (L_O) domains are often called 'rafts' in cell biology to describe subdomains at the plasma membrane with distinct lipid and protein composition (Day & Kenworthy, 2009; Hancock, 2006; Toulmay & Prinz, 2013). Previous studies suggest that cholesterol, glycospingolipid (GSL), inositol phospholipids or phosphatidylserine (PS) mediated raft formation play a crucial role in multiple pathways, including Ras signaling, cell adhesion, and endocytosis (Edidin, 2003; Hancock, 2006; Henis et al, 2009; Lingwood & Simons, 2010). Some of the evidence demonstrating the precise role of these lipids in forming subdomains will be further discussed in this section.

Glycosylphosphatidylinositol (GPI)-anchor protein (GPI-AP) is a common raft marker. GPI-AP organization is regulated by the cholesterol content of the plasma membrane (Varma & Mayor, 1998). GPI-AP clusters are present on the nanometer scale (< 5 nm) and contain less than 10 molecules, as measured by homo-FRET (fluorescence resonance energy transfer) based methods (Gowrishankar et al, 2012; Varma & Mayor, 1998). In addition, polarized epithelial cells contain micron-sized clusters at the apical membrane, emerging from the coalescence of small-sized GPI-AP clusters in the Golgi apparatus (Paladino et al, 2014). Cholesterol plays a crucial role in both systems, despite the differences in scale and composition (Goswami et al, 2008; Sharma et al, 2004).

Ras proteins, small GTPases involved in cell growth and proliferation, segregate into liquid ordered (L_O) subdomain structures at the plasma membrane (Henis et al, 2009). Three major isoforms of Ras, H-, N-, and K-Ras, are distinguished by different posttranslational processing at C-terminal membrane anchor region, mono-palmitoylation, di-palmitoylation, and polylysine, respectively (Hancock et al, 1989; Henis et al, 2009). Each nanometer sized Ras clusters contains only one type of isoform with distinct lipid composition, which is essential for accurate cytoplasmic signaling cascades. For example, lateral segregation of K-Ras clusters from H-Ras clusters is dependent on a lipid phase transition based on phosphatidylserine (PS) levels (Zhou et al, 2014).

Cholesterol and glycospingolipid (GSL) are crucial components in the liquid ordered phase (L_o) formation, which can be the initiation step in raft-mediated endocytosis of multiple membrane proteins including GPI-anchored proteins, interleukin 2 (IL-2) receptor, and cholera toxins (Lamaze et al, 2001; Le Roy & Wrana, 2005; Sabharanjak et al, 2002). In contrast to canonical endocytosis, many cargoes for raft-mediated endocytosis do not associate with typical coating proteins such as clathrins, which show electron dense structures with electron microscopy. Instead, most cargo proteins contain various lipid-binding domains that bind directly to the lipids (Howes et al, 2010). For example, galectin-3 (Gal3) requires GSL to trigger membrane invagination (Lakshminarayan et al, 2014).

Inositol phospholipids play a crucial role in numerous cellular processes at the plasma membrane. These phospholipids contain an inositol head group with one to three phosphate groups. In particular, phosphatidylinositol 4,5-biophosphate (PIP2), the most abundant phosphoinositide, binds to actin regulatory proteins directly or indirectly to regulate cell

morphology, adhesion and migration (McLaughlin et al, 2002). For example, vinculin, a major structural component at adherens junctions (AJ) and focal adhesions (FA), consists of a head (VA) domain, a disordered proline-rich region, and a vinculin tail (Vt) domain (Parsons et al, 2010). Upon binding to PIP2, the Vt region gets released from autoinhibition to form higher-order oligomers, which results in mature FA complexes at the plasma membrane (Chinthalapudi et al, 2014). PIP2 is also involved in neuronal exocytosis by clustering with syntaxin1A to form micron-sized domains (van den Bogaart et al, 2011).

Lipid mediated protein clustering occurs at internal membrane organelles as well, including the endoplasmic reticulum (ER) and Golgi. For example, stromal interacting molecule 1 (STIM1) is a calcium sensor located at the ER involved in store-operated Ca2+ entry (SOCE) (Liou et al, 2007). STIM1 requires cholesterol to form punctate structures at ER-PM contacts upon calcium depletion. (Pani et al, 2008; Wu et al, 2006) Also the Rim101 pathway in yeast vacuoles segregates protein components into lipid domains enriched with sterol (L_O), responding to pH stress and starvation (Toulmay & Prinz, 2013).

Biochemical studies of rafts have been performed mostly *in vitro,* using synthetic giant unilamellar vesicles (GUV) or membrane extraction of cells, which is resistant to nonionic detergent such as Triton X-100 (Day & Kenworthy, 2009; Hancock, 2006). However, it has been controversial whether phase transition of lipids in GUVs reflects microdomain formation in cells, because of differences in the complexity level between the plasma membrane and GUV system. Also, membrane extraction procedures using detergent will alter biochemical and biophysical properties of rafts (Edidin, 2003; Lingwood & Simons, 2010; Munro, 2003). For example, rafts studied in the *in vitro* systems show different sizes

and stability from structures at the plasma membrane (Kusumi et al, 2011). In addition, phase separated lipid domains in GUV are micron-sized structures, while super-resolution microscopy has revealed that many proteins form clusters smaller than the optical limit of conventional microscopy (~ 400 nm) in native conditions (Eggeling et al, 2009). Finally, physiological conditions of the plasma membrane are near the critical point of liquid ordered and disordered phases, which generates local fluctuations leading to the intrinsic heterogeneity of membranes with nanoscale subdomain structures. (Veatch et al, 2008) Recent studies suggest the large discrepancy between the *in vivo* and *in vitro* systems comes from the active role of proteins in microdomain formation at the plasma membrane, which, unlike lipids, the biophysical mechanism is not well understood.

Oligomerization of scaffold proteins at the plasma membrane

Most examples of protein-mediated receptor clustering implicate stochastic oligomerization of scaffold proteins at the plasma membrane as a key component of microdomain formation (Astro & de Curtis, 2015; Kholodenko et al, 2000; Wu, 2013). Scaffold proteins provide a signaling platform by interacting with membrane receptors and cytoplasmic effectors simultaneously (Langeberg & Scott, 2015; Zeke et al, 2009). Examples of the scaffold protein-based mechanisms proposed for receptor clustering will be discussed in this section.

The actin cytoskeletal machinery acts as a scaffolding network in numerous signaling pathways at the plasma membrane. For example, T cell activation requires active actin polymerization for proper T cell receptor (TCR) arrangement at the immunological synapse (Jaqaman & Grinstein, 2012; Sherman et al, 2011; Yu et al, 2013). Also actin meshwork of migrating cells associates with multiple proteins with a WH2 domain, which enhances actin polymerization at the leading edge (Gardel et al, 2010; Rafelski & Theriot, 2004). Feedback mechanism between rearrangement of actin filaments and associated proteins can be found with focal adhesion formation as well (Parsons et al, 2010).

Actomyosin at the cell cortex is a network of actin filaments crosslinked with myosin II molecular motors, which regulate cell migration and morphological changes (Paluch et al, 2006). Myosins are motor proteins associated with actin and include more than 20 classes subdivided into muscle and non-muscle myosins. They are involved in numerous cellular processes including cell migration, endocytosis, and vesicle trafficking (Arif et al, 2011). Recently, the Mayor group and the Rao group at the NCBS in Bangalore together

demonstrated that direct interactions between short and dynamic actin filaments at the cortex with GPI-anchored proteins resulted in concentration fluctuations to form nanoclusters at the plasma membrane (Gowrishankar et al, 2012; Rao & Mayor, 2014).

In addition to the actin cytoskeleton, self-assembly of other scaffolding proteins plays an essential role in initiating and maintaining cell-to-cell junctions. For example, cadherin, a major structural component at cell junctions, contains five extracellular immunoglobulin-fold (EC) domains in its extracellular region. Homo- and heterodimerization of EC domains between two cells reveal supramolecular structures (Harris & Tepass, 2010; Yap et al, 1997). A recent study demonstrated that oligomerization by *cis*-interactions between cadherins requires *trans*-interaction by cadherins presented by the neighboring cells (Wu et al, 2011).

Erythropoietin-producing hepatocellular (Eph) receptors respond to direct contact with a neighboring cell during nervous system development, resulting in rearrangement of the actin cytoskeleton (Himanen et al, 2007). Eph receptor-interacting proteins (ephrins) localize at the membrane with either glycosylphosphatidylinositol anchors or transmembrane domains and interact with Eph receptors at the cell-to-cell junctions. The N-terminal ligand-binding domain (LBD) of the Eph receptor interacts with the N-terminal receptor-binding domain (RBD) of ephrin, which requires matched subtypes on both sides (Nikolov et al, 2013). However, monovalent interactions between a single Eph receptor and an ephrin are not sufficient for Eph signaling (Janes et al, 2012). Also Eph receptor-ephrin complexes assemble into micron-sized structures at the contact sites despite of low expression level in the brain (Hafner et al, 2004). Thus, Eph signaling requires multimeric complex formation of Eph-ephrin at contact sites, which are made through positive feedback between extracellular

and intracellular signaling of Eph-ephrin. In addition, crystallography study proposed polymerization of the extracellular domains as an additional mechanism for protein clustering (Seiradake et al, 2013). Upon specific binding between Eph receptor and ephrin, both proteins function as scaffolding proteins for the intracellular pathway. The intracellular region of the Eph receptor consists of a sterile-alpha-motif (SAM) domain and a PDZ-binding motif, which results in *cis* oligomerization of Eph (Himanen et al, 2010). Cytoplasmic regions of ephrin also behave as 'receptor-like' signaling molecules and recruit an adaptor protein Nck2, which contains multi SH2/SH3 domains, through three phospho-tyrosine residues (Cowan & Henkemeyer, 2001). Nck2 binds to platelet-derived growth factor (PDGF) receptor or Src family kinases (SFKs) to facilitate phosphorylation of ephrin at the plasma membrane (Palmer et al, 2002). The c-terminal region of Ephrin contains a PDZ-binding motif as well, which interacts with PDZ-RGS3 in G protein-coupled receptor signaling (New et al, 2013).

Endocytosis is another cellular process that contains a wide range of self-assembling scaffold proteins (Le Roy & Wrana, 2005). Coating proteins such as clathrins and caveolin constitute an ordered array attached to the plasma membrane and induce endocytosis of most integrated proteins (Le Roy & Wrana, 2005; Martinez-Outschoorn et al, 2015). For example, COP protein clustering at the site of membrane bending is an essential step in clathrin-dependent endocytosis and cargo internalization (Crosby et al, 2013; Pucadyil & Schmid, 2009).

Multiple pathogens reorganize the cytoskeletal system and plasma membrane by hijacking scaffolding proteins of the host during the infection process. For example, type IV pili of *Neisseria meningitidis* are composed of oligomeric fibers of the main pilin protein, which acts as a scaffolding structure for minor pilin proteins to mediate adhesion to epithelial cells and autoaggregation. (Imhaus & Dumenil, 2014)

Also the death-inducing signaling complex is formed through homotyopic association of death domains (DD) from CD95 and FADD, followed by procaspase activation and initiation of apoptotic pathway. (Schleich et al, 2012)

Often protein-mediated and lipid-mediated receptor clustering processes are not exclusive, but cooperative with each other. For example, upon depletion of calcium in the ER, oligomerization of STIM1 enhances its accumulation at the ER-PM junctions, which requires cholesterol for formation. (Liou et al, 2007)

Raft-mediated endocytosis is often dependent on lipids as well as self-association of cargo protein itself. For example, annexin A4 (AnxA4) forms higher order arrays upon binding to Ca2+ and phospholipid. (Crosby et al, 2013)

Focal adhesions also require higher order oligomerization of Vinculin, an essential scaffold protein (Parsons et al, 2010). The higher order structure is mediated by binding to PIP2 as described previously, but the structure is further augmented by Vt-Vt self-association and binding to F-actin. (Chinthalapudi et al, 2014)

Multi-valent receptor clustering at the plasma membrane

Numerous receptors including Ephrin receptors, Cadherins, ZO-1, 836R and bacterial chemoreceptor Tsr contain multivalent domains (Astro & de Curtis, 2015; Groves & Kuriyan, 2010; Wu et al). Multivalent domains have been observed as clustered structures at the plasma membrane, even without the direct connection to sterols or oligomeric proteins. For example, cadherins at cell junctions have five EC domains interacting in-*cis* and in-*trans,* as described in the previous section (Yap et al, 1997). The intracellular domain of the Eph receptor contains three phosphorylation sites, while its interacting protein Nck2 has three SH3 domains (Palmer et al, 2002). Multi-valent interactions are often found simultaneously with lipid mediated or scaffold assembly mediated cluster formation. For example, phosphoinositides are known to be secondary signaling molecules involved in cytoskeletal regulation and vesicle trafficking (Comer & Parent, 2002). They bind to multiple proteins containing the Pleckstrin Homology (PH) domain, FYVE, and Phox (PX) domains (Lemmon, 2003). More specifically, vinculin, an essential component in focal adhesions, binds to α-catenin in a multivalent manner through its N-terminal domains (D1, D2 and D3), while c-terminal vinculin tail (Vt) region interacts with phosphatidylinositol 4,5-bisphosphate (PIP2) and F-actin as described in earlier session (Chinthalapudi et al, 2014; Ziegler et al, 2006).

However, there has been little discussion about the role of multivalency in cell signaling, despite its widespread prevalence in membrane signaling molecules. Furthermore, lipid mediated or scaffolding protein mediated supramolecular formation rarely consider the contribution of post-translational regulation to receptor clustering. In this thesis I propose

that phase separation of membrane-bound receptors can be driven by multivalent interactions, and that this process may be regulated by common post-translational modifications such as phosphorylation. I suggest these mechanisms are a general biophysical phenomenon used by cells to create functionally isolated compartments at the plasma membrane.

Phase separation in three-dimensional environment

Intracellular organization has been extensively studied in the context of membrane encapsulated structures such as the nucleus, ER, Golgi, and lysosomes. However, the cell contains numerous membrane-less organelles that are proposed to isolate biochemical reactions in a phase-separated environment spatially distinct from the rest of the cell. Some of these bodies found in the nucleus include nucleoli, Cajal bodies, nuclear speckles, and PML bodies, while the cytoplasm contains stress granules and P bodies. (Handwerger et al, 2005; Luby-Phelps, 2013; Spector, 2006) These bodies have been recently described as protein-rich organelles that are micron-sized, liquid-like droplets not contained by a membrane. The first example of liquid-like compartments was P granules, unique cytoplasmic membrane-less organelles in *Caenorhabditis elegans* germ cells. P granules are enriched in RNA and RNA-binding proteins and play an essential role in germ development (Hyman et al, 2014). Fluorescence imaging revealed that P granules coalesce and exchange components with the cytoplasm and that estimated viscosity and surface tension were also consistent with the properties of liquid droplets. Also asymmetric localization associated with condensation of P granules at the posterior suggested phase separation as an underlying mechanism for P granules formation (Brangwynne et al, 2009).

Nucleolus, an RNA/protein body structure in the nucleus, is another example of liquid droplets, consisting of hundreds of proteins and RNAs for ribosome biogenesis (Hyman et al, 2014). Despite the high complexity in composition, nucleoli have been shown to behave as viscous fluids. Two nucleoli can coalesce into a larger nucleolus. Moreover, nucleolar protein components diffuse rapidly when measured with fluorescence recovery after

photobleaching (FRAP) experiments (Brangwynne et al, 2011). Nucleoli dynamics are dependent on the level of ATP in cells, which may provide a regulatory pathway for ribosome production (Feric & Brangwynne, 2013).

Recent studies have demonstrated that disordered proteins can mediate phase separation *in vitro* and *in vivo*, suggesting that cells may use disordered proteins as a general mechanism to form proteinaceous and membrane-less organelles. For example, the MEG (maternal-effect germline defective) proteins, intrinsically disordered, serine-rich proteins, regulate phase separation of P granules (Wang et al, 2014). More specifically, phosphorylation of the MEG proteins by the kinase MBK-2 drives disassembly of P granules, while dephosphorylation by the phosphatase PP2A having an opposing effect (Wang et al, 2014).

Another example of disordered protein mediated phase transition is seen in the nuage/chromatoid body family structures that require Ddx4 protein for their assembly, a recruiting component of an RNAi pathway in spermatocytes (Kotaja & Sassone-Corsi, 2007). Ddx4 protein contains an extensive intrinsically disordered domain at its N-terminus, which can self-associate through electrostatic interactions between regions of alternating net charge (Forman-Kay & Mittag, 2013). Polymerization of Ddx4 protein leads to phase separation into isolated structures both *in vitro* and in cells (Hyman et al, 2014; Nott et al, 2015).

Recently the Mcknight group proposed another mechanism of RNA granule formation, which contains multiple RNA binding proteins with low complexity (LC) sequences. The LC sequences are found in disordered polypeptides and have little diversity in amino acid composition (Michelitsch & Weissman, 2000). The purified LC domain of the

fused in sarcoma (FUS) protein phase separates into hydrogel *in vitro* at high concentration and consists of amyloid-like fibers (Kato et al, 2012). Hydrogel droplets of FUS LC peptides mimic cellular RNA granules, as evidenced by their ability to trap other proteins with LC sequences as well as RNA molecules found in granules (Han et al, 2012; Kato et al, 2012).

Our lab has previously reported that multivalent interactions between proteins and ligands can drive phase separation of protein components. Biochemical interactions between multivalent molecules in three-dimensional solution, as well as in the cytoplasm, result in the formation of micron-sized droplets. This phase separation was dependent on the concentration of individual proteins, as exhibited by a sharp transition at a critical concentration. Phase separated proteins show highly dynamic behavior including coalescence into larger droplets and rapid component exchange between different phases. The model system we used in this study consisted of three synthetic peptides generated from nephrin, a major adhesion receptor in podocytes, and its downstream effectors Nck and N-WASP. (Li et al, 2012) My thesis work here extended analyses of phase separation phenomena of nephrin, Nck and N-WASP to the two-dimensional *in vivo* system.

Nephrin, Nck, and N-WASP signaling in podocytes

Nephrin is an essential structural component of the kidney glomerulus, a highly specialized structure for ultrafiltration of plasma (Ruotsalainen et al, 1999). Podocyte, a unique epithelial cell in the glomerular filtration assembly, consists of three regions, a cell body, major processes and foot processes (Faul et al, 2007). The foot processes form a finger-like, interdigitating network with the foot processes of neighboring podocyte. The slit diaphragm, a supramolecular complex similar to adherens junctions (AJs), localizes between opposing foot processes of two podocytes (Faul et al, 2007). Mutations of many AJ proteins are associated with various glomerular diseases including proteinuria and diabetic nephropathy (Jones et al, 2009; Qin et al, 2009).

Nephrin consists of eight extracellular IgG repeats, a transmembrane domain, and a short unstructured tail (Ruotsalainen et al, 1999; Welsh & Saleem, 2010). Nephrin maintains the extracellular junctions between foot processes while regulating actin cytoskeletal support within foot processes (Li et al, 2013; Welsh & Saleem, 2010). Nephrin clusters have been observed at the interface between opposing podocyte foot processes (Ruotsalainen et al, 1999; Welsh & Saleem, 2010). At these interfaces, the eight extracellular IgG domains of nephrin interact in-trans between kidney podocytes to create an interdigitating pattern of tight junctions that act as a biological filter (Gerke, 2003).

Nephrin gets phosphorylated during the early stage of kidney development or the wound recovery process upon injury, but is dephosphorylated in other developmental stages (Jones et al, 2006; Tryggvason et al, 2006). Also phosphorylation of nephrin triggers its internalization through raft mediated endocytosis without their extracellular interactions *in*

trans. (Quack et al, 2006) Overall, it is thought that the cytoplasmic signaling process triggers nephrin clustering along with actin cytoskeleton rearrangement, which is followed by stabilization of cell-cell junctions with trans-association of the extracellular IgG domains between podocytes. Based on such observations, we decided to focus on the role of multivalent interactions occurring in cytoplasm, which can be regulated by the phosphorylation state of nephrin.

Phosphorylation of tyrosine residues on the intracellular tail of Nephrin at the filtration barrier is dependent on the Src-family kinase Fyn. (Jones et al, 2006) In particular, three tyrosine residues have proven essential for nephrin signaling to the actin cytoskeleton. (Jones et al, 2006) Upon phosphorylation, the Src homology 2 (SH2)/SH3 adaptor protein Nck binds the phosphorylated tyrosine residues (Jones et al, 2009). Nck then recruits N-WASP and Arp2/3 complex to induce actin polymerization at sites of nephrin phosphorylation (Buday et al, 2002).

In mammals there are two Nck isoforms, Nck1 and Nck2, both of which are involved in numerous signaling pathways, including T cell activation, cell migration and focal adhesions (Buday et al, 2002; Lettau et al, 2009). Nck consists of three Src homology 3 (SH3) domains followed by a c-terminal SH2 domain. All SH3 domains interact with proline-rich motifs of N-WASP, which will be described further in the next paragraph. The SH2 domain binds to phosphorylated YDxV motifs on nephrin (Blasutig et al, 2008). Nck expression is required during kidney development, and conditional knock-out of Nck in podocytes resulted in various kidney diseases including proteinuria and glomerulosclerosis. (Jones et al, 2009)

N-WASP, an activator of Arp2/3 actin nucleation complex, consists of an N-terminal EVH1 domain, a central regulatory domain, a region containing multiple proline-rich motifs (PRMs) and a C-terminal activity-bearing domain called the VCA region (Padrick & Rosen, 2010). The VCA region can bind to actin directly through two tandem WH2 domains (V region) and to the Arp2/3 complex through the CA region (Takenawa & Suetsugu, 2007). Normally intramolecular interactions between the N-terminal regulatory domain and the VCA region locks N-WASP in an autoinhibited state (Cheng et al, 2008). Multiple activators including the Nck protein activate N-WASP by releasing the VCA domain from interactions with the regulatory domain (Mayer, 2001; Padrick & Rosen, 2010). For example, Cdc42 and phosphatidylinositol 4,5-bisphosphate (PIP2) independently and synergistically activate N-WASP by binding to the regulatory GTPase binding domain (GBD) and a short polybasic (B) motif, respectively (Padrick & Rosen, 2010; Takenawa & Miki, 2001). The Nck proteins interact with the PRMs and recruit N-WASP to the plasma membrane, where many other activators reside (Jones et al, 2009; Papayannopoulos et al, 2005).

Besides its structural role in podocytes described above, nephrin, a member of the immunoglobulin superfamily (IgSF) of cell adhesion molecules (Ig-CAMs), regulates interactions between neighboring cells in diverse systems (Li et al, 2013). For example, the nephrin homologs in *C. elegans*, SYG-1 and SYG-2, act between guidepost vulvar epithelial cells and the axon of the hermaphrodite-specific neurons (HSN) (Ozkan et al, 2014). In Drosophila, Dumbfounded (Duf) interacts with the nephrin homolog, Sticks and stones (Sns), to mediate myoblast fusion through extensive immunoglobulin (Ig) domain contacts (Chen & Olson, 2004; Shilagardi et al, 2013). Many Ig-CAMs recruit adaptor proteins to transmit

intracellular signaling as well, which is demonstrated with nephrin binding to Nck1 through phosphorylated tyrosine residues and with SYGs binding to ZO-1 through PDZ domain-binding motifs. (Ozkan et al, 2014)

Here I describe analyses of *in vivo* protein clustering in the cytoplasm and at the plasma membrane, driven by a multivalent interaction mediated phase separation. Both three-dimensional and two-dimensional systems revealed the sufficiency of multi-valent interactions between proteins to form higher-order structures in cells. The formation of protein clusters was dependent on concentration and valences, and all the components in the supramolecular complex were highly dynamic. Overall, our study proposes a multivalent interaction mediated phase separation as a fundamental mechanism for compartmentalization of a cell.

Chapter 2:

Multivalency mediated Protein Clustering at the Plasma Membrane

Multivalent interactions between nephrin, Nck1 and N-WASP have been well characterized, assigning three phospho-tyrosine residues on nephrin, three SH3 domains in Nck1 and an extensive proline-rich motif (PRM) of N-WASP, which makes them a great system to demonstrate multivalency mediated phase separation at the plasma membrane. Previous students in our lab, Hui-Chun Cheng and Pilong Li, showed that multivalent SH3 and PRM peptides can phase separate into a higher-order polymers, when mixed together in solution. (Li et al, 2012) However, the question remained whether this behavior observed *in vitro* could be mirrored in cells. To address this issue, I performed cellular experiments by expressing the synthetic SH3-PRM system in HeLa cells.

The result and discussion sections were adapted from the paper.

Results

Artificial cellular body formation by multivalent SH3-PRM interactions in cells

Co-expression of mCherry-$SH3_5$ and eGFP-PRM_5 in HeLa cells results in formation of numerous, 0.5~2 μm diameter, cytoplasmic puncta containing both fluorophores (Fig. 2-1A). Puncta are not observed in cells expressing either of the two proteins alone, or in cells co-expressing mCherry-$SH3_5$ + eGFP-PRM_3, indicating that their formation is dependent on interaction between the two high-valent molecules. The puncta do not stain with a large range of lipid and vesicle markers, suggesting they are phase-separated bodies rather than vesicular structures (Fig. 2-2). Both mCherry and eGFP fluorescence of the bodies recover in ~10 seconds after photobleaching (Fig. 2-1B), indicating rapid exchange of both components with the surrounding cytoplasm and suggesting a dynamic, liquid-like nature. Thus, interactions between multi-valent proteins can produce phase separated liquid droplets both *in vitro* and in cells. Interestingly, eGFP-PRM_5 showed a ring-like structure, which fluorescence at the center can be recovered upon photobleaching of mCherry-$SH3_5$. Such differential FRET effect between eGFP-PRM_3 and mCherry-$SH3_5$ revealed the heterogeneity within droplets. (Fig. 2-1A, Fig. 2-3).

Our initial studies performed in three-dimensional solution also showed that the intracellular tail of nephrin, interacting with natural Nck1 and N-WASP, followed the biophysical principle of multivalent phase separation, as well as resulted in functional consequences of active actin polymerization *in vitro*.

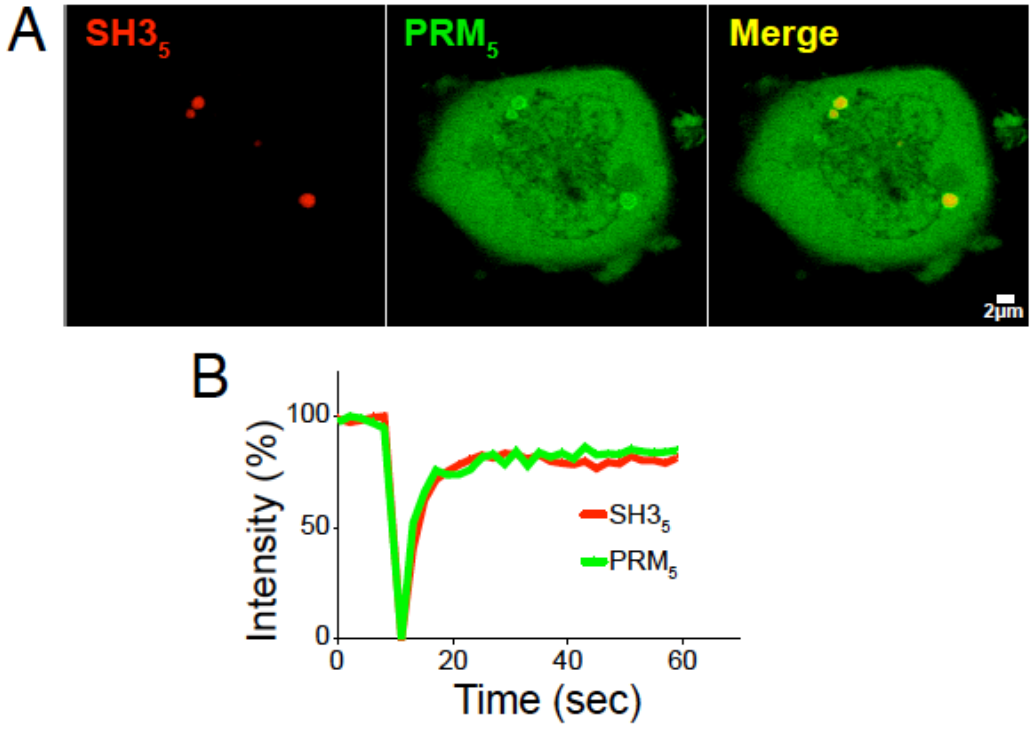

Figure 2-1. Coexpression of $SH3_5$ and PRM_5 in cells produces dynamic puncta. (A) mCherry–$SH3_5$ (left), eGFP–PRM_5 (center) and an image overlay in a cell expressing both proteins. It should be noted that the non-uniform eGFP fluorescence in the puncta results from mCherry–eGFP fluorescence resonance energy transfer (FRET) rather than from differential localization of the proteins (Figure 2-2). Scale bar, 2 mm. (B) Both mCherry and eGFP fluorescence recover rapidly after photobleaching.

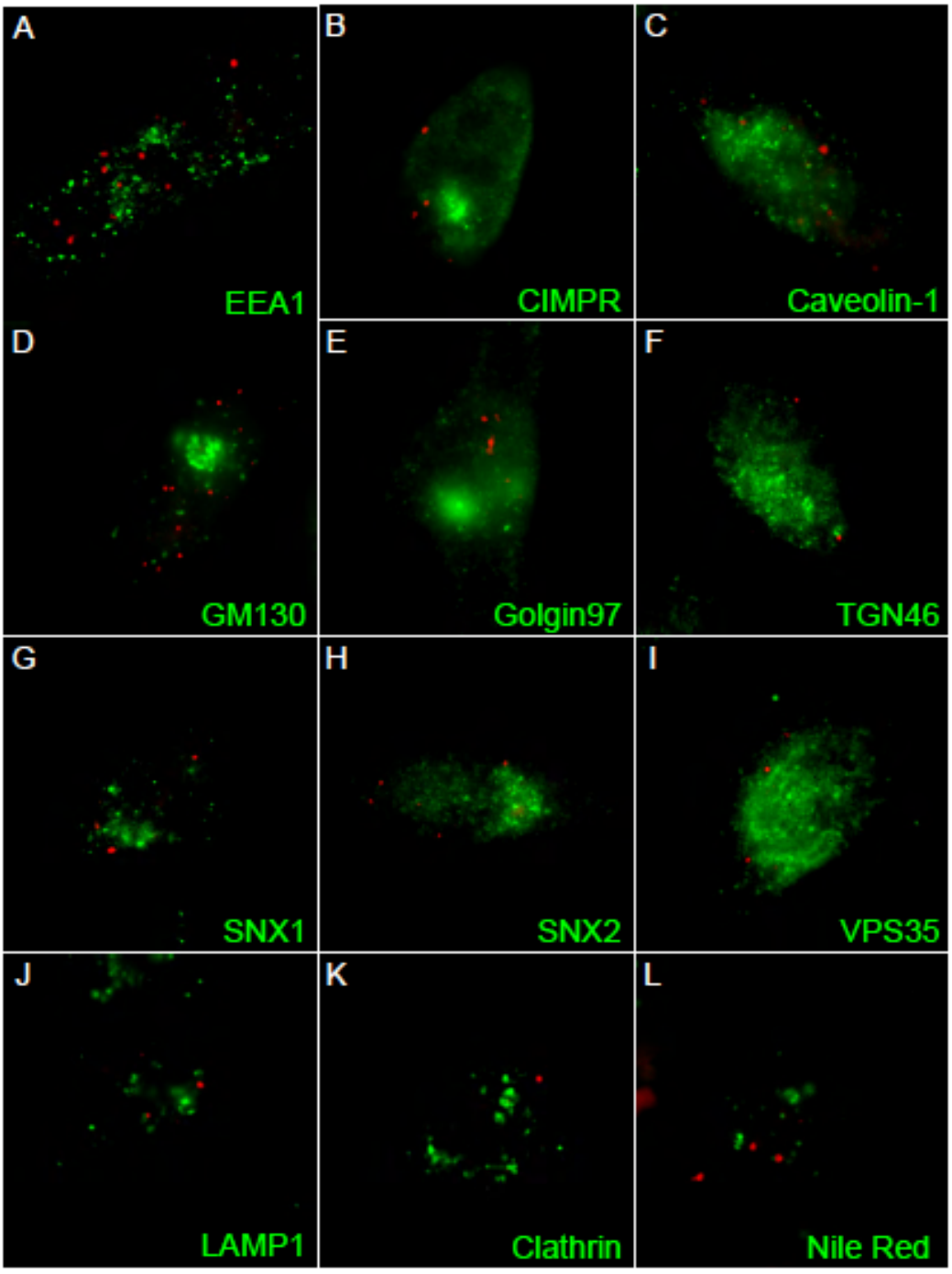

Figure 2-2. Cellular puncta formed by mCherry-SH3$_5$ and eGFP-PRM$_5$ are not vesicular. HeLa cells co-expressing mCherry-SH3$_5$ and eGFP-PRM$_5$ were stained with antibodies against various endocytic markers (identified with Cy5-labeled secondary antibodies) or co-expressing eGFP-SH3$_5$ and eGFP-PRM$_5$ were stained with a lipid dye (Nile

Red) as indicated. In all panels $SH3_5$-PRM_5 puncta are colored red and the various stains are colored green. Punctate structures did not coincide with cytoplasmic
vesicles or lipid. (A-C) Endocytic markers; (D-F) Golgi markers; (G-I) Retromer components; (J) lysosome
marker; (K) clathrin; (L) Nile red lipid marker.

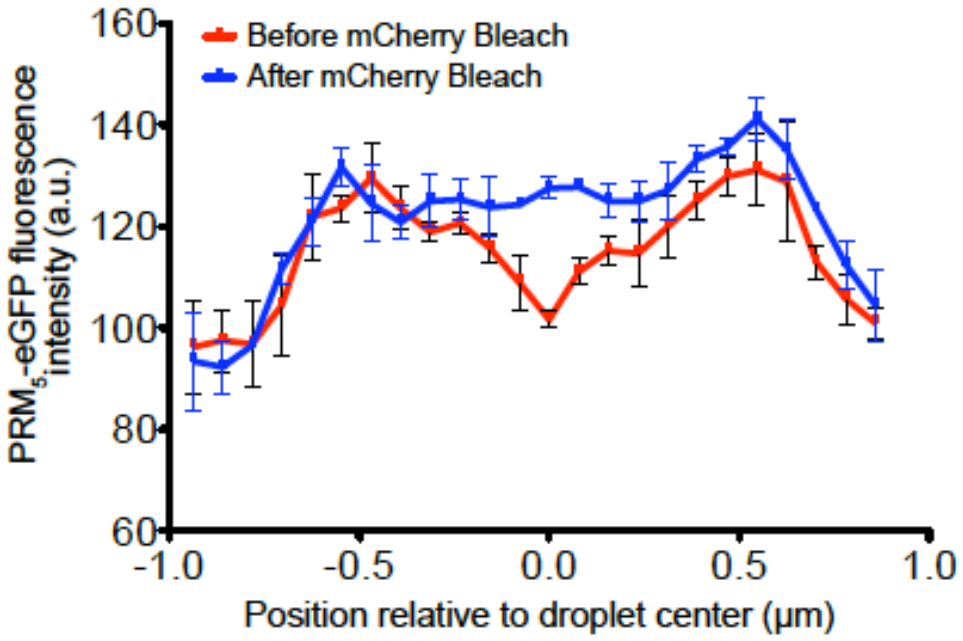

Figure 2-3. Non-uniform eGFP fluorescence in mCherry-SH3$_5$/eGFP-PRM$_5$ puncta is due to mCherry-eGFP FRET. Image shows eGFP fluorescence in a line-scan through the center of a cellular mCherry-SH3$_5$/eGFP-PRM$_5$ punctate structure before and after mCherry photobleaching. Error bars represent the standard error of the mean intensity for three closely spaced lines. The mCherry-SH3$_5$/eGFP-PRM$_5$ puncta have lower eGFP fluorescence at their centers than at their peripheries. Upon photobleaching of mCherry, the central green fluorescence increases appreciably, suggesting the initial non-uniformity is due to FRET between mCherry and eGFP. The different FRET properties at the periphery and center suggest that the bodies may be structurally inhomogeneous, for reasons we do not currently understand.

Phosphorylation of Nephrin induced by FKBP-FRB heterodimerization

Sudeep Banjade, a student in our lab recently published the *in vitro* work extended on the supported lipid bilayers, which demonstrated the polymerization of nephrin intracellular domain, Nck, and N-WASP on the two-dimensional surface concomitant phase transition. He measured the critical concentration of each component, above which the micron-sized cluster appears with temporal sharpness. The critical concentration of nephrin associated with the bilayer, Nck and N-WASP revealed valency-dependence and affinity dependence. He also showed that the protein clusters promote local actin polymerization in the presence of Arp2/3 complex. (Banjade & Rosen)

To test whether our *in vitro* observations were consistent with cellular systems involving the transmembrane domain and intracellular tail of nephrin, I needed to be able to regulate the interaction between nephrin and Nck. I employed an experimental system utilizing two well-known proteins, FKBP and FRB that bind each other with high affinity upon treatment of the small molecule, rapamycin. Nephrin and a Src family kinase are fused to FRB and FKBP, respectively, so that rapamycin addition to the cell will induce nephrin phosphorylation (Fig 2-4A). I also modified nephrin by truncating its extensive extracellular IgG repeats, leaving only its N-terminal membrane localization signal sequences, transmembrane domain and intracellular tail (called Δnephrin hereafter). This allowed me to isolate and study the function of the intracellular tail in nephrin clustering. The truncated construct was fused to FRB followed by fluorescent protein (mEGFP or mCherry) with $(GlyGlySer)_n$ linkers between each domain (Δnephrin-FRB hereafter). cSrc kinase was chosen for its potency over the natural kinase Fyn, and also modified to contain only the

kinase domain fused to FKBP (cSrcKD-FKBP hereafter). Activation of cSrc kinase requires substrate binding to the n-terminal SH2 and SH3 domains, releasing phosphorylation activity-bearing c-terminal kinase domain (Martin, 2001). Thus, I adapted the kinase domain without the regulatory domains, in order to increase K_M for Δnephrin, minimizing the background phosphorylation of Δnephrin prior to rapamycin addition as well as to reduce the phosphorylation of other undesired targets.

ΔNephrin-FRB localized on the plasma membrane, while Nck1 (fused to mEGFP for optical observation) remained cytoplasmic when both proteins were transiently expressed with cSrcKD-FKBP (Fig 2-4B). Upon rapamycin addition to the media, Nck translocated to the membrane. This translocation took less than one minute after the rapamycin addition to the media. Increased phosphorylation of Δnephrin on a similar timescale was observed by western blot using an antibody against phospho-tyrosine. Nck translocation was not observed when non-phosphorylatable mutant forms of Δnephrin were used, or when kinase was not co-expressed. Together, these data indicate that Nck translocation was due to binding to phosphorylated Δnephrin. Pull-down experiments confirmed the interaction between Nck1 and Δnephrin, as more Nck bound Δnephrin following rapamycin treatment (Fig 2-5A). Paralleling translocation, Nck binding was abolished when non-phosphorylatable mutant forms of Δnephrin were used, or when kinase was not co-expressed. This newly developed experimental platform allows us to observe the real-time behavior of Δnephrin and its interactions with binding partners in cells.

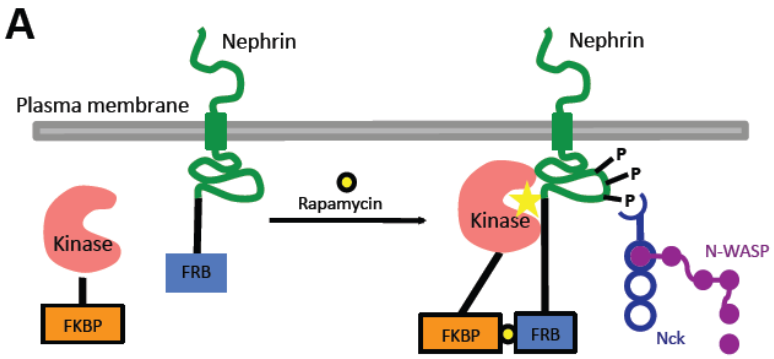
A
Nephrin
Plasma membrane
Kinase
FKBP
FRB
Rapamycin
Nephrin
Kinase
P
P
P
N-WASP
Nck
FKBP
FRB

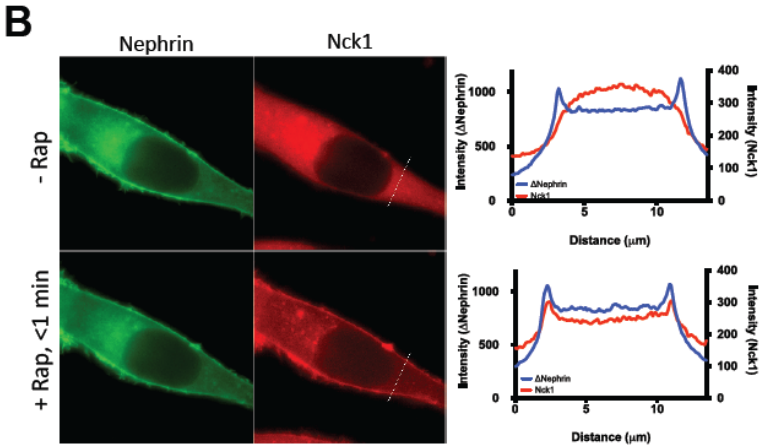
B
Nephrin
Nck1
- Rap
+ Rap, <1 min
Intensity (ΔNephrin)
Intensity (Nck1)
Distance (μm)
ΔNephrin
Nck1

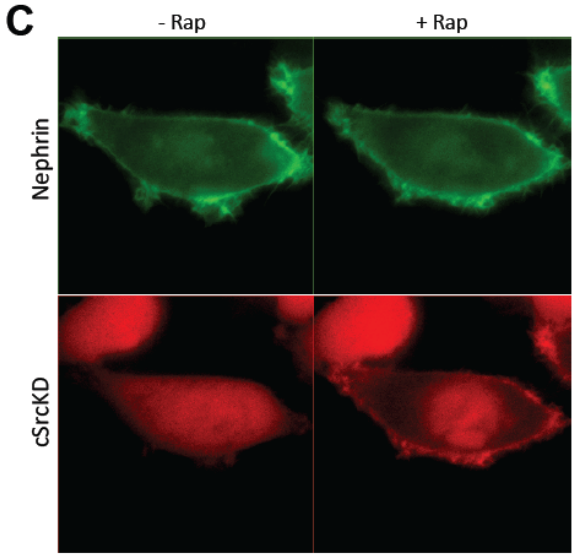
C
- Rap
+ Rap
Nephrin
cSrcKD

Figure 2-4. Development of a new tool manipulate the phosphorylation state of Δnephrin (A) cSrc and nephrin are fused to FKBP and FRB, respectively, so that rapamycin addition to the cell will induce nephrin phosphorylation, leading to the recruitment of Nck1 to the plasma membrane. (B) Addition of rapamycin into the medium resulted in rapid Nck1 translocation to the plasma membrane. Intensity profiles on the selected line were shown for Nck1 (red) and Δnephrin (green) (C) cSrcKD is recruited to the plasma membrane upon rapamycin treatment.

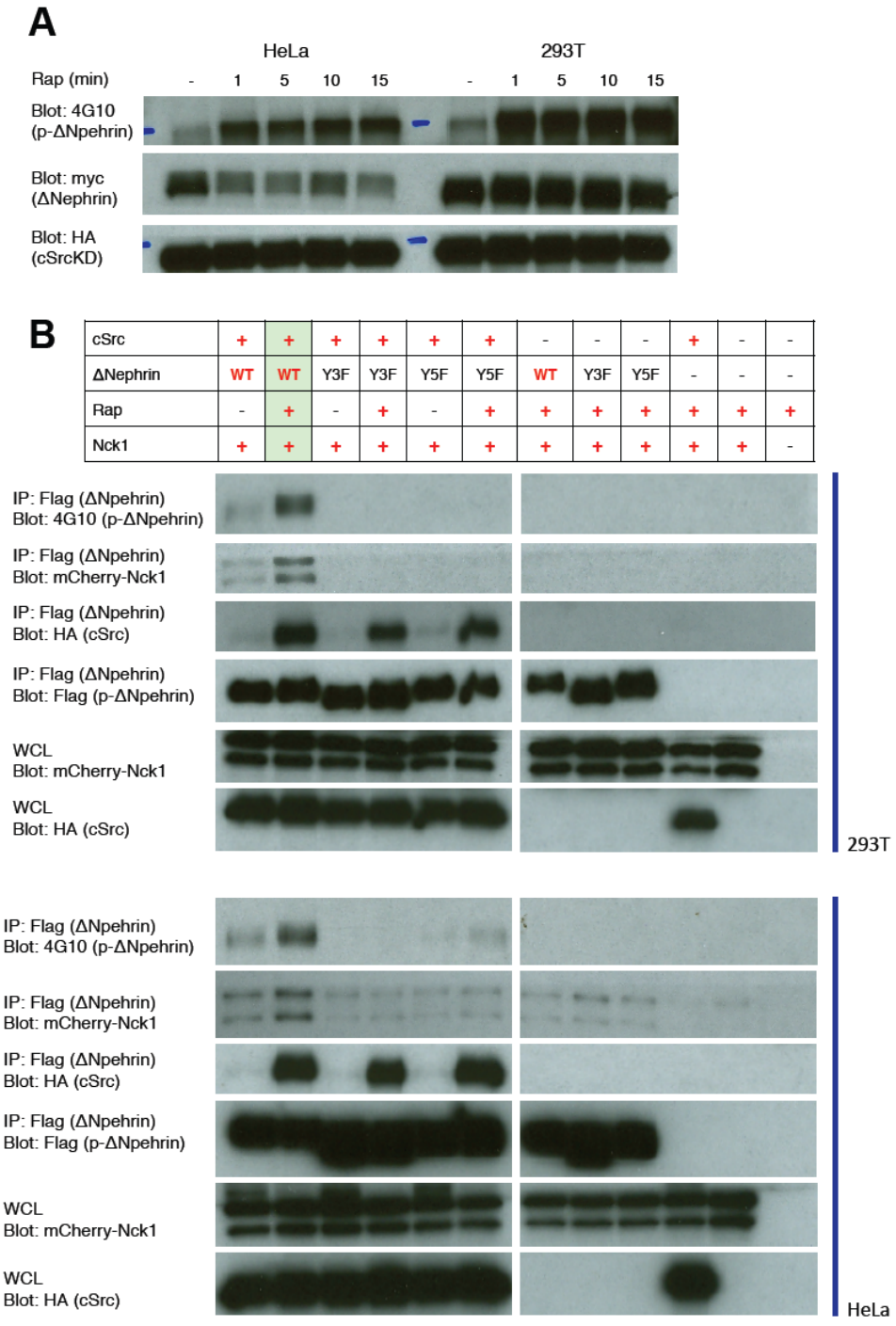

Figure 2-5. Increased phosphorylation level of Δnephrin can be detected with western blot analysis. (A) Western Blot analysis showed that cSrcKD phosphorylates Δnephrin within 1 minute after rapamycin treatment. Phosphorylated Δnephrin is detected using antibody against phosphor-tyrosines (4G10). (B) The increased phosphorylation level of

Δnephrin was observed in cells expressing Δnephrin (WT) and cSrcKD upon rapamycin treatment. Phosphorylation and Nck binding of Δnephrin was abolished when tyrosine sites on Δnephrin were mutated, when rapamycin was not added in media, or when kinase was not expressed. Two different cell lines, 293T and HeLa, were used for the experiments.

Formation of Nephrin clusters by binding to Nck1

To evaluate the consequences of interactions between Δnephrin and Nck1, total internal reflection fluorescence microscopy (TIRFM) was used to obtain live images. HeLa cells were transiently transfected with cSrcKD-FKBP, Δnephrin and Nck1.

Phosphorylation of Δnephrin following rapamycin treatment induced protein cluster formation on the plasma membrane. These clusters were enriched in both Δnephrin and Nck1 (Fig. 2-6A). Irregularly-shaped Δnephrin clusters were observed by both light microscopy and stochastic optical reconstruction microscopy (STORM) (Fig. 2-6B). Irregular shapes and sizes are consistent with phase transitions of these proteins observed in *in vitro* reconstitutions on supported lipid bilayers (Banjade & Rosen, 2014).

Cluster formation was dependent on the both the valency of Δnephrin, rapamycin treatment, and kinase fusion overexpression. The mutant form of Δnephrin (Δnephrin(Y3F)) was generated by replacing three tyrosine residues required for Nck1 binding. Because this construct was unable to interact with Nck1 at the plasma membrane, fewer clusters formed. The absence of rapamycin or kinase also resulted in a significantly lower fraction of cells showing clusters. (Fig. 2-7A)

However, I observed that almost twenty percent of Δnephrin (Y3F)-transfected cells still had clustered domain structures on their plasma membranes. This raised the question whether these clusters are the same as those formed by wild type phosphorylated Δnephrin. A distinguishing feature of p-Δnephrin (WT) clusters is the enrichment of Nck1 upon chemical induction. I, therefore, compared Nck1 enrichment in clusters of p-Δnephrin (WT) and Δnephrin(Y3F). The cluster areas were selected by Otsu thresholding. The intensities for

Δnephrin and Nck1 were measured and their ratio was calculated. This analysis clearly showed that clusters composed of p-Δnephrin (WT) can be distinguished from clusters of Δnephrin (Y3F) by the higher ratio of Nck1 to Δnephrin within clusters. More than 90% of clusters from all control samples (cells expressing Δnephrin (Y5F), cells without cSrcKD expression, cells without rapamycin treatment) had Nck1/Δnephrin fluorescence intensity ratio lower than 0.9, while this ratio was greater than 0.9 in almost 60% of cells expressing Δnephrin (WT). These data suggest that there are at least two forms of Δnephrin clusters, those induced by Δnephrin-Nck1 interactions and those that are Nck1-independent. Nck1-dependent clusters are further studied in the following sections.

Because multivalency-driven phase separation is dependent on the protein concentration, I tested whether Δnephrin clusters also depend on cellular concentrations, as would be expected if they were phase-separated entities. For these experiments, I transiently transfected the HeLa cells to produce a wide range of protein expression levels. The fluorescence of Δnephrin or Nck1 was measured in every transfected cell, quantified as the average intensity of each protein, to determine the expression level of each protein. Within a population of cells with a certain range of fluorescence intensities, the fraction of cells showing clusters demonstrates how the concentration of each protein is important for cluster formation following rapamycin treatment. Both the data binned over protein expression and fitted with logistic regression showed a clear distinction between cells with p-Δnephrin(WT) and control samples (cells expressing non-phosphorylatable Δnephrin mutants, cells without cSrcKD expression, cells without rapamycin treatment) with the measured p-value of less than 0.0001. (Table 2-1) Also comparing cells with p-Δnephrin(WT) showed that the

likelihood of clusters formation increases with Nck1 expression in cells. (Fig. 2-7A). However, cluster formation was insensitive to the Δnephrin concentration, as shown in Fig. 2-7D.

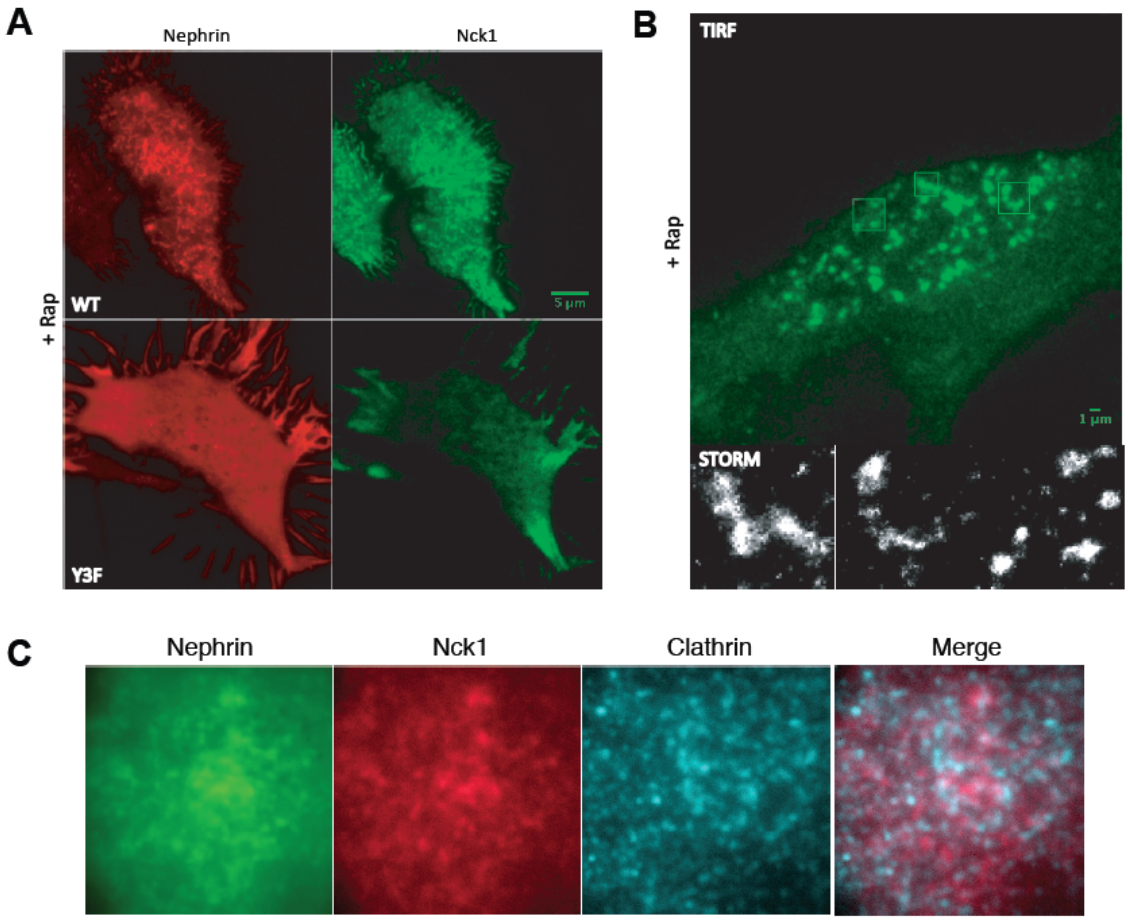

Figure 2-6. ΔNephrin forms clusters enriched with Nck1 (A) ΔNephrin clusters were enriched with Nck1, while mutant Δnephrin did not form any clusters upon rapamycin treatment. (B) STORM imaging revealed irregular shaped Δnephrin clusters. Zoomed in images were shown for three regions. (C) ΔNephrin clusters did not co-localize with the clathrin heavy-chain staining.

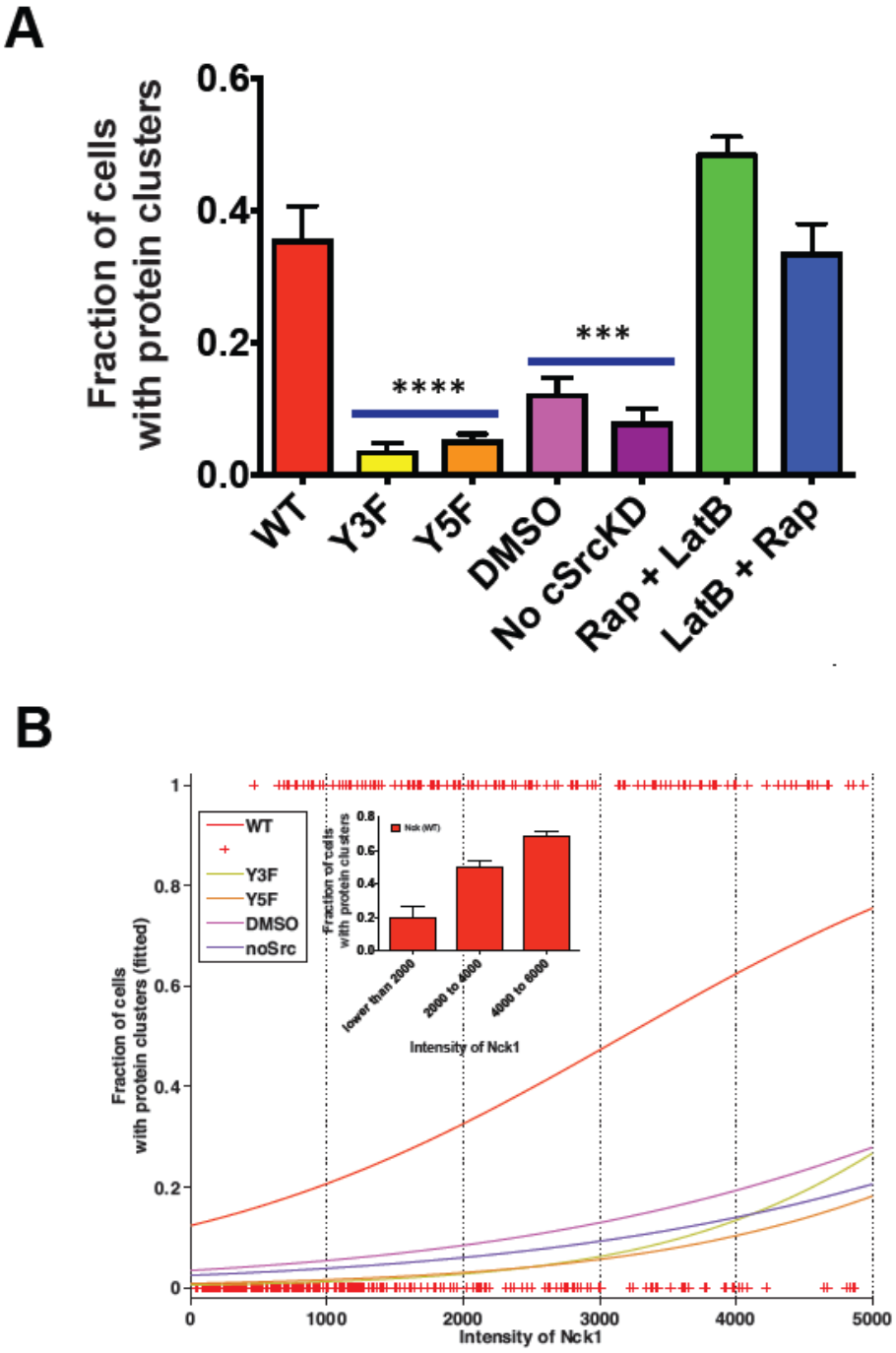

Figure 2-7. ΔNephrin forms clusters dependent on Nck1 concentration, but independent on Δnephrin concentration. (continued on next page)

C

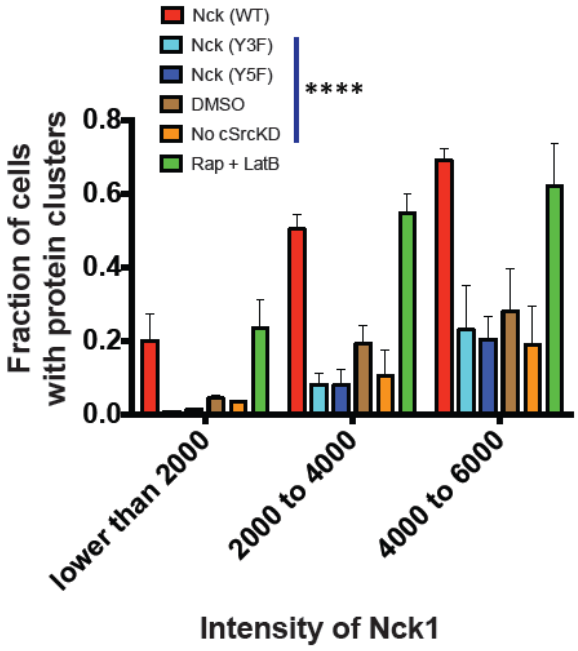
Nck (WT)
Nck (Y3F)
Nck (Y5F)
DMSO
No cSrcKD
Rap + LatB
****
Fraction of cells with protein clusters
0.8
0.6
0.4
0.2
0.0
lower than 2000
2000 to 4000
4000 to 6000
Intensity of Nck1

D

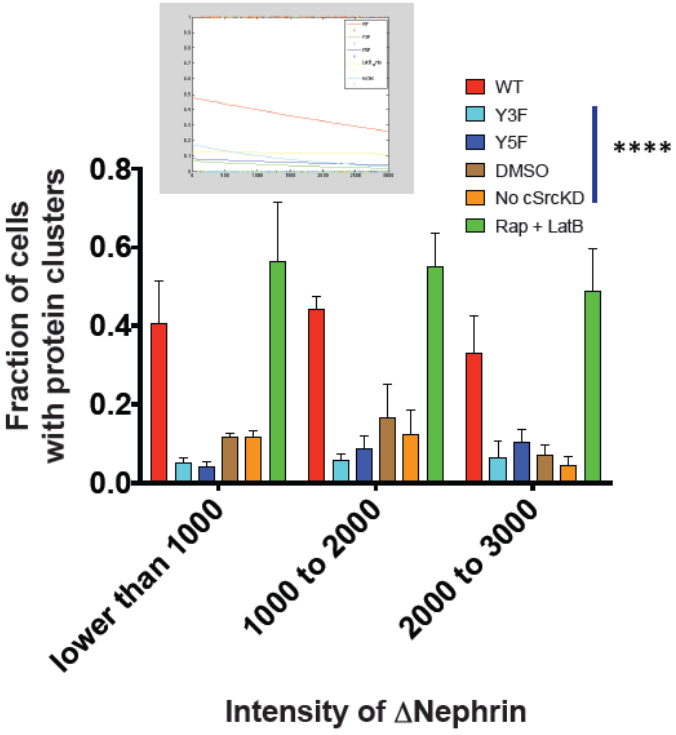
WT
Y3F
Y5F
DMSO
No cSrcKD
Rap + LatB
****
Fraction of cells with protein clusters
0.8
0.6
0.4
0.2
0.0
lower than 1000
1000 to 2000
2000 to 3000
Intensity of ΔNephrin

Figure 2-7. ΔNephrin forms clusters dependent on Nck1 concentration, but independent on Δnephrin concentration. (A to D) Error bars, s.e.m. (n=3, total more than 450 cells counted) (A) Approximately 40% of cells with phospho-Δnephrin and Nck1 (WT) showed clusters, in contrast to about 10% of cells without rapamycin treatment (DMSO) or kinase expression (No cSrcKD) and less than 5% of cells with non-phosphorylatable mutants of Δnephrin (Y3F and Y5F). LatB treatment does not prevent cluster formation. (Rap+LatB and LatB+Rap) (B) Logistic regression fitting of the proportion of cells to the Nck1 intensities showed increasing probability of cluster formation with higher Nck1 concentration in cells. The fraction of cells with clusters within binned Nck1 intensities was also measured to confirm the logistic regression analysis data. (C) High expression level of Nck1 favors clustering of Δnephrin(WT). Mutation of Nck1 binding sites prevented clustering. (D) ΔNephrin expression level does not affect protein clustering efficiency.

	Nck1	Nephrin
WT-Y3F	<0.0001	<0.0001
WT-Y5F	<0.0001	<0.0001
WT-DMSO	<0.0001	<0.0001
WT-no cSrc	<0.0001	<0.0001
Y3F-Y5F	5.070391e-01	2.906806e-01
Y3F-DMSO	1.480095e-03	1.943427e-06
Y3F-no cSrc	.3.058038e-02	2.684041e-02
Y5F-DMSO	4.153947e-03	1.162443e-03
Y5F-no cSrc	1.148804e-01	1.456619e-01
LatB Only-no cSrc	3.095268e-01	1.113016e-03

Table 2-1. P-values from logistic regression fitting of concentration dependency data
Values colored in red shows that sample with phospho-Δnephrin(WT) and Nck1 are significantly different from control samples.

Nephrin cluster formation is independent of actin polymerization

To determine how actin polymerization affects Δnephrin cluster formation, I inhibited actin polymerization by treatment with Latrunculin B (LatB) for 20 minutes and then induced Δnephrin phosphorylation with rapamycin. LatB was added to the media before rapamycin induction to eliminate any possible roles of actin polymerization in protein clustering. Pre-treatment with LatB abruptly changed the shape of cells and cortical actin structures but did not alter the organization of Δnephrin at the plasma membrane. Subsequent addition of rapamycin induced recruitment of Nck1 to the plasma membrane within one minute, followed by the formation of micron-sized clusters of within 30 minutes. (Fig. 2-8A,B)

The dependence of cluster formation on protein expression level was also evaluated following the addition of LatB (Fig, 2-8C). This analysis showed that the proportion of cells with clusters increased within the population with higher Δnephrin and Nck1 expression. Notably, almost no difference was observed between the conditions with or without LatB treatment. Such observations reveal that Δnephrin clustering on the plasma membrane is independent of actin polymerization.

To eliminate the possibility that Δnephrin clustering was induced by association with other membrane-localized structures, I performed the following experiments. Cells were stained for paxillin, caveolin, or clathrin to determine if Δnephrin clusters simply localized to focal adhesions or endocytic machinery. ΔNephrin clusters did not colocalize with these structural markers, suggesting that they are independent from focal adhesion complexes or endosomal vesicles. (Fig. 2-9) In addition, all clustering experiments here were performed with concurrent methyl-beta-cyclodextrin (MbCD) treatment to prevent the endocytosis of

Δnephrin upon phosphorylation. (Qin et al, 2009) Treating cells with MbCD not only helped to increase the Δnephrin concentration on the membrane (not shown), but also eliminates the possibility that the clustering I observed is generated primarily by cholesterol-dependent raft formation.

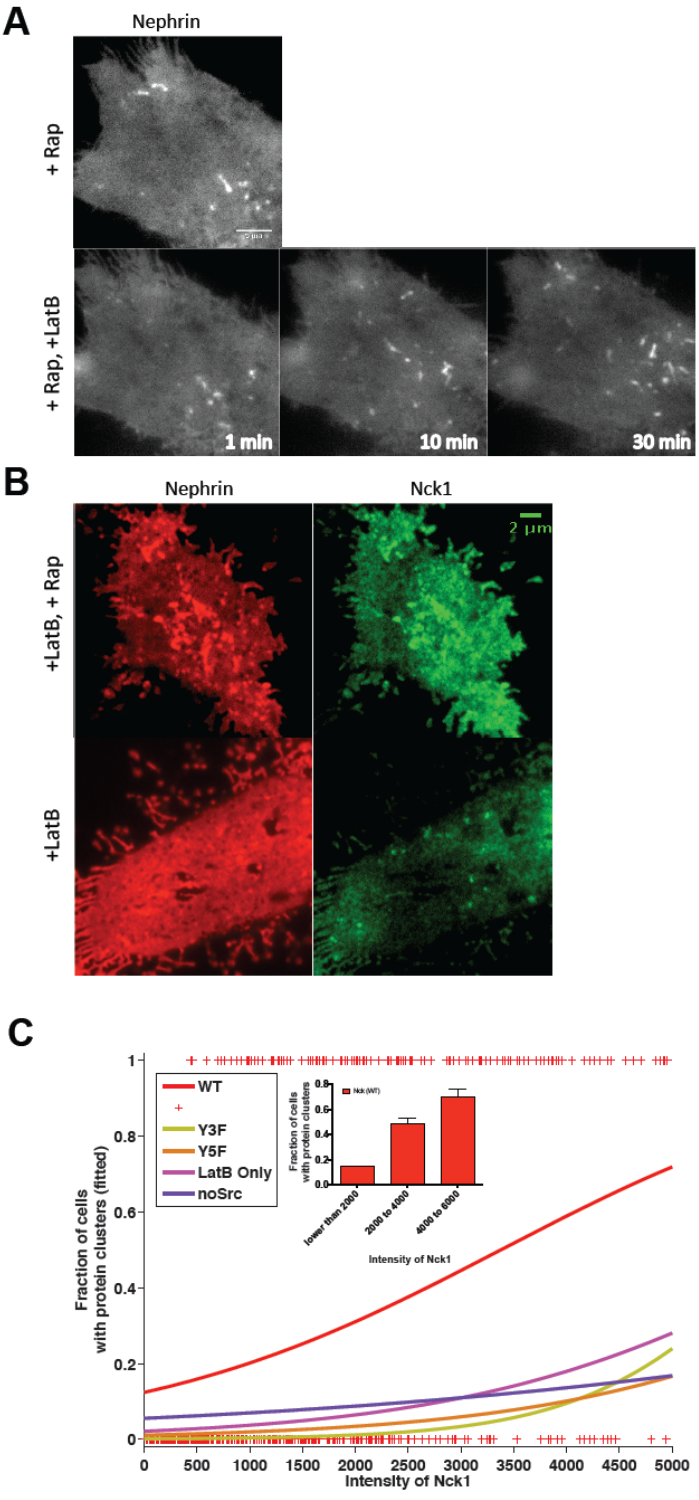
A
Nephrin
+ Rap
+ Rap, +LatB
1 min
10 min
30 min
B
Nephrin
Nck1
2 µm
+LatB, + Rap
+LatB
C
WT
Y3F
Y5F
LatB Only
noSrc
Fraction of cells with protein clusters (fitted)
Intensity of Nck1
Nck (WT)
lower than 2000
2000 to 4000
4000 to 6000

Figure 2-8. ΔNephrin forms clusters via interactions with Nck1 in the absence of actin cytoskeleton (A) Clustering of Δnephrin was observed using TIRFM within 10 minutes after rapamycin treatment. LatB treatment before rapamycin did not affect Δnephrin clustering. (B) ΔNephrin clusters in LatB treated cells were enriched in Nck1. (C) Logistic regression fitting of the proportion of cells to the Nck1 intensities showed increasing probability of cluster formation with higher Nck1 concentration in cells treated with LatB. The fraction of cells with clusters within binned Nck1 intensities was also measured to confirm the logistic regression analysis data. Error bars, s.e.m. (n=3, total more than 450 cells counted)

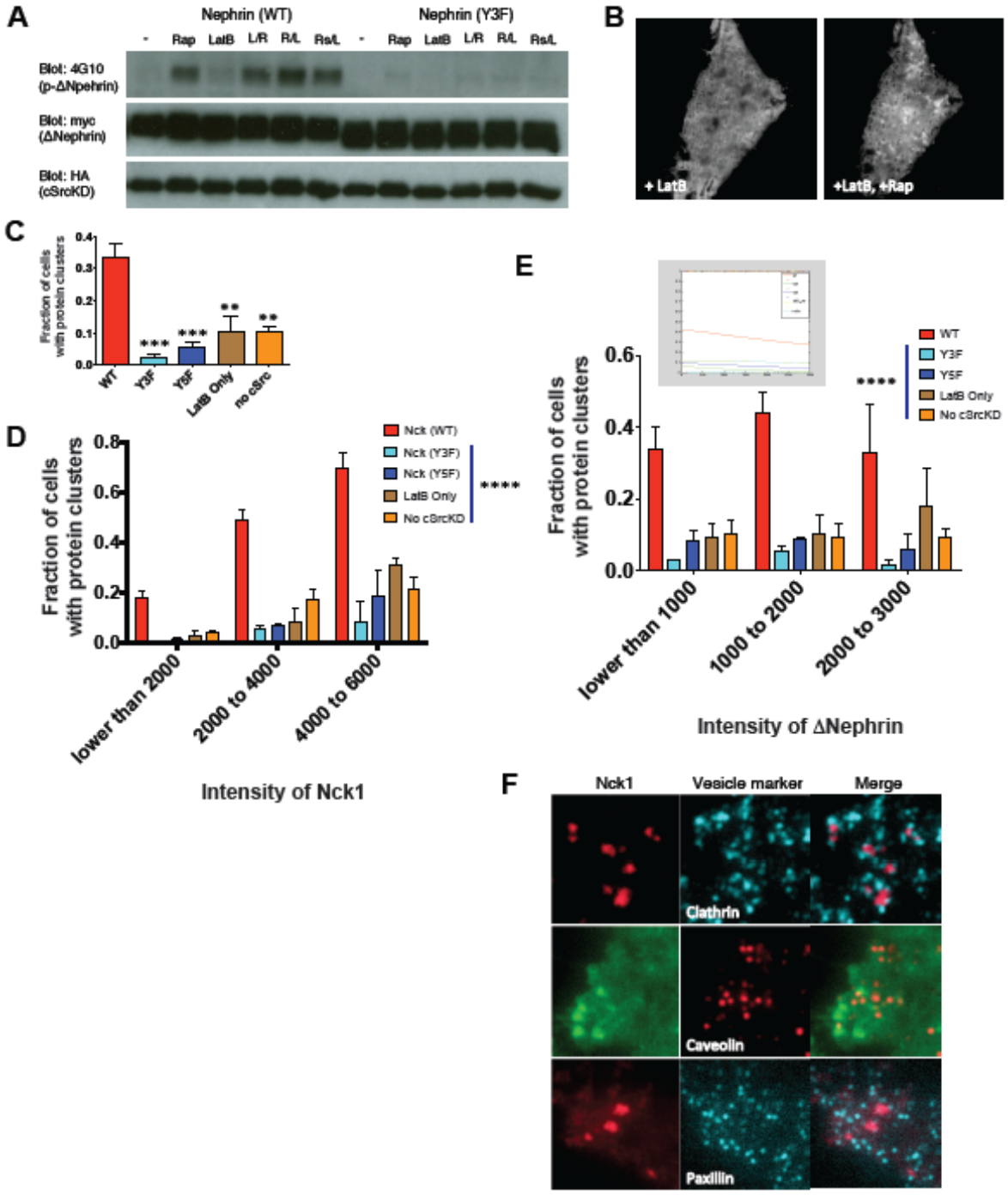

Figure 2-9. Latrunculin B treatment did not interfere with Δnephrin cluster formations. (A) Latrunculin B treatment did not affect phosphorylation of Δnephrin upon rapamycin treatment. (B) Cells were treated with LatB for 20minutes and with rapamycin without changing the media. Live imaging of a cell showed Δnephrin clusters within 10 minutes after rapamycin treatment. (C, D, E) Error bars, s.e.m. (n=3, total more than 450 cells counted) (C) Almost 40% of cells with phospho-Δnephrin and Nck1 showed clusters, in contrast to less

than 10% of cells in control samples without rapamycin treatment (LatB Only) or kinase expression (No cSrc) and less than 5% of cells with non-phosphorylatable mutants of Δnephrin (Y3F and Y5F). (D) Concentration dependency of Δnephrin-Nck1 clustering following LatB treatment. (E) The proportion of cells with clusters did not show significant differences between the ranges of Δnephrin intensity level. Logistic regression fitting data was also measured to confirm the result. (F) ΔNephrin clusters did not co-localize with endocytic (clathrin and caveolin) or focal adhesion (paxillin) markers.

	Nck1	Nephrin
WT-Y3F	<0.0001	<0.0001
WT-Y5F	<0.0001	<0.0001
WT-DMSO	<0.0001	<0.0001
WT-no cSrc	<0.0001	<0.0001
Y3F-Y5F	3.104231e-02	1.429694e-02
Y3F-DMSO	5.597473e-04	<0.0001
Y3F-no cSrc	<0.0001	<0.0001
Y5F-DMSO	6.433213e-02	3.032447e-02
Y5F-no cSrc	4.013633e-04	1.692041e-02
LatB Only-no cSrc	1.310527e-03	9.424898e-01

Table 2-2. P-values from logistic regression fitting on concentration dependency data acquired from samples treated with LatB before rapamycin. Values colored in red shows that two sample in comparison are significantly different to each other.

Characterization of Nephrin clusters as multi-valent phase separated polymers

In vitro studies have shown that clustering of ΔNephrin on model membranes and phase separation of the protein in solution are both driven through multivalency-based hetero-oligomerization with Nck1 and N-WASP (Li et al, 2012). A hallmark of this behavior is the dependence of phase separation on the valency of the interacting species. As described above, Nck1 contains three consecutive SH3 domains, which interact with up to six proline-rich motifs in N-WASP. To test how Nck1 valency affects protein clustering, I generated a series of proteins composed of tandem repeats of the second SH3 domain of the protein followed by the SH2 domain. The SH3 domains were connected to each other by the linker that naturally joins the first and second SH3 domains of Nck1. (Fig. 2-10A) These engineered constructs are denoted below as SH3b(3), SH3b(2), and SH3b(1) for proteins with three, two, and one SH3 domain(s), respectively.

Initially I found that cells expressing SH3b(3) were much more likely to form clusters on the membrane than those expressing SH3b(1) (Fig. 2-10A). Further investigations performed together with fluorescence intensity analysis quantitatively compared cluster formation in cells expressing either SH3b(3), SH3b(2), or SH3b(1) to determine the effect of valency on cluster formation. Cells expressing higher valency constructs were more likely to contain clusters with lower expression of the engineered proteins. (Fig. 2-10B) Without LatB treatment, cells expressing SH3b(2) were nearly as likely as cells expressing SH3b(3) to contain clusters. But in LatB treated cells the SH3b(2) construct had a significantly lower ability to form clusters. Cells expressing SH3b(1) induced clusters similarly to negative control samples expressing Δnephrin(Y3F) with or without LatB treatment.

In vitro Δnephrin clusters formed on supported lipid bilayers by addition of Nck1 and N-WASP were dynamic liquid-like structures (Banjade & Rosen, 2014). All three molecules showed rapid fluorescence recovery after photobleaching (FRAP), and the macroscopic clusters merged with each other on seconds to minutes timescales. I characterized the dynamics of Δnephrin clusters in cells using FRAP. I found that Δnephrin recovers more slowly than Nck1 following photobleaching ($t_{1/2}$ of 32.49 seconds for Δnephrin vs. 23.62 seconds for Nck1, Fig. 2-10D). This is expected, as Δnephrin can only exchange molecules within the two dimensional membrane, whereas Nck1 can exchange both along the membrane as well as in the third dimension with the cytosol. Comparison of clustered versus unclustered regions revealed that both Δnephrin and Nck1 recover with substantially slower rates within clusters than outside of clusters ($t_{1/2}$ of 32.49 seconds for Δnephrin in clustered regions vs. 11.84 seconds in unclustered regions, $t_{1/2}$ of 23.62 seconds for Nck1 in clustered regions vs. 3.359 seconds in unclustered regions, Fig. 2-10D). This decreased recovery rate would be consistent with highly crosslinked, SH2- and SH3-mediated, oligomers/polymers within the phase separated clusters. These results support our proposal that the clusters are complex, non-covalent polymer networks that can freely exchange components with the local environment through the dissociation of SH2-pTyr and SH3-PRM interactions.

I further evaluated the assembly state of proteins in the clustered domains by measuring the dependence of the fluorescence anisotropy of YFP-Δnephrin on the density of the fluorophore, which reports on homo-fluorescence resonance energy transfer (homo-FRET) between the YFPs. (Goswami et al, 2008) I found that the fluorescence anisotropy gradually increased as Δnephrin clusters were photobleached, indicating homo-FRET

between YFP-Δnephrin molecules. This result suggests that YFP-Δnephrin molecules are within 10 nm of each other inside the clusters, consistent with a network crosslinked by Nck1 and N-WASP. (Fig. 2-10D)

Together, these data suggest that our *in vivo* nephrin clusters are very similar to the phase separated protein structures that we have observed in our previous *in vitro* experiments. (Banjade & Rosen, 2014) Also the experimental setup and coordinated controls eliminated mechanisms for protein clustering based on lipid raft formation and actin assembly.

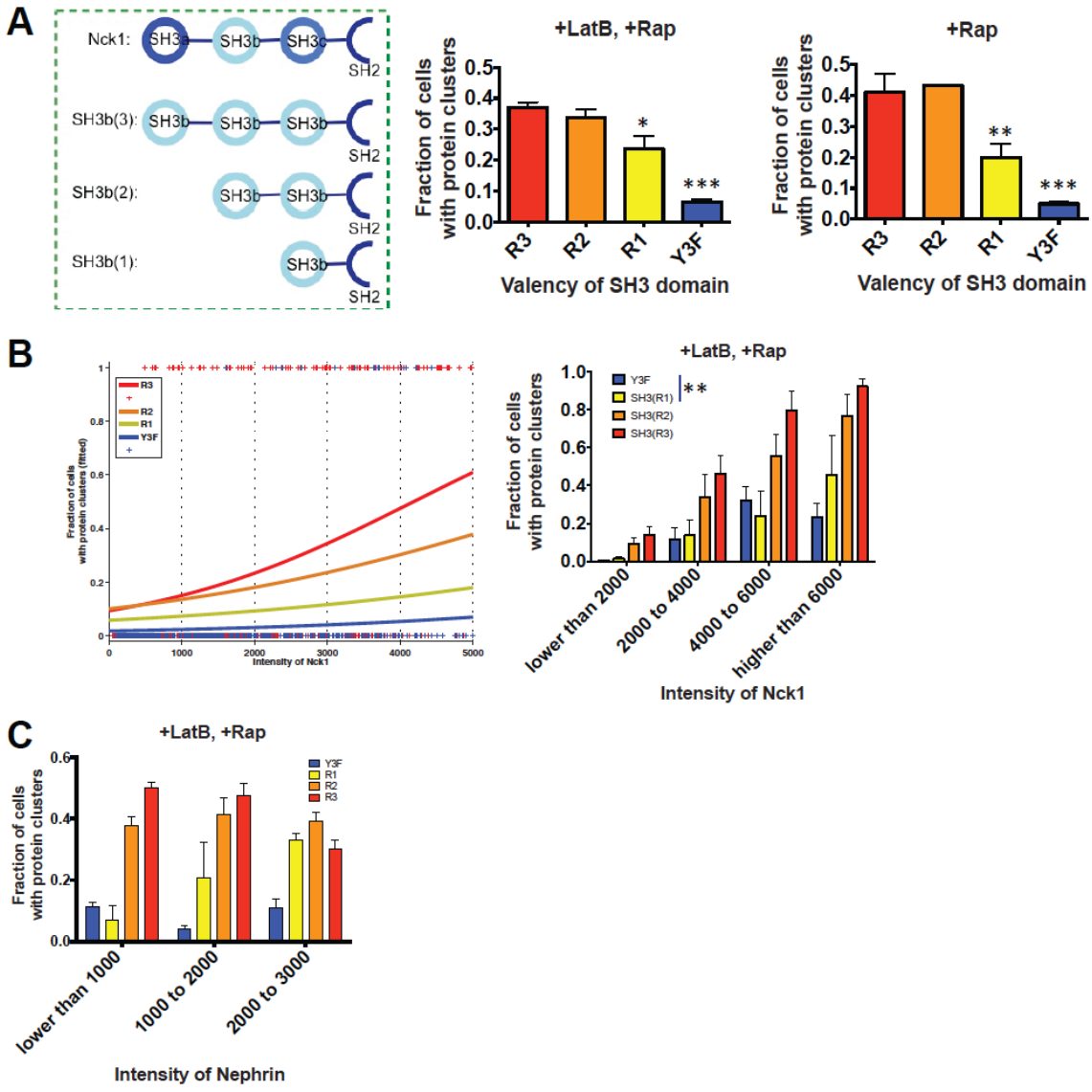

Figure 2-10. ΔNephrin clustering is mediated by phase separation. (continued on next page)

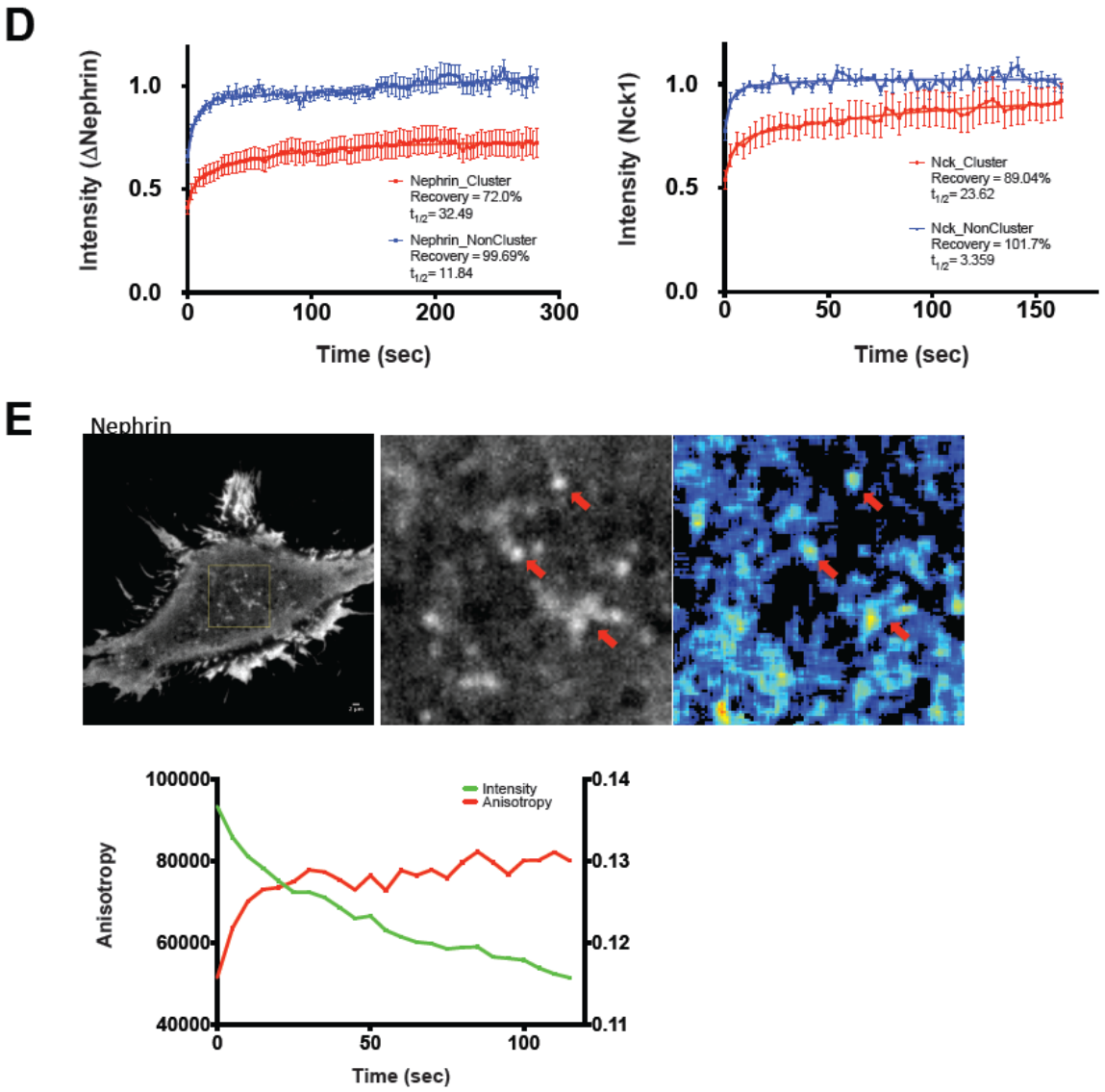

Figure 2-10. ΔNephrin clustering is mediated by phase separation. (A, B, C) Error bars, s.e.m. (n=3, total more than 450 cells counted) (A) Recombinant Nck1 constructs were designed with different SH3 valency. Higher fraction of cells showed Δnephrin clusters when expressing higher SH3 valency constructs. Samples with triple- (R3), di- (R2), and mono-SH3 (R1) constructs were colored in red, orange, and yellow, respectively. (B) Logistic regression fitting of the proportion of cells to the Nck1 intensities showed increasing probability of cluster formation with higher SH3 valencies as well as higher recombinant Nck1 concentration in cells. The fraction of cells with clusters within binned Nck1 intensities was also measured to confirm the logistic regression analysis data. (C) ΔNephrin expression level did not affect clustering efficiency of triple- or di-SH3 constructs. However, samples with higher level of Δnephrin showed higher fraction of cells with clusters. (D) ΔNephrin and Nck1 intensity levels recovered after photo-bleaching at slower rates at the regions with

clusters compared to those without clusters. (n=3, total more than 15 cells measured) (E) ΔNephrin clusters showed homo-FRET using anisotropy microscopy imaging. Image of a region with Δnephrin clusters (middle) in a cell (left) before photobleaching revealed high anisotropy level at clusters (right, red arrows). Photobleaching of YFP fused to Δnephrin showed reverse relationship between anisotropy and intensity level.

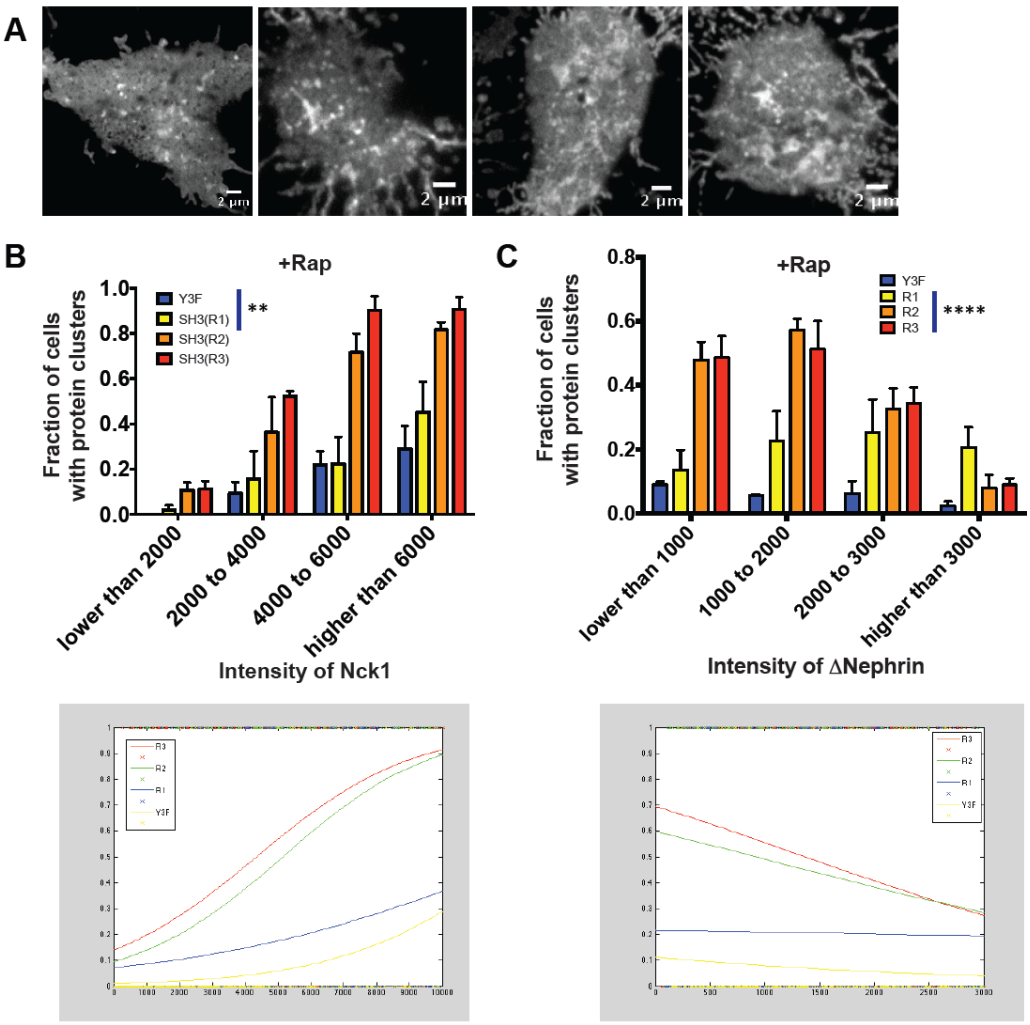

Figure 2-11. ΔNephrin clustering is mediated by phase separation in the presence of actin cytoskeleton. (A) ΔNephrin clusters formed with recombinant SH3b(3) construct were morphologically similar to the clusters formed with Nck1. (B,C) Error bars, s.e.m. (n=3, total more than 450 cells counted) (B) Higher recombinant Nck1 expression favored protein clustering. The proportions of cells with tri- and di-SH3 were similar in all intensity ranges. Logistic regression data were shown to confirm the data of fraction of cells within binned intensity level. (C) Lower Δnephrin expression favored protein clustering in samples with tri- and di-SH3 constructs, while the sample with mono-SH3 constructs with different Δnephrin expression showed comparable clustering efficiency.

Actomyosin mediated movement of protein clusters

ΔNephrin clusters formed *in vitro* on supported bilayers move very little on the membrane surface. Clusters merge over time as their dynamic edges encounter one another, but their centers of mass do not change appreciably. In contrast, the Δnephrin clusters formed in cells are highly mobile throughout the time course of our experiments. They travel across the cell surface with rates as high as a couple of micrometers per minute. This mobility could be eliminated, however, by treating cells with LatB before induction of Δnephrin phosphorylation by rapamycin. Clusters formed in this manner showed only Brownian-like motion on the membrane surface. These data suggest that cluster motility is dependent on actin filaments, likely the dynamic behavior thereof. (Fig 2-12A) Based on a recent study demonstrating the role of actomyosin on GPI anchored protein *in vitro* and on T cell receptor clusters at the immunological synapse, I further examined other factors that could contribute to the diffusion of protein clusters on the plasma membrane. (Goswami et al, 2008; Sherman et al, 2011; Yi et al, 2012; Yu et al, 2013)

First I tested the effect of Blebbistatin, a potent myosin inhibitor, on Δnephrin cluster mobility (Kovacs et al, 2004). When Blebbistatin was applied to cells containing Δnephrin clusters, cluster mobility was inhibited. (Fig 2-12B) However, the inactive Blebbistatin enantiomer had no effect on cluster movement. These data demonstrate the importance of an active actomyosin network in cluster mobility on membranes and further suggest together with our observations following LatB treatment, that various disruptions of the cytoskeleton may affect the movement of protein clusters. However, treatment of cells with Δnephrin clusters by inhibitors of the Arp2/3 complex, CK869 or CK666, (Pollard & Cooper, 2009)

did not alter the behavior of clusters (Fig 2-13). These results demonstrate that the diffusion of protein clusters is driven by myosin-mediated cortical actin rearrangements rather than by Arp2/3 complex-dependent actin branch nucleation.

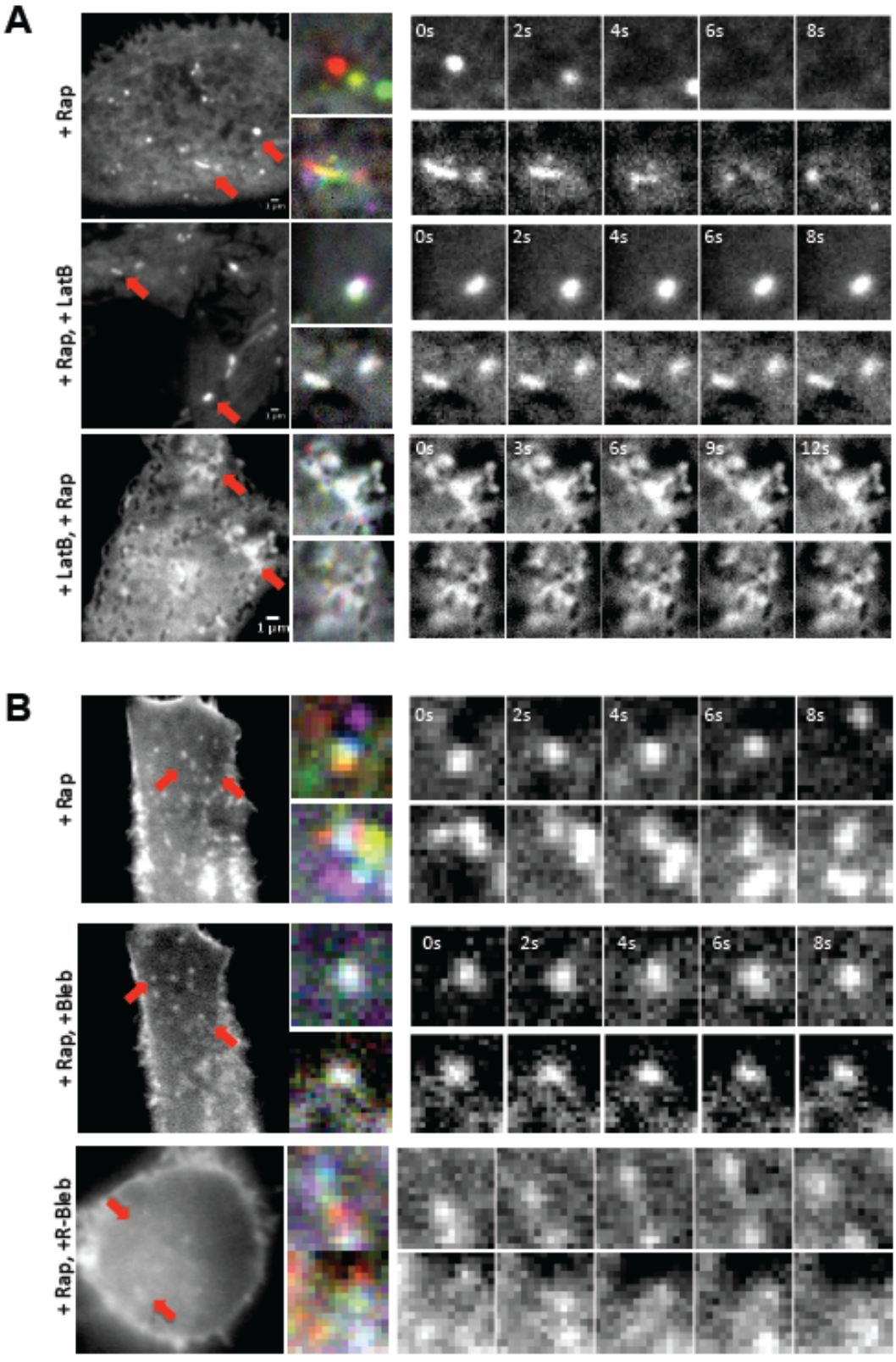
A
+ Rap
+ Rap, + LatB
+ LatB, + Rap
0s
2s
4s
6s
8s
0s
2s
4s
6s
8s
0s
3s
6s
9s
12s
1 μm
B
+ Rap
+ Rap, +Bleb
+ Rap, +R-Bleb
0s
2s
4s
6s
8s
0s
2s
4s
6s
8s
0s
2s
4s
6s
8s

Figure 2-12. Movement of protein clusters at membrane is driven by the cortical actomyosin system. (A) ΔNephrin clusters moved upon formation. Single cluster in a cell (red arrow) were tracked for 8 or 12 seconds. Images at each time points were color coded with ImageJ. LatB treatment before or after rapamycin slowed Δnephrin cluster mobility. (B) Inhibition of myosin with blebbistatin treatment slowed cluster mobility and induced partial cluster disassembly. Inactive form of blebbistatin did not affect the mobility of Δnephrin clusters.

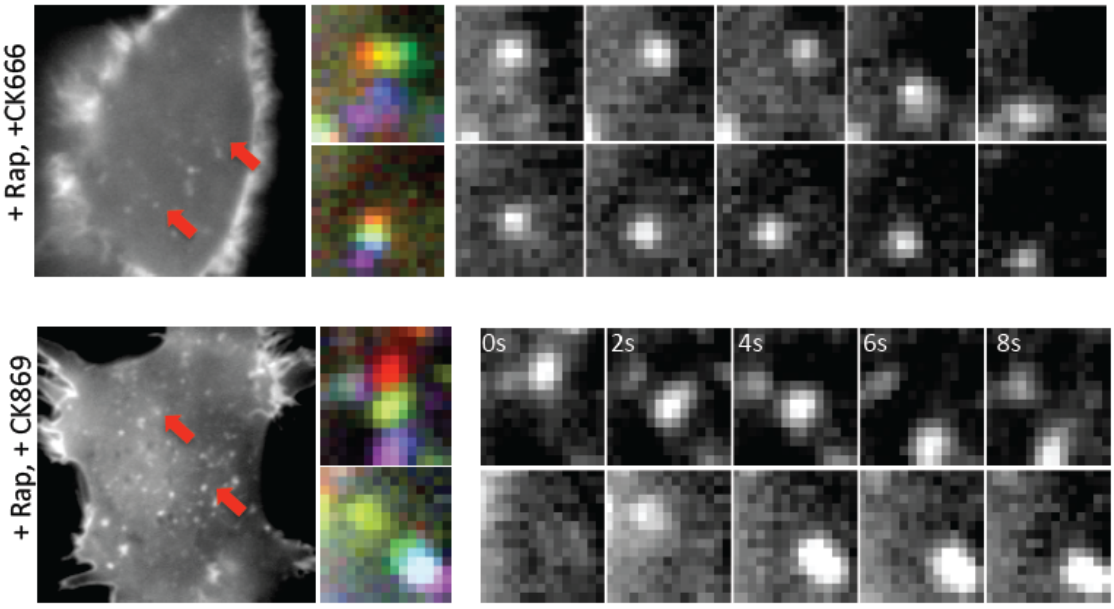

Figure 2-13. Inhibition of Arp2/3 complex does not affect cluster mobility.
Inhibitors of Arp2/3 complex, CK CK666 and CK869 did not alter the Δnephrin cluster mobility.

Peripheral membrane protrusion mediated by Nephrin clusters

As described in earlier studies, nephrin is known for its important role in generating the slit diaphragm of the glomerular filtration barrier. Although the extracellular domain of nephrin is the major structural component of the interdigitating pattern of cellular junctions that compose the slit diaphragm, it has been proposed that the initial cell protrusion process prior to stable cell-to-cell contact may be mediated by intracellular signaling of Nephrin to the actin cytoskeleton. (Faul et al, 2007) This proposal suggests that induced Δnephrin clusters may induce distinctive changes in the local cytoskeleton.

Live cell confocal imaging showed a dramatic change in the distribution of Δnephrin as well as the morphology of cell edges over a 30 minutes time course following rapamycin treatment. (Fig 2-14A) Cells formed micron-sized clusters enriched with Δnephrin and Nck1, from which generated multiple filopodia-like or microspike structures. These changes occurred concomitant with a large increase in F-actin at the sites of nephrin clustering. Clusters at the peripheral membrane in the middle confocal section of a cell, where membrane did not attach to the glass surface, showed the same biophysical and biochemical characteristics with those observed with the TIRF imaging on the basal surface. Their formation required binding to Nck1, whose localization in the peripheral clusters was dependent on the phosphorylation state of Δnephrin (Fig 2-14B). Also the fraction of cells with clusters increased with increasing number of Nck1 SH3 domains. (Fig 2-14C)

LatB treatment resulted in a notable difference between cells containing Δnephrin clusters and those without clusters. Following LatB treatment, membrane bending was observed at the regions containing actin-rich Δnephrin clusters, while those without clusters

merely shrank with the cell rounding. The actin in these clusters is resistant to even high dose of LatB (5 μM) for more than 30 minutes. In contrast, pre-treatment of LatB prevented the formation of Δnephrin clusters at the peripheral membrane. However, it is still possible that small peripheral clusters, of a scale below the resolution limit of confocal microscopy and similar to those observed on the basal membrane by TIRF microscopy still formed in the presence of LatB. These results suggest a possible role of the cortical actomyosin network in the maturation of peripheral Δnephrin clusters.

Using confocal microscopy, I examined the dynamics of large (2~3 microns) peripheral Δnephrin clusters by FRAP. Similar to the behavior of the basal clusters, Δnephrin at the periphery recovered more slowly than Nck1 recovery following photobleaching. (Fig 2-14D) ΔNephrin and Nck1 also recovered more slowly within clusters than outside of clusters (Table 2-3). Interestingly, the rate of Δnephrin recovery within clusters significantly decreased upon LatB treatment, while Δnephrin recovery throughout the rest of membrane was not affected by the compound. This behavior is reminiscent of previous observations that the dynamics of N-WASP at sites of vaccinia virus adhesion to eukaryotic cells are decreased by LatB treatment. (Weisswange et al, 2009) However, recovery rates of Nck1 were unaffected by LatB treatment. This observation is interesting in that Nck1, the adaptor component in the protein network, may be highly dynamic regardless of changes to its surrounding environment. This feature of adaptor proteins has been demonstrated in a previous study with EBP50 (ERM-binding phosphoprotein of 50kD), PDZ contacting scaffolding proteins in microvillar biogenesis. (Garbett & Bretscher, 2012) Therefore, maintenance of dynamics of adaptor proteins may be a general mechanism for a cell to

induce fast cytoplasmic responses to membrane signals, such as the change of phosphorylation state of Δnephrin.

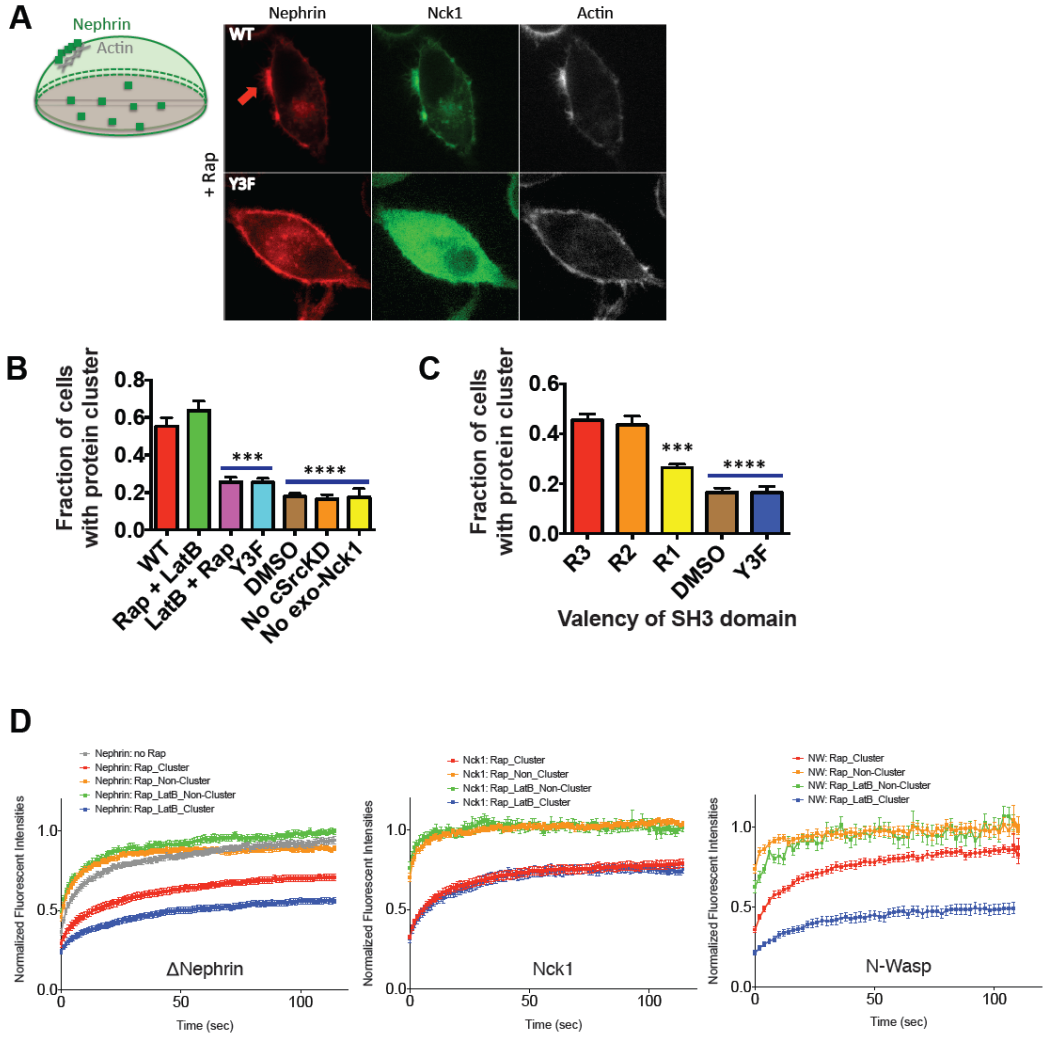

Figure 2-14. ΔNephrin forms clusters via interactions with Nck1 at the periphery of a cell. (A) Clustering of Δnephrin(WT) was observed at the cellular periphery 10 minutes after rapamycin treatment. ΔNephrin clusters were enriched with Nck1 and F-actin. (B, C) Error bars, s.e.m. (n=3, total more than 100 cells counted) (B) About 60% of cells with phospho-Δnephrin(WT) and Nck1 showed clusters, in contrast to the 20% of cells with nonphosphorylated mutant of Δnephrin (Y3F), no rapamycin treatment, no cSrc expression, or no exogenous Nck1 expression. LatB treatment before rapamycin also interfered with Δnephrin cluster formation at the cell periphery. (C) ΔNephrin clustering at cellular periphery favors higher SH3 valency of Nck1. (D) FRAP experiments demonstrated that dynamics of Δnephrin, Nck1, and N-WASP molecules within clusters were slower compared to those outside of clusters. LatB treatment after cluster formation slowed down the recovery

rate of Δnephrin and N-WASP, while did not affect Nck1 dynamics. Error bars, s.e.m. (n=3, total more than 25 cells counted for Δnephrin, total more than 15 cells counted for Nck1 and N-WASP)

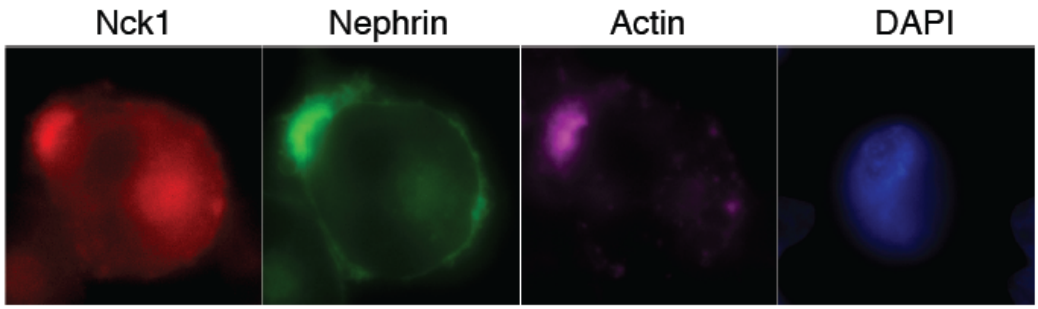

Figure 2-15. ΔNephrin clusters at the periphery of a cell are resistant to the actin depolymerization drug. ΔNephrin clusters enriched in Nck1 were resistant to LatB treatment for more than 30 minutes.

ΔNephrin					
	Rap _Cluster	Rap _Non-Cluster	Rap_LatB _Cluster	Rap_LatB _Non-Cluster	no Rap
Plateau	0.7310	0.8829	0.5780	1.023	0.9735
Half Life (Slow)	30.04	9.042	29.12	44.10	39.04
Half Life (Fast)	3.411	1.522	2.242	4.553	3.494
Tau (slow)	43.35	13.05	42.01	63.62	56.32
Tau (fast)	4.922	2.196	3.234	6.568	5.041

Nck1				
	Rap _Cluster	Rap _Non-Cluster	Rap_LatB _Cluster	Rap_LatB _Non-Cluster
Plateau	0.7875	1.043	0.7567	1.022
KFast	0.2099	0.3114	0.6472	0.7525
KSlow	0.03224	0.02963	0.04976	0.1106
Fast HalfLife	3.303	2.226	1.071	0.9212
Slow HalfLife	21.50	23.39	13.93	6.268

N-Wasp				
	Rap _Cluster	Rap _Non-Cluster	Rap_LatB _Cluster	Rap_LatB _Non-Cluster*
Plateau	0.8777	1.000	0.5088	0.9780
KFast	0.1621	0.4462	0.09386	0.07810
KSlow	0.02504	0.02702	0.02212	
Fast HalfLife	4.276	1.553	7.385	8.876
Slow HalfLife	27.68	25.65	31.34	

Table 2-3. Measurement from FRAP experiment

Discussion

Regulation of receptor signaling by multivalency-driven phase separation

I have demonstrated here that intracellular binding of nephrin to its adaptor Nck1 can induce protein clustering and actin polymerization at the plasma membrane. Comprehensive analysis of imaging experiments suggested that in vivo nephrin clustering is driven by a multivalent interaction phase transition, as cluster formation is dependent on protein concentration and valencies, while being independent of actin polymerization. These observations are consistent with previous observations made using *in vitro* model systems.

However, there are noteworthy differences between our in vivo and in vitro studies. First, the relative potency of SH3b(2), the recombinant Nck1 protein with two repetitive SH3 domains, is quite different when measured in cellular contexts than in *in vitro* contexts. In cells, the clustering ability of the SH3b(2) construct is comparable to SH3b(3) or natural Nck1, whereas *in vitro* experiments using model membranes require much higher concentration of SH3b(2) to induce phase separation. Notably, the clustering ability of SH3b(2) was reduced with the LatB treatment, suggesting a compensating role of actin polymerization activity in protein clustering. Additionally, phase separation occurs at a clearly measured critical concentration *in vitro*. However, our analysis using *in vivo* clustering showed a gradual increase in tendency to induce protein clustering as assessed by the fraction of cells showing clusters. It is likely that cells also behave in a switch-like manner, and the experimental data on the population of cells demonstrated a collective behavior of gradual increase of the protein clustering ability. Such differences could also be derived from the involvement of other proteins involved in the regulation of actin

polymerization. For example, WIP may compensate or even be necessary within cellular systems by adding more poly-Proline rich motifs, to increase valency of interacting partners, as well as interacting with Nck1 and N-WASP. (Cortesio et al, 2010; Padrick & Rosen, 2010) Also it would be interesting to test how the addition of different protein components would change the response pattern of multivalent proteins. Additional components may either induce the system to react in a more switch-like fashion or in a stochastic manner.

Our work on macroscopic spatial control of proteins can benefit not only studies that focus on signaling systems that locally regulate activity, such as actin polymerization or adhesion, but also benefit other receptor signaling systems in general. In the context of amplifying an extracellular signal into an intracellular signaling cascade, the change of overall activity could be made through phase transition as observed in H-Ras segregation into nanoclusters including PI3K activation. (Henis et al, 2009; Zhou et al, 2014)

Another implication of the study to general receptor biology comes from the observation on the movement of protein clusters at the TIRF focal plane. Movement of most receptors including A36R in vaccinia infection and cadherins were known to be mediated by actin polymerization often initiated by receptor signaling. (Weisswange et al, 2009) A36R, upon vaccinia attachment to the membrane, resulted in actin comet tails, which contain highly mobile protein complexes. The A36R and nephrin systems share components involved in actin polymerization such as Nck1 and N-WASP, whose dynamics are both dependent on the actin network. However, the mechanisms used to achieve such motility seem to be distinct. Actin comet generation is mediated by its own actin polymerization activity, which

can be blocked with actin inhibitors such as Latrunculin B. However, nephrin clusters are affected by both actin and myosin activity, but not by the activity of Arp2/3 complex.

The dynamics of the Δnephrin clusters across the plasma membrane may be comparable to those of T cell receptor clusters at the immunological synapses. We recently showed that the T cell receptor and its interacting components can be phase separated *in vitro* to form clusters on supported lipid bilayers. These clusters are also dynamic and dependent on valency as well as concentration (Su, et al., 2015, submitted). T cell receptor clusters moves across the T cell surface dependent on the underlying actomyosin network, leading to maturation of the interface between a T cell and an antigen presenting cell. (Groves & Kuriyan; Yi et al, 2012; Yu et al, 2013) Such observations suggest that cells may utilize two different mechanisms to move a receptor complex at the plasma membrane, one that requires actin polymerization activity, and the other mediated by rearrangements of the cortical actomyosin network.

Another interesting property of this mechanism is that it sustains molecule dynamics even within micron-sized clusters. These observed dynamics prompts us to consider phase separation as a reversible signaling system controlled by modulating the number of valences. For example, common post-translational modification mechanisms like phosphorylation of tyrosine residues may be used as a dial to tune the number of interacting motifs. In nephrin signaling, Fyn, the natural kinase targeting nephrin, may induce nephrin clustering similar to my experimental system, while PTP1B, the phosphatase of nephrin, disassemble the phase separated structures (Takano, 2011; Holzman, 2003). It is notable that excess amount of pTyr peptide in the system could reverse the phase separation of nephrin *in vitro* (Bajade, 2014).

Phase separated structures in cells may also be regulated through a two-way communication system with a positive feedback mechanism. My study demonstrated that nephrin phosphorylation by cSrc kinase could induce nephrin clustering at the plasma membrane. However, it has been reported that irreversible clustering of nephrin tails fused to CD16/7 extracellular/transmembrane domains with antibodies can function as an upstream signal to induce phosphorylation of nephrin, followed by rearrangements of the actin cytoskeleton in the cytoplasm (Blasutig et al, 2008; Rivera et al, 2004). Also previous study showed that the SH3 domains of Nck proteins enhanced the phosphorylation activity of Fyn, the natural kinase for Nephrin (New et al, 2013). Overall, these findings suggest that phase separation of phosphorylated nephrin can, in turn, increase the local phosphorylated nephrin concentration.

This indicates that the system does not behave as just a simple mixture of various proteins, rather this system creates a cellular compartment with a distinct function determined by its composition.

Implication in nephrin biology and next question

The study of kidney development has demonstrated that the phosphorylation level of nephrin is increased at the initial stages of foot processes formation, and also during slit diaphragm recovery after injury. (Faul et al, 2007; Li et al, 2013; Ruotsalainen et al, 1999; Welsh & Saleem, 2010). Interactions between nephrin and Nck are also reported to be crucial for normal nephron formation. However, it is still largely unknown how a common signaling process can result in the formation of the complicated structures seen in the slit diaphragm. Our study, along with the previously reported *in vitro* experiments, proposes that the appearance of actin-rich structures at microdomains condensed with nephrin may be the initial step for the creation of the interdigitated pattern of podocyte junctions. In addition, nephrin clustering may be utilized to induce the myoblast fusion activity (Chen & Olson, 2004; Sens et al, 2010; Shilagardi et al, 2013; Sohn et al, 2009). Recently, the Chen group at Johns Hopkins University reconstituted a cell fusion system in *Drosophila* cells using Sticks and stones (Sns), a nephrin homolog (Shilagardi et al, 2013). The cell fusion process involves many multivalent interactions between fusogenic proteins and cell-to-cell adhesion molecules, which may form a phase separated structure with potent actin polymerization activity (Chen & Olson, 2004).

Based on our observations, the next question is why biological systems have evolved to utilize multivalent proteins to form clusters through phase transitions. In other words, how does the local polymerization of proteins benefit the living organisms? A cell may utilize multivalent systems to either inhibit or amplify signals depending on the oligomerization process. For example, it has been shown that glutamine synthetase (Gln1) can be inactivated

through filament formation in yeast. (Petrovska et al, 2014) In contrast, liquid-like structures made by nephrin, Nck1, and N-WASP increase the efficiency of signal transduction by promoting high local concentrations of involved components with reduced energy consumption.

Nephrin clustering can potentially lead to two different pathways, depending on the involvement of other components after microdomain formation. Multiple studies propose the stabilization of nephrin dimerization *in trans* by podocin, another crucial protein in foot process formation (Saleem et al, 2002; Shono et al, 2009), while others suggested internalization of residual nephrin as a mechanism of quality control (Qin et al, 2009). Combined with the reports implying the role of cargo clustering in the process of endocytosis, the nephrin system may utilize the clustering mechanism to facilitate both the formation of junctions as well as the repression of protrusion at unwanted sites.

Methods and Materials

Constructs

All Nephrin-FRB, cSrcKD-FKBP were cloned into pcDNA vectors (Invitrogen). Nephrin-FRB construct is cloned by conjugation of Nephrin and FRB tethered by $[GGS]_3$ linker. cSrcKD-FKBP construct is cloned by conjugation of cSrcKD and FKBP tethered by $[GGS]_3$ linker. For imaging experiments, mCherry or mEGFP (EGFP with mutation: A206K) was cloned after FKBP or FRB. All Nephrin-FRB constructs contained Flag probe at the C-terminal end. All cSrcKD-FKBP constructs contained HA probe at the C-terminal end. Nck1 was cloned into pEGFP vector containing EGFP with A206K mutation (Clontech). Recombinant proteins were cloned with second SH3 domain (SH3b) of Nck1. Further information on cloned constructs is provided in Table 2-4.

Proteins	Sequence Information	Notes
Nephrin(WT)	MALGTTLRASLLLLGLLTE GLAQLAIPASM**EQKLISEE D**LNNGSGGSGTGSGGSPGL HQPSGEPEDQLPTEPPSGPS GLPLLPVLFALGGLLLLSNA SCVGGVLWQRRLRRLAEGI SEKTEAGSEEDRVRNEYEES QWTGERDTQSSTVSTTEAE PYYRSLRDFSPQLPPTQEEV SYSRGFTGEDEDMAFPGHL YDEVERTYPPSGAWGPLYD EVQMGPWDLHWPEDTYQD PRGIYDQVAGDL DTLEPDSLPFELRGHLV	Nephrin plasma membrane targeting signal peptide (residues 1-29) – **myc probe**– Linker(LNNGSGGS – KpnI – GSGGS) – Nephrin intracellular domain after Fibronectin type-III domain (residues 1036-1241)
Nephrin(Y3F)	MALGTTLRASLLLLGLLTE GLAQLAIPASMEQKLISEED LNNGSGGSGTGSGGSPGLH QPSGEPEDQLPTEPPSGPSG LPLLPVLFALGGLLLLSNAS	Mutations: Y1176F, Y1193F, Y1217F

	CVGGVLWQRRLRRLAEGIS EKTEAGSEEDRVRNEYEES QWTGERDTQSSTVSTTEAE PYYRSLRDFSPQLPPTQEEV SYSRGFTGEDEDMAFPGHL FDEVERTYPPSGAWGPLFD EVQMGPWDLHWPEDTYQD PRGIFDQVAGDLDTLEPDSL PFELRGHLV	
Nephrin(Y5F)	MALGTTLRASLLLLGLLTE GLAQLAIPASMEQKLISEED LNNGSGGSGTGSGGSPGLH QPSGEPEDQLPTEPPSGPSG LPLLPVLFALGGLLLLSNAS CVGGVLWQRRLRRLAEGIS EKTEAGSEEDRVRNEYEES QWTGERDTQSSTVSTTEAE PYYRSLRDFSPQLPPTQEEV SYSRGFTGEDEDMAFPGHL FDEVERTFPPSGAWGPLFDE VQMGPWDLHWPEDTFQDP	Mutations: Y1176F, Y1183F, Y1193F, Y1210F, Y1217F

	RGIFDQVAGDLDTLEPDSLP FELRGHLV	
Nck1	MAEEVVVVAKFDYVAQQE QELDIKKNERLWLLDDSKS WWRVRNSMNKTGFVPSNY VERKNSARKASIVKNLKDT LGIGKVKRKPSVPDSASPAD DSFVDPGERLYDLNMPAYV KFNYMAEREDELSLIKGTK VIVMEKCSDGWWRGSYNG QVGWFHSNYVTEEGDSPLG DNVGSLSEKLAAVVNNLNT GQVLHVVQALYPFSSSNDE ELNFEKGDVMDVIEKPEND PEWWKCRKINGMVGLVPK NYVTVMQNNPLTSGLEPSP QQCDYIRPSLTGKFAGNPW YYGKVTRHQAEMALNERG HEGDFLIRDSESSPNDFSVSL KAQGKNKHFKVQLKETVY CIGQRKFSTMEELVEHYKK	Full-length (residues 1-377)

	APIFTSEQGEKLYLVKHLS	
SH3b(3)	**MPAYVKFNYMAEREDELS LIKGTKVIVMEKSSDGWW RGSYNGQVGWFPSNYVTE EGDSPL**SARKASIVKNLKD TLGIGKVKRKPSVPDSASPA DDSFVDPGERLYDLN**MPAY VKFNYMAEREDELSLIKG TKVIVMEKSSDGWWRGS YNGQVGWFPSNYVTEEGD SPL**SARKASIVKNLKDTLGI GKVKRKP SVPDSASPADDSFVDPGERL YDLN**MPAYVKFNYMAER EDELSLIKGTKVIVMEKSS DGWWRGSYNGQVGWFPS NYVTEEGDSPL**NNPLTSGL EPSPPQSDYIRPSLTGKFAG NPWYYGKVTRHQAEMALN ERGHEGDFLIRDSESSPNDF SVSLKAQGKNKHFKVQLKE	N-terminal Nck1 domain (residues 1-251) was replaced by three repeated **SH3b (residues 109-168)** domains tethered by Linker domain between SH3a and SH3b (residues 61-108).

	TVYSIGQRKFSTMEELVEH YKKAPIFTSEQGEKLYLVK HLS	
SH3b(2)	**MPAYVKFNYMAEREDELS LIKGTKVIVMEKSSDGWW RGSYNGQVGWFPSNYVTE EGDSPL**SARKASIVKNLKD TLGIGKVKRKPSVPDSASPA DDSFVDPGERLYDLN**MPAY VKFNYMAEREDELSLIKG TKVIVMEKSSDGWWRGS YNGQVGWFPSNYVTEEGD SPL**NNPLTSGLEPSPPQSDYI RPSLTGKFAGNPWYYGKVT RHQAEMALNERGHEGDFLI RDSESSPNDFSVSLKAQGK NKHFKVQLKETVYSIGQRK FSTMEELVEHYKKAPIFTSE QGEKLYLVKHLS	N-terminal Nck1 domain (residues 1-251) was replaced by two repeated **SH3b (residues 109-168)** domains tethered by Linker domain between SH3a and SH3b (residues 61-108).
SH3b(1)	**MPAYVKFNYMAEREDELS LIKGTKVIVMEKSSDGWW**	N-terminal Nck1 domain (residues 1-251) was replaced

	RGSYNGQVGWFPSNYVTE **EGDSPL**NNPLTSGLEPSPPQ SDYIRPSLTGKFAGNPWYY GKVTRHQAEMALNERGHE GDFLIRDSESSPNDFSVSLK AQGKNKHFKVQLKETVYSI GQRKFSTMEELVEHYKKAP IFTSEQGEKLYLVKHLS	by **SH3b (residues 109-168)** domain.
cSrcKD	WEIPRESLRLEVKLGQGCFG EVWMGTWNGTTRVAIKTL KPGTMSPEAFLQEAQVMKK LRHEKLVQLYAVVSEEPIYI VTEYMSKGSLLDFLKGETG KYLRLPQLVDMAAQIASGM AYVERMNYVHRDLRAANI LVGENLVCKVADFGLARLI EDNEYTARQGAKFPIKWTA PEAALYGRFTIKSDVWSFGI LLTELTTKGRVPYPGMVNR EVLDQVERGYRMPCPPECP ESLHDLMCQCWRKEPEERP	Kinase domain (residues 263-522)

	TFEYLQAFLEDY	
FKBP	VQVETISPGDGRTFPKRGQT CVVHYTGMLEDGKKFDSSR DRNKPFKFMLGKQEVIRGW EEGVAQMSVGQRAKLTISP DYAYGATGHPGIIPPHATLV FDVELLKLEG	
FRB	ELIRVAILWHEMWHEGLEE ASRLYFGERNVKGMFEVLE PLHAMMERGPQTLKETSFN QAYGRDLMEAQEWCRKY MKSGNVKDLTQAWDLYYH VFRRISKQ	

Table 2-4. Information on protein expression constructs used in Chapter 2

Cell Culture and transfection

HeLa cells and HEK293T were cultured in Dulbecco's modified Eagle's medium (DMEM) containing 10% FBS and 1mM penicillin/streptomycin (Invitrogen) and 1mM GlutaMAX (Invitrogen). Cells were transfected using Effectene (QIAGEN) and incubated for 27h at 37°C.

Co-immunoprecipitation

HeLa cells and HEK293T cells were plated on 6-well plates (#BRAND) and transfected for 27h at 37°C. Cells were harvested with 1mM EDTA in PBS by scraping and cell lysates were prepared in lysis buffer (50mM Tris, pH8.0, 150mM NaCl, 1% TritonX-100, 1mM PMSF, 1mM benzamidine, 1μg/ml leupeptin, 1μg/ml antipain, 10mM NaF, 1M beta glycerophosphate, 0.2M Na_3VO_4 and 0.5mM Okadaic acid) for 30min at 4°C. The cleared lysate was incubated and immunoprecipitated with anti-Flag M2 affinity gel (Sigma) for 2h at 4°C. Immune complexes were eluted with 0.5mg/mL of Flag peptide in lysis buffer and western blotted with the antibodies against phosphor-tyrosine (4G10), Nck1/2, Flag probe (Nephrin), HA probe (cSrc).

TIRF microscopy imaging and data analysis

HeLa cells were plated on glass-bottom 35mm dishes (MatTek), which were coated with 0.1% L-lysine (Sigma) for 30min at RT. Before imaging, cells were starved for 7h with DMEM with no FBS, and then treated with 1mg/mL methyl-beta-cyclodextrin (Sigma) for 30m. Rapamycin (Toronto Research) was used with 1μM concentration, and Latrunculin B

(Sigma) was used with 5μM concentration. For cluster motility assay, blebbistatin (Toronto research chemical), Arp2/3 complex inhibitors CK666 and CK869 were used up to 50μM for 30min. After drug treatment, cells were fixed with 4% paraformaldehyde (Sigma) for 20min at RT followed by mounting in PBS.

For immunofluorescence staining experiment, transfected and then fixed cells were permeablized with 0.1% Saponin in PBS for 5 min. The antibodies used for staining were anti-clathrin heavy chain (provided by D.Billadeau and T.Gomez), anti-caveolin-1, and anti-paxillin antibodies. Secondary antibodies conjugated with Alexa Fluor 647 (Invitrogen) were used.

Nikon Eclipse Ti microscope equipped with an Andor iXon Ultra 897 EM-CCD camera was used to collect images with a 100 X objective in TIRF-fluorescence mode. Images were corrected for background and uneven illumination as described previously. (REF) Cells were detected by thresholding an image with Otsu method in ImageJ. Images were further thresholded by applying Otsu algorithm two or three times to select clustered area on the membrane. For each experimental condition, at least 450 cells from three independent procedures were analyzed to measure intensities of whole cell area or of clustered area. Macro was used in ImageJ to automate the imaging analysis process. (Table 2-5)

Measured intensities were used to fit the probability that a cell produced clusters on the plasma membrane with logistic regression method on MatLab. Individual samples were checked for their suitability to the logistic regression method. To evaluate whether two samples were significantly different each other, data from two samples were combined to one

data, which is fitted as one or two population distributions to calculate a p-value. Detailed calculations were demonstrated in Table 2-6.

```
numStr="File number";

fileStr="Image name_"+numStr+"_MMStack.ome.tif"

// Open images


imageCalculator("Subtract create 32-bit", ""+fileStr+":1","Background Standard Image for Nephrin");

// Background subtraction of Nephrin images

imageCalculator("Divide create 32-bit", "Result of "+fileStr+":1","Normalization standard Image for Nephrin");

// TIRF normalization of Nephrin images

imageCalculator("Subtract create 32-bit", ""+fileStr+":2","Background Standard Image for Nck1");

// Background subtraction of Nck1 images

imageCalculator("Divide create 32-bit", "Normalization standard Image for  Nck1");

// TIRF normalization of Nck1 images


selectWindow("Result of "+fileStr+":1");

close();

selectWindow("Result of "+fileStr+":2");

close();

selectWindow(""+fileStr+":2");

close();

imageCalculator("Divide create 32-bit", "Result of Result of "+fileStr+":2","Result of Result of "+fileStr+":1");

// Calculate the ratio image between Nephrin and Nck1


selectWindow("Result of Result of "+fileStr+":2");

close();

roiManager("Delete");
```

```
roiManager("Show All");
selectWindow("Result of Result of "+fileStr+":1");
waitForUser("Cell Selection","Select a cell in the "+fileStr+"");
// Selet a region of interest containing a single cell


selectWindow("Result of Result of Result of "+fileStr+":2");
run("Restore Selection");
run("Crop");
selectWindow("Result of Result of "+fileStr+":1");
run("Crop");
setAutoThreshold("Otsu dark");
run("Create Selection");
// Select a cell by detecting boundary


roiManager("Add");
waitForUser("Cluster Selection","Otsu Applied to the image: #1");
roiManager("Delete");
setAutoThreshold("Otsu dark");
run("Create Selection");
roiManager("Add");
waitForUser("Cluster Selection","Otsu Applied to the image: #2");
roiManager("Delete");
setAutoThreshold("Otsu dark");
run("Create Selection");
roiManager("Add");
waitForUser("Cluster Selection","Otsu Applied to the image: #3");
```

```
selectWindow("Result of Result of Result of "+fileStr+":2");

roiManager("Combine");

// Select clustered area in a cell – this procedure was repeated when the appropriate clustered regions was not selected



run("Measure");

// Measure intensities on a whole cell area and clustered regions



selectWindow("Result of Result of "+fileStr+":1");

roiManager("Delete");

setAutoThreshold("Otsu dark");

run("Create Selection");

roiManager("Add");

waitForUser("Cluster Selection","Otsu Applied to the image: #4");

selectWindow("Result of Result of Result of "+fileStr+":2");

roiManager("Combine");

run("Measure");

// Procedure of selection of clustered area and measurement of intensities was repeated until an appropriate clustered region was used for analysis.
```

Table 2-5. Macro used to measure intensities

Load data from excel files of each experimental set

```
clear all; % clear all variables in workspace

clc; % clear command window

close all hidden; % close all opened & hidden figure windows


% input data folder

folderName = uigetdir('/folder name/');


% create a cell array of file names (demonstrated with examples sets, files with '_C' were data from cells with clusters, files with '_NC' were data from cells without clusters)

expNames = {'R3_C','R3_NC','R2_C','R2_NC','R1_C','R1_NC','Y3F_C','Y3F_NC'};


% create a empty object map

dataMap = containers.Map();


% iterate i from 1 to the length of expName

for i=1:length(expNames)

    % get an experiment name of index i

    expName = expNames{i};


    % get a file path to read

    fileName = sprintf('%s/%s.xls',folderName,expName);


    % load data
```

```
    data = dataset('XLSFile',fileName);


    % insert data into map `dataMap` with a name (expName)
    dataMap(expName)=data;
end


% Now I can get experiment data for the experiment name 'R3_C' by
% calling dataMap('R3_C')



%   Logistic Regression as two population distribution (two samples)
%   Logistic Regression as one population distribution (two samples)
proc1(dataMap)
%   Logistic Regression as one population distribution (one sample)
proc2null(dataMap)
```

Logistic regression analysis on two samples (proc1.m)

```
function p = proc1(dataMap)


% Process
%   Logistic Regression as two population distribution (two samples)
%   Logistic Regression as one population distribution (two samples)
fprintf('## Logistic Regression as two population distribution (two samples)\n');
```

```
fprintf('## Logistic Regression as one population distribution (two samples)\n');



processNames = {{'R3','R2'},{'R3','R1'},{'R3','Y3F'},{'R2','R1'},{'R2','Y3F'},{'R1','Y3F'}};


fieldNames = {'Nck_Mean','Nephrin_Mean'};



for fi=1:length(fieldNames)


 FieldName = fieldNames{fi};


 for i=1:length(processNames)


   A=processNames{i}{1};

   B=processNames{i}{2};


   fprintf(['# Processing ' A '-' B '(' FieldName ')\n']);


    % dataMap('R3_C').Nck_Mean' ==> postfix ' transposes matrix.
    % ex> 100x1 ==> 1x100 vector

    A_C=getfield(dataMap([A '_C']),FieldName)';

    % = dataMap([A '_C']).Nck_Mean';

    A_NC=getfield(dataMap([A '_NC']),FieldName)';

    % = dataMap([A '_NC']).Nck_Mean';

    B_C=getfield(dataMap([B '_C']),FieldName)';
```

```
% = dataMap([B '_C']).Nck_Mean';

B_NC=getfield(dataMap([B '_NC']),FieldName)';

% = dataMap([B '_NC']).Nck_Mean';


% [V1 V2 V3] ==> vector concatenation

intensity= [A_C A_NC B_C B_NC];


% ones(A,B)  get a A x B matrix with ones.

% zeros(A,B)  get a A x B matrix with zeros.

% sample indicator (0: first sample 1: second sample)

sampleIndicator = [ zeros(1,length(A_C)) zeros(1,length(A_NC)) ones(1,length(B_C)) ones(1,length(B_NC))];


% response vector (0: non-cluster 1: cluster)

response = [ ones(1,length(A_C)) zeros(1,length(A_NC)) ones(1,length(B_C)) zeros(1,length(B_NC))];



fprintf('\tLogistic Regression as two population distribution (two samples)\n');


beta = [0 0 -0.0001 0.0001];


% http://www.mathworks.co.kr/kr/help/matlab/ref/optimset.html

options = optimset();


% http://www.mathworks.co.kr/kr/help/matlab/ref/fminsearch.html

[beta,fval] = fminsearch(@loglike_tp_ts,beta, options, intensity, sampleIndicator, response);
```

```
fprintf('\t\tBeta = %e %e %e %e\n',beta(1),beta(2),beta(3),beta(4));

probFunc = @(beta0,beta1,beta2,beta3,intensity,sampleIndicator) 1./(1+exp(-beta0 - beta1.*sampleIndicator - beta2.*intensity - beta3.*intensity.*sampleIndicator));

probValue = probFunc(beta(1),beta(2),beta(3),beta(4),intensity,sampleIndicator);



% calculate the likelihood value as two population distribution

fprintf('\t\tLikelihood value = %f\n', -loglike_tp_ts(beta,intensity, sampleIndicator, response));


% loglike_tp_ts function (Probability function for two population fitting) is shown below

lnLTwo=-loglike_tp_ts(beta,intensity, sampleIndicator, response);




fprintf('\tLogistic Regression as one population distribution (two samples)\n');


beta = zeros(1,2);

% http://www.mathworks.co.kr/kr/help/matlab/ref/optimset.html

options = optimset();

% http://www.mathworks.co.kr/kr/help/matlab/ref/fminsearch.html

[beta,fval] = fminsearch(@loglike_op,beta, options, intensity, response);

fprintf('\t\tBeta = %e %e \n',beta(1),beta(2));
```

```
    probFunc = @(beta0,beta1,intensity) 1./(1+exp(-beta0 - beta1.*intensity));
    probValue = probFunc(beta(1),beta(2),intensity);



    % calculate the likelihood value as one population distribution
    fprintf('\t\tLikelihood value = %f\n', -loglike_op(beta,intensity,response));
    % loglike_op function (Probability function for one population fitting) is shown below
        lnLOne=-loglike_op(beta,intensity,response);



    % calculate the p-value from two likelihood values
    LR = 2*abs(lnLTwo - lnLOne);
    fprintf('\tLR = %e\n', LR);


    % http://www.mathworks.co.kr/kr/help/stats/chi2cdf.html
    % https://www.mathworks.com/matlabcentral/newsreader/view_thread/103019
    Chi = 1-chi2cdf(LR,2);
    fprintf('\tChi = %e\n', Chi);
  end
end
```

Logistic regression analysis on one samples with generation of graphs for Nephrin and Nck1 (proc2null.m)

```
function p = proc2(dataMap)

% Process
% Logistic Regression as one population distribution (one sample)
fprintf('## Logistic Regression as one population distribution (one sample)\n');

processNames = {'R3','R2','R1','Y3F'};
scatterOptions = {'rx','gx','bx','yx'};
plotOptions = {'r','g','b','y'};


fieldNames = {'Nck_Mean','Nephrin_Mean'};


for fi=1:length(fieldNames)

   FieldName = fieldNames{fi};


   % plotting the graph for each data set
   figure('name',[FieldName ':Logistic Regression as one population distribution (one samples)']);


   for i=1:length(processNames)
```

```
A=processNames{i};
ScatterOption = scatterOptions{i};
PlotOption = plotOptions{i};



fprintf(['# Processing ' A '(' FieldName ')\n']);


   A_C=getfield(dataMap([A '_C']),FieldName)';
   A_NC=getfield(dataMap([A '_NC']),FieldName)';


   intensity= [A_C A_NC];


   response = [ ones(1,length(A_C)) zeros(1,length(A_NC))];


  fprintf('\tLogistic Regression as one population distribution (one samples)\n');



      beta = zeros(1,2);
      options = optimset();
      [beta,fval] = fminsearch(@loglike_op,beta, options, intensity, response);
      fprintf('\t\tBeta = %e %e \n',beta(1),beta(2));


      probFunc = @(beta0,beta1,intensity) 1./(1+exp(-beta0 - beta1.*intensity));
      probValue = probFunc(beta(1),beta(2),intensity);
```

```
intensity_A= [A_C A_NC];
response_A = [ones(1,length(A_C)) zeros(1,length(A_NC))];

% the range of the plot can be changed here
fplot(@(x) probFunc(beta(1),beta(2),x),[0,10000],PlotOption);
hold on;

% print the scatter graph of raw data
scatter(intensity_A,response_A,10,[0 1 0],ScatterOption);
hold on;



% print
fprintf('\t\tLikelihood value = %f\n', -loglike_op(beta,intensity,response));

lnLOne=-loglike_op(beta,intensity,response);

fprintf('\tLogistic Regression as one population distribution without intensity (one samples)\n');

beta = zeros(1,1);
options = optimset();
[beta,fval] = fminsearch(@loglike_op_null,beta, options, intensity, response);
fprintf('\t\tBeta = %e \n',beta(1));

probFunc = @(beta0,intensity) 1./(1+exp(-beta0));
```

```
            probValue = probFunc(beta(1),intensity);


            fprintf('\t\tLikelihood value = %f\n', -loglike_op_null(beta,intensity,response));


            % loglike_op_null function (Probability function to test suitability of datasets for logistic regression analysis) is shown below
        lnLTwo=-loglike_op_null(beta,intensity,response);




        LR = 2*abs(lnLTwo - lnLOne);
        fprintf('\tLR = %e\n', LR);


        % http://www.mathworks.co.kr/kr/help/stats/chi2cdf.html
        % https://www.mathworks.com/matlabcentral/newsreader/view_thread/103019
        Chi = 1-chi2cdf(LR,1);
        fprintf('\tChi = %e\n', Chi);


   end
   legend(processNames{1},'',processNames{2},'',processNames{3},'',processNames{4},'');
end
```

Probability function for one population fitting of two samples (loglike_op.m)

```
function f = loglike_op(beta,intensity, response)
beta0=beta(1);
```

```
beta1=beta(2);


PROB = 1./(1+exp(-beta0 - beta1.*intensity));
% prevent 0 or 1 for technical reasons
PROB=min(PROB,0.99999999999999999999999999999);
PROB=max(PROB,0.00000000000000000000000000001);


lik = response .* log(PROB) + (1-response) .* log(1-PROB);
f=-sum(lik);
```

Probability function for two population fitting of two samples (loglike_tp_ts.m)

```
function f = loglike_tp_ts(beta,intensity, sampleIndicator, response)
beta0=beta(1);
beta1=beta(2);
beta2=beta(3);
beta3=beta(4);


PROB = 1./(1+exp(-beta0 - beta1.*sampleIndicator - beta2.*intensity - beta3.*intensity.*sampleIndicator));
% prevent 0 or 1 for technical reasons
PROB=min(PROB,0.99999999999999999999999999999);
PROB=max(PROB,0.00000000000000000000000000001);


lik = response .* log(PROB) + (1-response) .* log(1-PROB);
f=-sum(lik);
```

Probability function to test suitability of datasets for logistic regression analysis (loglike_op_null.m)

```
function f = loglike_op_null(beta,intensity, response)

beta0=beta(1);


PROB = 1./(1+exp(-beta0));

% prevent 0 or 1 for technical reasons

PROB=min(PROB,0.99999999999999999999999999999);

PROB=max(PROB,0.00000000000000000000000000001);


lik = response .* log(PROB) + (1-response) .* log(1-PROB);

f=-sum(lik);
```

Table 2-6. Logistic Regression

STORM microscopy

Cells were transfected with Nephrin-FRB conjugated with mEOS2 photo-switchable proteins along with cSrcKD-FKBP and Nck1 proteins. (The Luby-Phelps group generously provided mEOS2 protein construct.) STORM images were acquired and processed with Localization Microscopy plugin of Micromanager, which utilize the Nikon Eclipse Ti microscope equipped with an Andor iXon Ultra 897 EM-CCD camera and a 100 X objective in TIRF-fluorescence mode. More than 200,000 images were used to generate a STORM image followed by corrected for X-Y drifting and rendered by 4X.

Homo-FRET experiment

Nephrin-FRB fused with mEYFP was used to collect anisotropy data with Nikon Eclipse Ti microscope equipped with two Andor iXon Ultra 897 EM-CCD cameras and a 100 X objective in TIRF-fluorescence mode. Acquired images were analyzed with MatLab as described previously. (Goswami et al, 2008)

Confocal microscope imaging

Cell images were acquired with Perkin Elmer Spinning Disk Ultraview ERS equipped with Hamamatsu C9100-50 EMCCD to analyze Nephrin clustering at the periphery of a cell. F-actin was stained by phalloidin conjugated with Alexa 647 (Invitrogen).

Fluorescence Recovery After Photobleaching (FRAP) experiment

Cells were collected with Zeiss LSM510 confocal microscope with 100X objective. Two squares of 20 by 20 pixels on clustered area and unclustered area were sequentially bleached with scanning laser and imaged up to 5 min afterwards. (Dundr & Misteli, 2003; McNally, 2008)

Chapter 3

Concluding Remarks I

Through the work described in the previous chapter, I propose that microdomains condensed with nephrin can be generated at the plasma membrane of eukaryotic cells when multivalent interaction with Nck1 and N-WASP was induced. Importantly, clusters of membrane-bound nephrin, even in a cellular environment crowded with molecules, are consistent with multivalent interaction driven phase separated polymers previously observed in solution and on model membranes. The formation of nephrin clusters is dependent on both concentration and valences of nephrin and Nck1, but independent of actin polymerization. Also all components are dynamic even when they are recruited into clusters. Finally, nephrin clusters result in the formation of actin rich structures, unless a dominant negatively active form of N-WASP is used to prevent actin polymerization. Overall, our study demonstrates that a unique microdomain structure at two-dimensional cellular surfaces can be generated solely by multivalent interactions between receptors and its cytoplasmic effectors.

Despite the multivalency mediated phase separation has been shown all in three-dimensional solution and cytoplasm as well on supported lipid bilayer and at the plasma membrane, there are still questions remaining to be answered. For example, it is not yet clear whether how well these phase separated structures reflect natural nephrin clusters observed during kidney development. Intrinsic difficulty to study nephrin punctate structures *in vivo* comes from the limited availability of immortal podocyte cell lines. Also there is no known

protocol so far to reconstitute foot processes from cell culture system. In addition, nephrin protein used in my study lacks extracellular domain, which also contributes to its clustering by *trans*-association between neighboring cells. Another contributing factor for nephrin clusters *in vivo* is the association of cholesterol to the transmembrane region of nephrin. Below are three interesting observations that I made with nephrin system at the plasma membrane, which suggest cooperativity between lipid and multivalency mediated nephrin clustering.

1. Without the treatment of cyclodextrin, a cholesterol depletion drug, endocytosis of nephrin occurred almost immediately after phosphorylation. Raft mediated endocytosis of nephrin was reported previously, suggesting its regulatory role in quality control.
2. Small fraction of cells showed nephrin clusters not bound to Nck1, which indicates its ability to cluster by its own.
3. Membrane staining with Nile red showed that micron-sized nephrin clusters are also enriched with lipid. Previous study demonstrated that protein crowding resulted in membrane bending, which may be a possible mechanism behind my observation.

Further study with purified, full-length nephrin protein combined with GUV system will address the contribution of lipid to the nephrin clustering. Recently developed technology will enable us to prepare nephrin embedded GUV system with the intracellular domain oriented in the vesicles. (Coyne et al, 2014)

Multivalency occurs in numerous pathways in both cytoplasm and plasma membrane, conserved along different species. However, its contribution to the biological consequences beyond the avidity effect upon interacting with other proteins is still lacking. Along with the posttranslational modification, multivalency mediated polymerization of proteins can be a generally applied mechanism for cell signaling.

Chapter 4

Introduction II

Numerous experimental methods have been developed to investigate the role of individual proteins in signaling processes. Visualization of fluorescently-tagged proteins using light microscopy is a powerful tool to investigate a single cell in real time (Shaner et al, 2005). There are very few methods used in cell biology to properly study protein dynamics. For example, genetic techniques, including transient expression or suppression of a specific protein of interest, only generate effects after hours of treatment. Cell-permeable small molecules enable faster stimulation of signal transduction but often have non-specific targets and toxicity. Therefore, development of tools that can be used to modulate a protein's activity with spatiotemporal control are necessary to properly study dynamic processes such as rearrangement of the actin cytoskeleton.

Optogenetic tools

Recently light was recognized as an ideal tool to regulate localization and function of proteins with greater temporal and spatial control. In some early attempts to utilize light in biological systems, phytochromes, a family of sensory photoreceptors, were used to induce gene expression or protein splicing in yeasts (Shimizu-Sato et al, 2002). Phytochromes from *Arabidopsis thaliana* were also used in a mammalian system to localize activators of Rho-family GTPases at the plasma membrane to induce actin-dependent cell protrusion (Levskaya et al, 2009). The mechanism behind a phytochrome system will be further discussed in the next section.

Neurobiology benefits from engineered opsins that can depolarize or hyperpolarize the membrane in neurons when exposed to light (Rana & Dolmetsch, 2010). For example, an algal protein, chanelrhodopsin-2 (ChR2) was adopted to induce various spike firing patterns on a milli-second-timescale. NpHR, an archaeal light-driven chloride pump from *Natronomonas pharaonis*, has opposing effect from ChR2 by optically inhibiting neural activity (Zhang et al, 2007). Since NpHR and ChR2 respond to separate wavelengths, they could be used together to control muscles and motor neurons in *C. elegans* (Zhang et al, 2007). For studies of a complex mammalian system, a pair of opsin-receptor chimaeras (the optoXR family) was developed for opposing effects on spike firing in neurons, which resulted in spatial preference in living mice. (Airan et al, 2009)

Multiple photoreceptors that respond to blue light were also investigated as tools to optogenetically manipulate other biological systems. For example, light-mediated interactions between *Arabidopsis* cryptochrome 2 (CRY2) and CIB1 was used to induce

DNA transcription and recombination (Konermann et al, 2013). The CRY2-CIB1 system can operate with endogenous chromophore, flavin and pterin, and does not require any exogenous cofactors. A previous study also demonstrated that CIB1, when anchored at the plasma membrane through CAAX box motif, could recruit CRY2 on a subsecond time scale (Kennedy et al, 2010).

Melanopsin, a member of the opsin subfamily of G protein, was used in combination with calcineurin and nuclear factor of activated T cells (NFAT) to activate transgene expression (Ye et al, 2011). The melanopsin system adopts proteins that are specifically expressed in intrinsically photosensitive retinal ganglion cells (ipRGCs) (Hankins et al, 2008). Relatively long-exposure and high-irradiant blue light is required to activate melanopsin to increase the intracellular calcium level. Elevated calcium level in cells, in turn, activates calcineurin to phosphorylate and relocalize NFATs to the nucleus (Ye et al, 2011).

Lastly, a light oxygen voltage 2 (LOV2) domain from *Avena sativa* phototropin was used for activation of small GTPases, Rac1 and Cdc42 (Hahn & Kuhlman, 2010). LOV domain was from phototropins, a blue light-activated serine/threonine kinase in plants and algae. LOV domain requires a flavin chromophore (either FMN or FAD), which covalently associates with a cysteine residue of LOV upon illumination, undocking and unfolding the C-terminal Jα helix (Yao et al, 2008). Cease of illumination reverts LOV domain to the dark state with folded Jα helix on a time scale of hours. Expressed LOV-photoactivatable Rac (PA-Rac1) was developed to investigate Rac-induced protrusion of lamellipodia. (Hahn & Kuhlman, 2010; Wu et al, 2009) Further optimizations of LOV-based optogenetic systems

were made through stabilization of LOV-Jα docking in the dark state, which led to an increased dynamic range of activity. (Strickland et al, 2010; Yao et al, 2008)

Arabidopsis LOV domain protein FKF1 and GIGANTEA (GI) proteins were introduced as the blue light-activated heterodimerization (LAD) system (Yazawa et al, 2009). The LAD system had a wide range of application, from recruiting Rac1 to the membrane to modulating gene expression in cells. However, LOV domain-mediated LAD system showed slow kinetics, taking more than ten minutes for activation and hours for reversion (Yazawa et al, 2009).

Dronpa dimerizes or tetramerizes in a light dependent manner to control the activity of Cdc42 or protease (Ando et al, 2004; Zhou et al, 2012). Dronpa mediated optogenetics have three advantages over other systems. First, Dronpa uses cyan light (~500nm), which contains less energy than toxic blue light. Second, Dronpa does not require any exogenous or endogenous cofactors, which may alter the efficiency of the system. Third, oligomerization of Dronpa switches on the fluorescence of Dronpa, which allows live imaging without the use of an additional fluorescence protein. (Zhou et al, 2012)

Although all these methods opened new avenues in studying cellular dynamics, they are used to investigate a limited number of molecules with a limited number of cellular outputs. Here I present a general approach for designing optogenetic tools with either intra-molecular or inter-molecular control that can be used to study a wide range of biological problems.

Light mediated interactions between PhyB and Pif3

Phytochromes (PhyA to PhyE in *Arabidopsis thaliana*) are responsible for growth and development of plants and bacteria in response to light. (Rockwell et al, 2006; Schepens et al, 2004; Sharrock, 2008) Phytochromes use a covalently-attached tetrapyrrole chromophore, phycocyanobilin (PCB), to interconvert between two states: red light absorbing (Pr) and far-red light absorbing (Pfr) states. Without light, Pr is predominant. Pr can be converted to Pfr by red light (650nm) illumination. Phytochromes in the Pfr state transmit signals by binding to phytochrome interacting factor 3 (Pif3). (Khanna et al, 2004; Ni et al, 1998; Ni et al, 1999) Phytochrome in the Pfr state can revert to the Pr state in less than one second by far-red (730nm) illumination. This same transition occurs slowly by thermal energy over a course of a few hours (Schepens et al, 2004). The wavelengths of lights used to induce phytochrome transitions between active and inactive states (650nm and 730nm) makes phytochromes particularly useful to achieve light-mediated control among naturally developed photoregulatory systems. They are separated from the excitation spectrum of commonly used fluorescence protein such as GFP (488nm) or RFP (568nm) allowing visualization of molecules without disturbing the optogenetic system (Rockwell et al, 2006). Also the red and far-red wavelengths can penetrate deeper into the tissue compared to the blue-light, which makes phytochromes suitable for *in vivo* study.

Previous studies suggest that PhyB and Pif3 may be engineered into a useful light-mediated heterodimerization tool. PhyB interacts with Pif3 with K_D=100μM in vitro, which is relatively affinity compared to other Pif proteins. (Khanna et al, 2004) Using PhyB and Pif3, gene expression was regulated in yeast. (Shimizu-Sato et al, 2002) Pif6, another

phytochrome interacting factor, was used to recruit upstream activators of Rho-GTPases to the plasma membrane inducing a protrusion at the regions of interest. (Levskaya et al, 2009)

SopE Biology

SopE is a potent guanine nucleotide exchange factors (GEF) protein that targets Rho GTPases and functions in the bacterial type III secretory system of *Salmonella typhimurium* (Patel & Galan, 2005; Zhou & Galan, 2001). During invasion of bacteria into mammalian cells, SopE induces local changes in the actin cytoskeleton that induces ruffles on the plasma membrane by activating the host-cell Rho GTPases, Cdc42 and Rac1 (Erickson & Cerione, 2004). The activated Cdc42, together with phosphatidylinositol 4,5-biophosphate (PIP2) binds to the family of Wiskott-Aldrich syndrome proteins (WASp), releasing its C-terminal VCA region for Arp2/3 activation (Padrick & Rosen, 2010). Cdc42 mediated WASp activation is further described in the next section. Rac1 induces Scar/WAVE complex mediated Arp2/3 activation (Takenawa & Suetsugu, 2007). In addition to rapid cellular morphological changes upon SopE light-induced activation, the structure of SopE is also known, making it an ideal protein for testing our newly proposed optogenetic technique. (Buchwald et al, 2002)

Cdc42 and WASp

Cdc42 is a Rho family GTPase that binds to the GTPase binding domain (GBD) of WASp. GTP-Cdc42 readily binds WASp while GDP-Cdc42 is inactive and binds WASp with a much lower affinity (Padrick & Rosen, 2010). Upon binding to Cdc42, WASp releases from its autoinhibited state to expose its C-terminal VCA (for Verprolin homology, Central hydrophobic and Acidic domain) domain to recruit Arp2/3 complex and induce actin nucleation and polymerization. (Goley & Welch, 2006; Padrick & Rosen, 2010; Pollard, 2007) WASp activation is further described in Chapter 2. Cdc42 and WASp were chosen as binding partners to test our proposed optogenetic tool to regulate intra-molecular interactions using red or far-red illumination in cells, based on our previous work testing their optogenetic control *in vitro*. (Leung et al, 2008)

Chapter 5:

Development of a generally applicable optogenetic tool

The result and discussion sections were adapted from the paper.

Result

Light-mediated interactions between PhyB and Pif3 in mammalian cells

I first validated light-mediated interaction between PhyB and Pif3 in mammalian cells by engineering a nucleus-targeted PhyB and observed the Pif3 localization pattern upon red or far-red light illumination. (Fig 5-1A) I fused an N-terminal fragment of holo-PhyB, which is the minimal region for Pif3 interaction upon light illumination (residues 1-651 covalently attached to PCB; PhyB hereafter), with a C-terminal nucleus localization sequences (NLS) from vaccinia virus. (Yoneda, 1997) The N-terminal binding domain of Pif3 (residues 1-100; Pif3 hereafter) was also used for our experiments. (Khanna et al, 2004)

HeLa cells were transiently transfected with PhyB and Pif3. PhyB localized exclusively in the nucleus, while $Pif3_N$ localized in both the nucleus and in the cytoplasm. As shown previously, PCB chromophore treatment in the media was enough to make PhyB responding to the light. (Levskaya et al, 2005; Shimizu-Sato et al, 2002) (Data not shown) This step did not disrupt the localization pattern of PhyB or Pif3 after dark adaptation or upon continuous far-red illumination. (Fig 5-2A) Upon red light illumination, Pif3 co-localized with PhyB in the nucleus within 15 minutes. As predicted, Pif3 localization returned to the pre-illumination state when the cells were exposed to far-red light. (Fig 5-1B)

When PCB chromophore was not supplied in the media or when the fluorescence protein without Pif3 domain was used, Pif3 did not alter its localization pattern. (Fig 5-1C, Fig 5-2B)

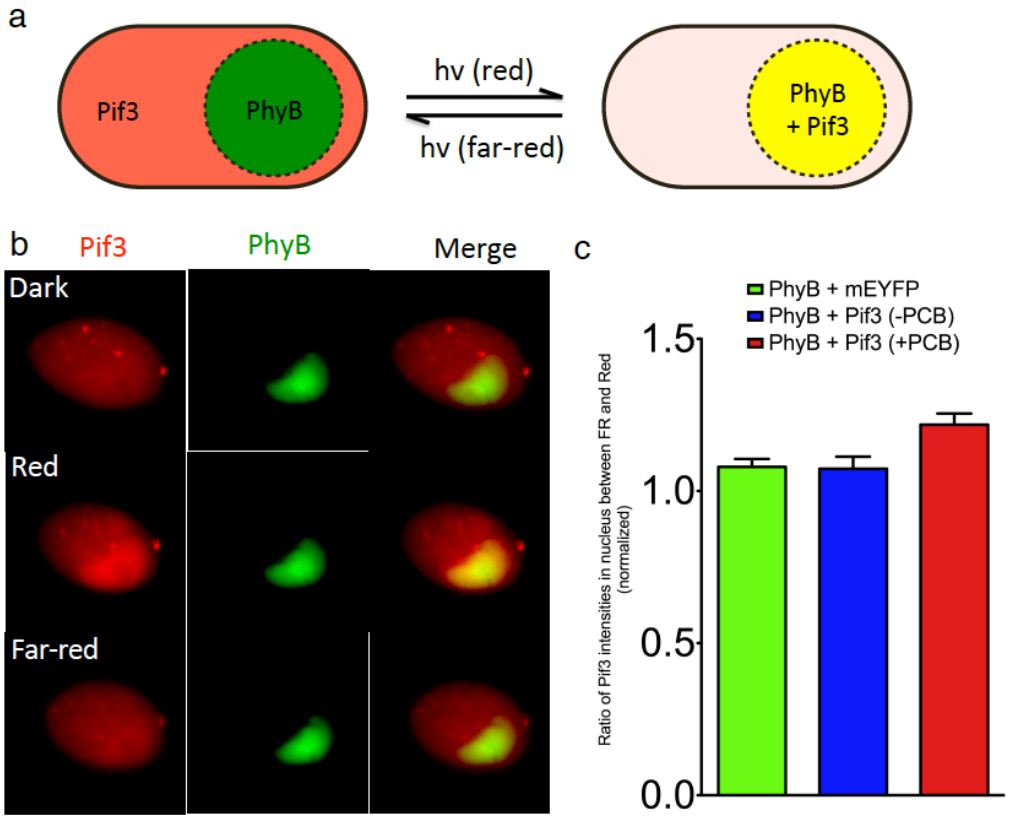

Figure 5-1. PhyB recruits Pif3 under the red light illumination in HeLa cells. (A) Binding between PhyB and Pif3 in cells can be verified by measuring the localization change of Pif3. Under the condition that PhyB is tagged with the nucleus localization signal, Pif3 would accumulate in the nucleus under the red light. This effect would be reverted under the far-red illumination. (B) Pif3 showed diffusive pattern under dark state, while PhyB exclusively resided in the nucleus. (first panel) After 15min of the red light (650nm) stimulation, the nucleus localization became dominant for Pif3. (middle panel) As the spectrum of light changed to far-red (730nm) region, Pif3 released back to the cytoplasm within 15min. (bottom panel) (C) Ratio of the Pif3 intensities between the red and the far-red condition has been measured in live cells. Only under the condition that the cell expressed both PhyB and Pif3 and was supplied with PCB, Pif3 recruitment into the nucleus was observed. Error bars, s.d. (n=2, total more than 20 cells.)

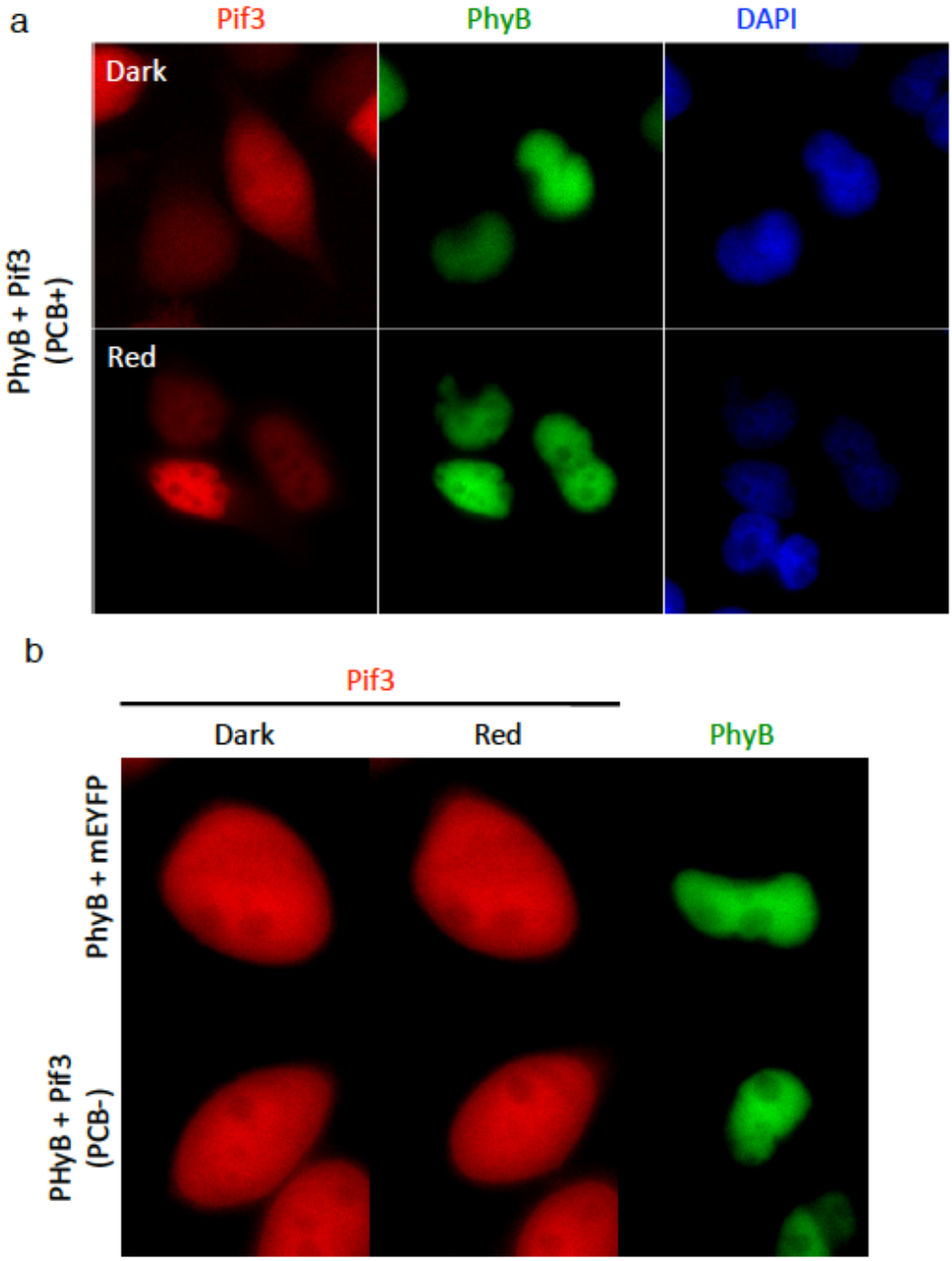

Figure 5-2. PhyB recruits Pif3 into the nucleus. (A) Pif3 localization change upon the red light was confirmed with the fixed samples. As observed in live cells, Pif3 accumulated in the nucleus with PhyB-NLS after the light induction. (B) Cells without treatment of PCB or without Pif3 did not respond to the light stimulation.

Ruffle formation by light-mediated intra-molecular interaction of SopE

To engineer SopE into an optogenetic probe, I first identified potential sites where I could SopE into non-functional fragments that would only gain function when fragment pairs bound one another via PhyB-Pif3 interactions. To efficiently and accurately screen SopE fragment pairs, I tested combination *in vitro* rather then in cells by quantitatively measuring its GEF activity to Rac GTPase. As a positive control for molecular interactions, I replaced PhyB/Pif3 with the well-established FKBP/FRB interacting pair so that I could control SopE function by treatment with the small molecule, rapamycin. (Banaszynski et al, 2005) Thus, I were able to test the efficacy of each light-induced PhyB/Pif3 fragment pair as well as the wild-type, intact SopE. (Fig 5-3A) To optimize our protein purification, I generated recombinant SopE proteins fused to an N-terminal FKBP and a C-terminal FRB (FKBP-SopE-FRB hereafter), or vice versa (FRB-SopE-FKBP hereafter), with TEV protease sites positioned to enable fragment generation upon TEV protease treatment. This strategy enabled us to purify a single protein and then modify the protein into the desired fragments post-purification. Screening of the SopE structure revealed seven candidate cleavage sites (residues 78-240; SopE hereafter), mostly on turns or loops between helices that would most likely not affect SopE folding or activity upon activation. (Fig 5-3B) Overall, I purified total sixteen SopE recombinant proteins including fourteen constructs with inserted TEV cleavage sites and two constructs without insertion in SopE.

I then systematically tested SopE fragment pairs using a three-step evaluation process. First, full-length SopE GEF activity was evaluated by measuring the decay rate of Rac-loaded mantGDP fluorescence prior to TEV protease addition. Recombinant SopE constructs

with pre-TEV-cleavage activity levels similar to that of wild-type SopE were subjected to TEV protease cleavage to generate pairs of SopE fragments. (John et al, 1990; Leonard et al, 1994) For example, FKBP-SopE-FRB protein was cleaved to form an N-terminal fragment of SopE fused to FKBP (FKBP-$SopE_N$ hereafter) and a C-terminal fragment of SopE fused to FRB (FRB-$SopE_C$ hereafter). Each pair of SopE fragments was tested for its GEF activity. Only those with no GEF activity underwent rapamycin treatment. Inactive SopE fragment pairs were treated with rapamycin, and GEF activity was partially restored in two pairs with different cleavage sites. (Fig 5-3C) This three-step process can be used to evaluate proteins for their use with the general optogenetic described here.

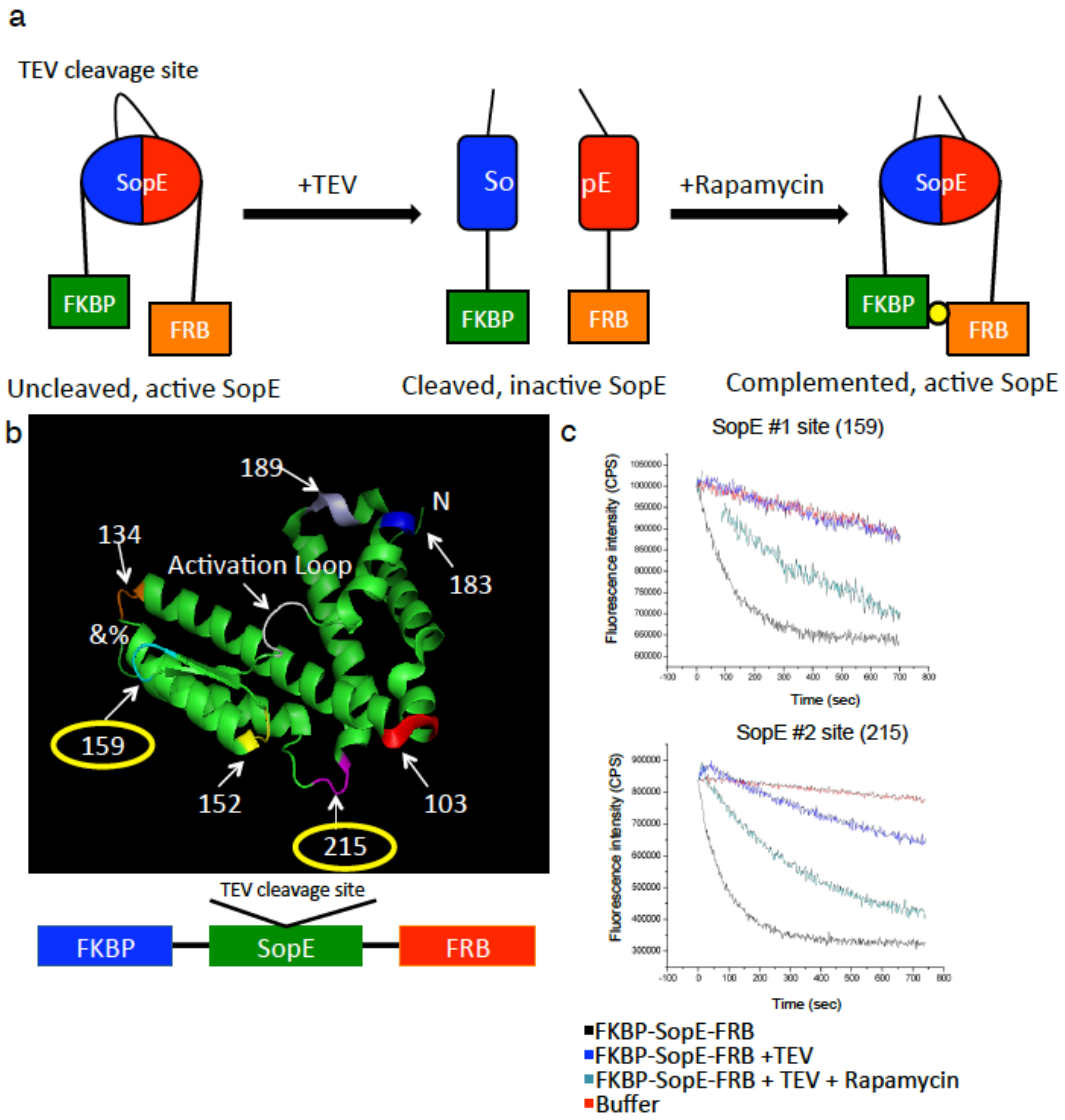

Figure 5-3. The cleavage site for SopE protein screened *in vitro*. (A) To generate the SopE fragments which enable to complement to each other in proximity, FKBP-FRB heterodimerization system was adopted. The chimeras of SopE flanking with FKBP and FRB were evaluated whether any of them can meet the following criteria: 1) The construct without any protease treatment should be at the active state. 2) The cleaved fragments of the construct after TEV enzyme incubation would lose its GEF activity. 3) By supplying the dimerization mediator, the rapamycin, the construct would regain the activity. (B) Seven different sites were pre-selected for the cleavage sites based on the known structure of SopE protein. The TEV protease cleavage residues were inserted at each site. The yellow circles indicated the selected sites after the screening. (C) Two sites (159 and 215) satisfied all three conditions for the switchable SopE pair. The fluorescence intensity measured in the graphs here represents SopE activity.

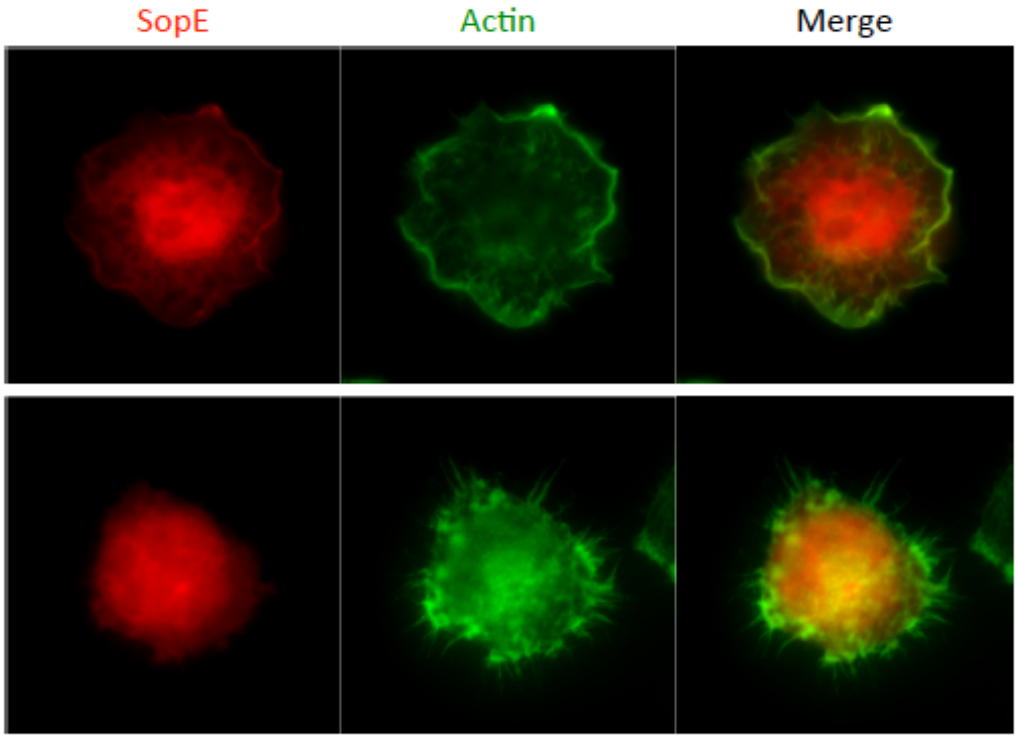

Figure 5-4. The uncleaved SopE (78-240) construct induces heavy actin ruffles. Depending on the expression level of SopE, either the membrane ruffling or the microspike structures were observed.

Using fragment pairs that were successfully evaluated by the process previously described, two optogenetic pairs of SopE fragments were generated by fusing the N-terminal SopE fragment with PhyB (PhyB-$SopE_N$ hereafter) and the C-terminal SopE fragment with Pif3 ($SopE_C$-Pif3). The rationale behind such arrangement was that PhyB requires free N-terminus for proper folding and that SopE fragments requires its cleaved sites to be spatially available for complementation. $SopE_C$-Pif3 was further modified to contain three tandem repeats of Pif3 ($SopE_C$-$[Pif3]_3$ hereafter) to generate a high affinity interaction that resulted in a stable complementation of SopE fragments. (Fig 5-5A) HeLa cells were transfected with each pair, treated with PCB chromophore, illuminated with red light and observed for a morphological change over a time course of 30 minutes. Whole cell red light exposure successfully induced lamellipodia structures in cells transfected with the pair of PhyB-$SopE_N$ ($SopE_N$ residue 78-215) with $SopE_C$-$[Pif3]_3$ ($SopE_C$ residue 216-240). This effect was partially reversed when the cell was exposed to far-red illumination. (Fig 5-5B) Subcellular red light exposure generated ruffle formations within the illuminated area that were eliminated by far-red light illumination. (Fig 5-5C) Cells without treatment of PCB chromophore or without a complete pair of optogenetic SopE did not show any change in cell shape upon red light illumination. (Fig 5-6C) I then further verified that the morphological changes resulted from GEF activity of optogenetic SopE pair by Rho GTPases assay. (Hardt et al, 1998) (Fig 5-5D) Cells expressing optogenetic pairs of SopE illuminated with the red light showed increased level of active, GTP-loaded Rac1 compared to those illuminated with the far-red light, although cells transfected with uncleaved, full-length, SopE contained significantly higher levels of active Rac1. I repeated these experiments with another

optogenetic pair of SopE, cleaved at the residue 159, and were able to induce ruffle formation under whole-cell red-light illumination. However, morphological changes were not observed with the local illumination. (Fig 5-6B) Overall, I demonstrated that our systematic approach generated a new optogenetic tool for SopE protein, which can be generally applicable to other proteins.

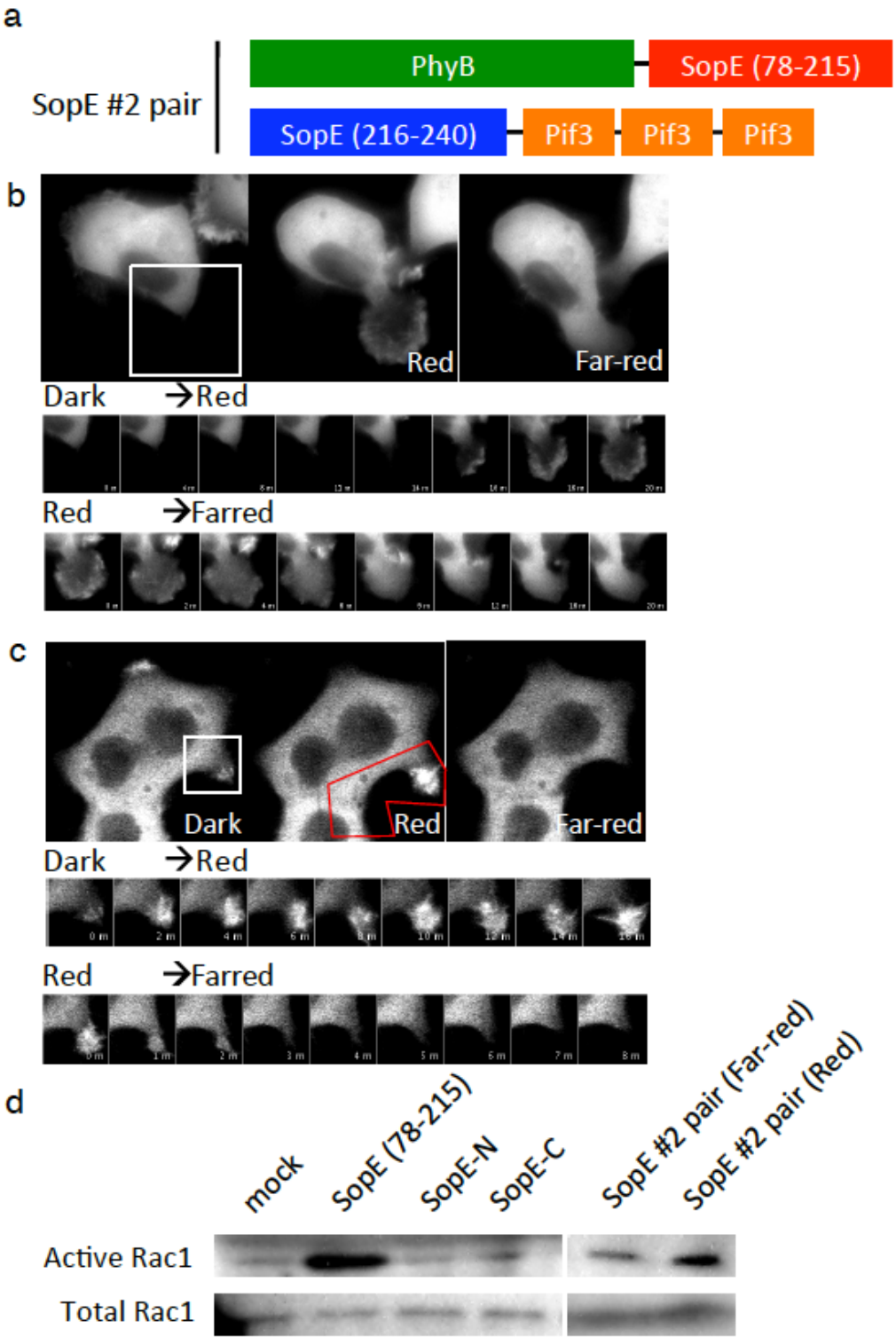

Figure 5-5. Light mediated switchable SopE generates ruffles in HeLa cells. (A) The chimera of SopE with the split site at the residue of 215 was generated by paring with PhyB-

Pif3 light-mediated binding partners. (B) A cell expressing switchable SopE was illuminated by the red or the far-red light on the whole cell area and the actin structure rearrangement was observed using the fluorescence protein tagged actin. The ruffles at the plasma membrane were emerged under the red light, which effect can be reverted by exposing cells to the far-red light. The boxed region is presented in a time series. (C) The ruffling effect was induced locally under a focal illumination. This phenotype was diminished with the far-red background light only. The region indicated by the white box is presented in a time series. (D) Rac1 activation under the red irradiation was measured by the pull down assay with its downstream effector, Pak1-CRIB domain.

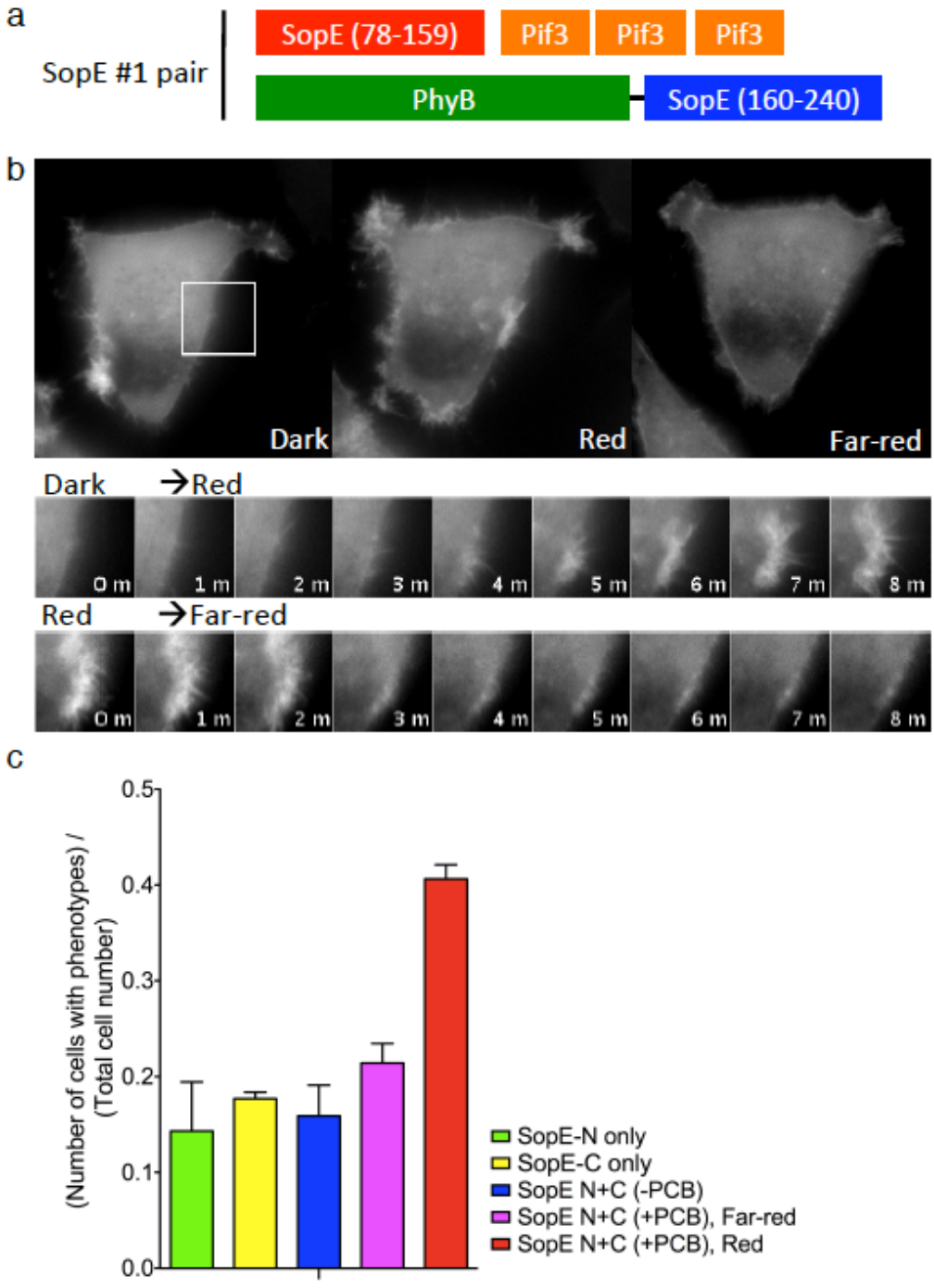

Figure 5-6. Light mediated switchable SopE generates the ruffling structure. (A) The genetically cleaved SopE at the 159 residue were also tested for its switchable activity in HeLa cells. The N-terminus of SopE was conjugated with three-repeated Pif3 while the C-terminus of SopE was coupled with PhyB. (B) Cells expressing the SopE #1 pair were

irradiated under the red light covering the whole cell region. Ruffling phenotype emerged after 10min under the red light could be reverted by exposing cells to the far-red light. The boxed region is presented in a time series. (C) Control transfection conditions were tested to validate the switchable SopE #2 pair. Cells with either one part of the pair or without PCB supply did not induce the cytoskeleton rearrangement. Error bars, s.d. (n=2, total more than 100 cells counted.)

Cell spreading mediated by light-mediated inter-molecular interactions between PhyB-Cdc42 (GDP) and Pif3-WASp

I fused PhyB and Pif3 to Cdc42 and WASp, respectively, to generate optogenetic pairs (PhyB-Cdc42 and Pif3-WASp hereafter). PhyB-Cdc42, localized to the Golgi upon expression in HeLa cells, similar to endogenous Cdc42 localization. (Figure S5) Therefore, I exchanged the C-terminal CAAX box domain of Cdc42 to that of K-Ras protein (PhyB-$Cdc42_{PM}$ hereafter) to target, PhyB-Cdc42 to the plasma membrane. (Michaelson et al, 2001)

HeLa cells were transfected with PhyB-$Cdc42_{PM}$ and Pif3-WASp and incubated with PCB chromophore in the media. Upon illumination, with red light for 30 minutes, cells generated extensive filopodia began to spread. (Fig 5-7A) A significantly lower fraction of cells responded to the red light when expressing either PhyB-$Cdc42_{PM}$, Pif-WASp, or when PhyB alone was used without Cdc42. (Fig 5-7B) PhyB-Cdc42 without a native CAAX box domain or with the CAAX box domain of Rac protein also induced rearrangement of actin cytoskeleton following red-light illumination, although the extent of morphological changes were varied. (Fig 5-8 and Fig 5-9) Overall, I demonstrated optogenetic control of Cdc42/WASp intra-molecular interactions and propose that this control could be extended to other intra-molecular interactions in other signaling pathways.

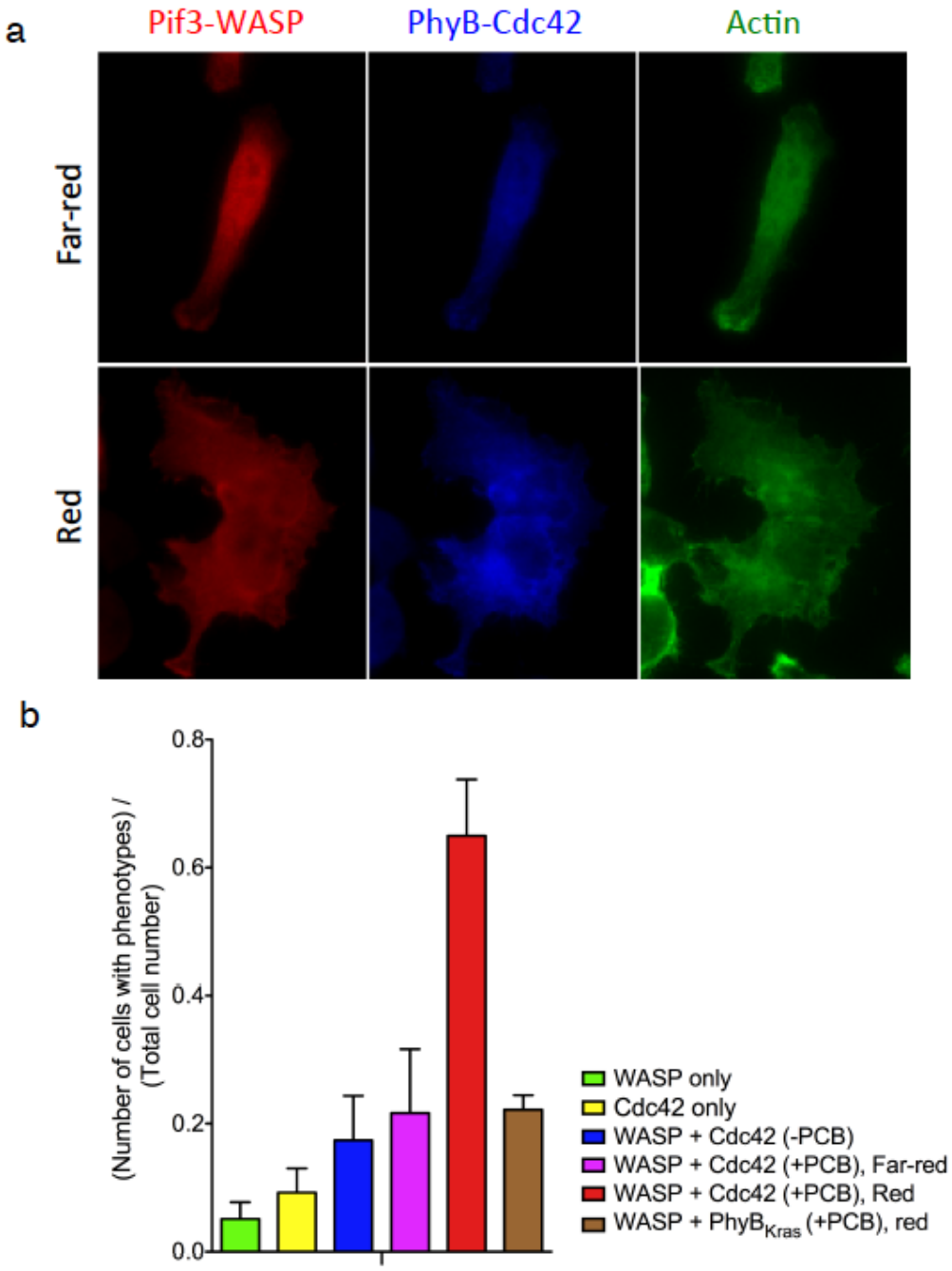

Figure 5-7. Cdc42 (GDP) activates WASP to induce the filopodium formation in HeLa cells. (A) Cells expressing PhyB-Cdc42 (GDP) and Pif3-WASP pair showed a global filopodium formation when illuminated with the red light. A distinct actin structure was confirmed with the phalloidin staining. (B) Cells with only one part of the switchable Cdc42-WASP pair did not respond to the light stimulation. Also when cells were not supplied PCB, the phenotype could not be observed. When PhyB was not paired with Cdc42, the fraction of

cells with the distinct actin structure was decreased. Error bars, s.d. (n=3, total more than 100 cells counted.)

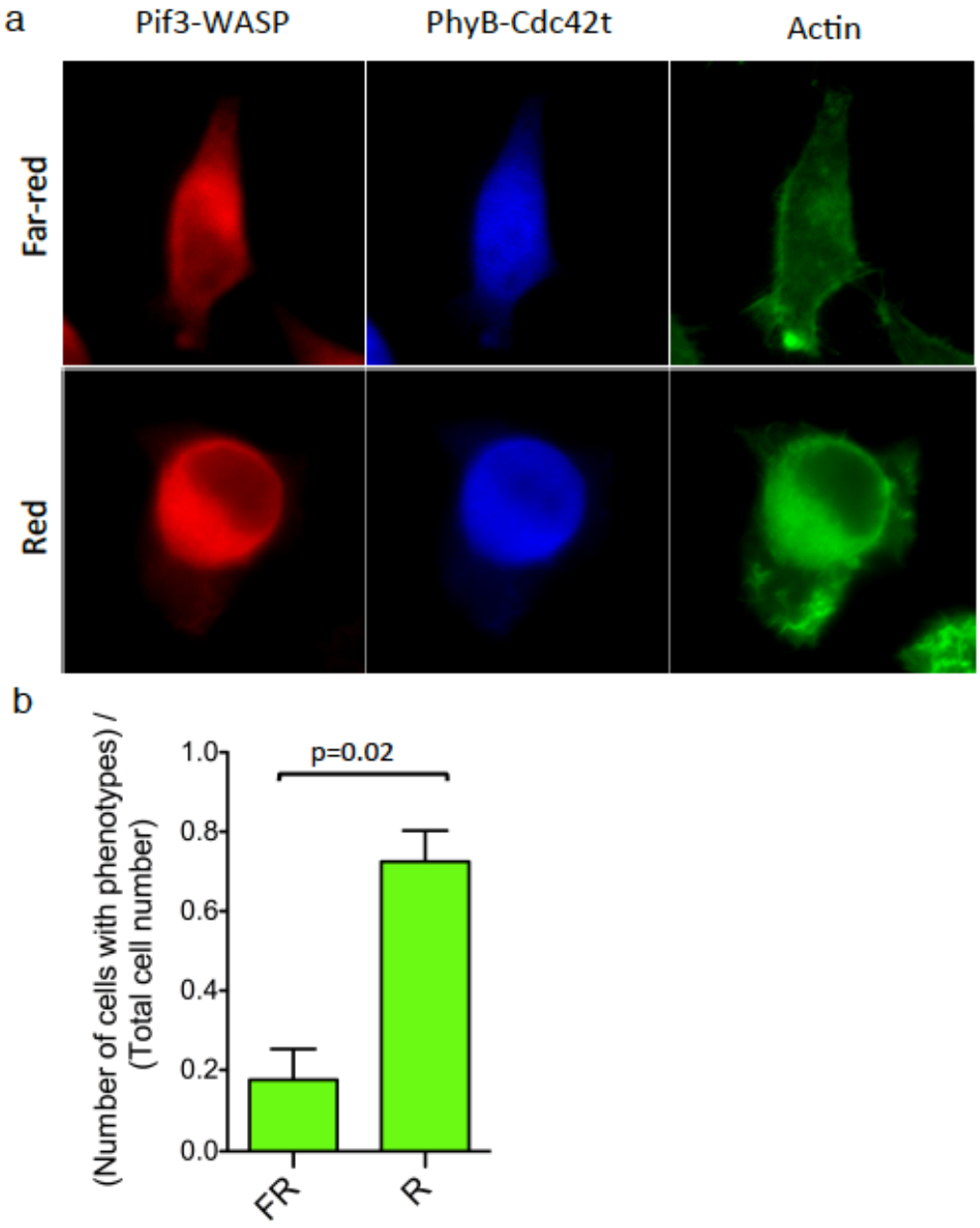

Figure 5-8. Cdc42 in the cytoplasm activates WASP to affect on the cytoskeleton structure of cells through the light-mediated control. (A) After 30min of the red light stimulation, cells expressing Pif3-WASP and PhyB-Cdc42 without any CAAX box domain, showed the centered actin staining pattern compared to the sample irradiated with the far-red light. (B) The number of the cells showing the abolished actin structure was counted to evaluate the functionality of Cdc42t-WASP pair. Error bars, s.d. (n=2, total more than 60 cells counted.)

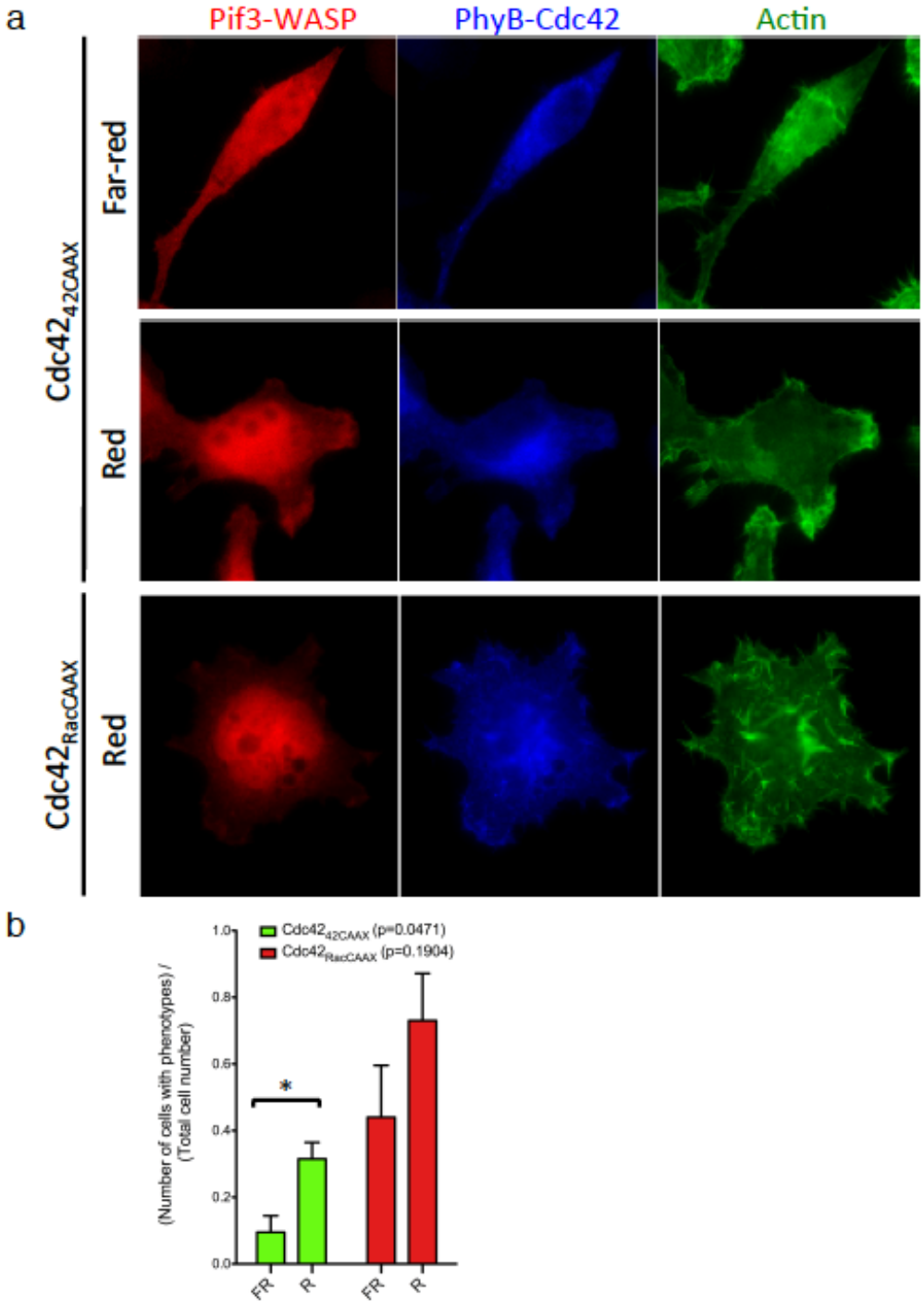

Figure 5-9. Cdc42 with the different CAAX boxes and WASP induced the different phenotypes in HeLa cells. (A) Cdc42 with its own CAAX box (unmodified) was targeted mostly at the Golgi network. When this wild-type Cdc42 was paired with WASP, cells

showed much weaker phenotype in terms of filopodium formation than when Cdc42 was used with K-Ras CAAX box region. On the contrary, when Cdc42 was modified to have Rac1 CAAX box, there was huge effect on the cytoskeleton even under the inactive condition with the far-red light. (B) Each phenotype with the different Cdc42 constructs was evaluated by counting the cells with the distinct actin structures. Error bars, s.d. (n=2, total more than 60 cells counted.)

Discussion

I have introduced an *in vivo* method to engineer optogenetic tools that can be applied to numerous systems and signaling pathways. I used two model systems to demonstrate that the activity of a single protein, SopE, or the binding of two proteins, Cdc42 and WASp, can be regulated by light-mediated interactions between PhyB and Pif3.

Previous study showed that PhyB did not bind or very weakly bound to Pif3 when PhyB localized to the plasma membrane. I also observed that partitioning of Pif3 in the nucleus by PhyB was weak and occurred very slowly, which was at least partially caused by slow trafficking between nucleus and cytoplasm in mammalian cells. Such low affinity between this optogenetic pair may increase the dynamic range of activation by reducing the background activity, that is often caused by overexpression, prior to the red-light illumination.

After optogenetic pairs generation, treatment of PCB chromophore in media is the only additional step besides typical transient transfection. PCB chromophore can be extracted from commercially available *Spirulina* cell lysates, using a well-established procedure. The constitution of holo-PhyB, which interconverts between Pr and Pfr, can be tested by measuring the 650nm absorbance of cell lysates upon red or far-red illumination. (Data not shown)

It is noteworthy that whole-cell or partial illumination on SopE resulted in different morphological change and that changing of Cdc42 localization by exchanging CAAX box domain caused diverse effect on cell shape. Such observations suggest the importance of spatial control of GTPases in many cellular processes such as bacterial invasion and cell migration.

Although I only utilized the optogenetic tool to the proteins involved in rearrangement of actin cytoskeleton, the method potentially provides a direct approach to probe an individual protein's role in many complicated signaling pathways. Especially along with the further optimized irradiation device with better focal stimulation control of μm-scale length, any dynamic cellular behavior with rapidly changing processes will benefit greatly by generally applicable light-mediated control.

Methods and Materials

Constructs

All PhyB (residues 1-651) and Pif3 (residues 1-100) conjugated constructs were cloned into pcDNA vectors (Invitrogen). PhyB-$SopE_N$ and $SopE_C$-$[Pif3]_3$ constructs were cloned as described in Figure 4a, with each domains tethered by $[GGS]_3$ linker. For imaging experiments, mCerulean or mEYFP (Cerulean and YFP with mutation: A206K) was cloned after PhyB or SopE. PhyB-Cdc42 and Pif3-WASp constructs were cloned as previously described. (Leung et al, 2008) Further information of PhyB and Pif3 constructs is provided in Table 5-1. All FKBP-SopE-FRB constructs were cloned into P15Cool2 vector, which contains N-terminal MBP and His tag. Further information of SopE mutants with TEV cleavage sites is provided in Table 5-2.

Proteins	Sequence Information	Notes
PhyB	MVSGVGGSGGGRGGGRGG EEEPSSSHTPNNRRGGEQAQ SSGTKSLRPRSNTESMSKAI QQYTVDARLHAVFEQSGES GKSFDYSQSLKTTTYGSSVP EQQITAYLSRIQRGGYIQPF GCMIAVDESSFRIIGYSENA REMLGIMPQSVPTLEKPEIL AMGTDVRSLFTSSSSILLER AFVAREITLLNPVWIHSKNT GKPFYAILHRIDVGVVIDLE PARTEDPALSIAGAVQSQKL AVRAISQLQALPGGDIKLLC DTVVESVRDLTGYDRVMV YKFHEDEHGEVVAESKRDD LEPYIGLHYPATDIPQASRFL FKQNRVRMIVDCNATPVLV VQDDRLTQSMCLVGSTLRA PHGCHSQYMANMGSIASLA	Residues 1-651. DNS sequences were optimized for mammalian cell expression system.

	MAVIINGNEDDGSNVASGR SSMRLWGLVVCHHTSSRCI PFPLRYACEFLMQAFGLQL NMELQLALQMSEKRVLRT QTLLCDMLLRDSPAGIVTQS PSIMDLVKCDGAAFLYHGK YYPLGVAPSEVQIKDVVEW LLANHADSTGLSTDSLGDA GYPGAAALGDAVCGMAVA YITKRDFLFWFRSHTAKEIK WGGAKHHPEDKDDGQRM HPRSSFQAFLEVVKSRSQP WETAEMDAIHSLQLILRDSF KESEAAMNSKVVDGVVQP CRDMAGEQGIDELGA	
Pif3	MPLFELFRLTKAKLESAQD RNPSPPVDEVVELVWENGQ ISTQSQSSRSRNIPPPQANSS RAREIGNGSKTTMVDEIPMS VPSLMTGLSQDDDFVPWLN H	Residues 1-100.

NLS	MTAPKKKRKMTAPKKKRK	
SopE	MTKITLSPQNFRIQKQETTL LKEKSTEKNSLAKSILAVKN HFIELRSKLSERFISHKNTES SATHFHRGSASEGRAVLTN KVVKDFMLQTLNDIDIRGS ASKDPAYASQTREAILSAV YSKNKDQCCNLLISKGINIA PFLQEIGEAAKNAGLPGTTK NDVFTPSGAGANPFITPLISS ANSKYPRMFINQHQQASFKI YAEKIIMTEVAPLFNECAMP TPQQFQLILENIANKYIQNTP	
Cdc42	QTIKCVVVGDGAVGKTCLL ISYTTNKFPSEYVPTVFDNY AVTVMIGGEPYTLGLFDTA GQEDYDRLRPLSYPQTDVF LVCFSVVSPSSFENVKEKW VPEITHHCPKTPFLLVGTQI DLRDDPSTIEKLAKNKQKPI TPETAEKLARDLKAVKYVE	CAAX box region

	CSALTQKGLKNVFDE AILAALEPPEPKKSRRCVLL	
Kras CAAX box	EKMSKDGKKKKKKSKTKC VIM	
WASp	KKKISKADIGAPSGFKHVSH VGWDPQNGFDVNNLDPDL RSLFSRAGISEAQLTDAETS KLIYDFIEDQGGLEAVRQE MRRQGGSGGSVPAGGLAP GGGRGALLDQIRQGIQLNK TPGAPESSALQPPPQSSEGL VGALMHVMQKRSRAIHSSD EGEDQAGDEDEDDEWD	GBD-VCA
FKBP	VQVETISPGDGRTFPKRGQT CVVHYTGMLEDGKKFDSSR DRNKPFKFMLGKQEVIRGW EEGVAQMSVGQRAKLTISP DYAYGATGHPGIIPPHATLV FDVELLKLEG	
FRB	ELIRVAILWHEMWHEGLEE	

	ASRLYFGERNVKGMFEVLE PLHAMMERGPQTLKETSFN QAYGRDLMEAQEWCRKY MKSGNVKDLTQAWDLYYH VFRRISKQ	

Table 5-1. Information on protein expression constructs used in Chapter 5

Mutant Name	Insertion site	Notes
FKBP-SopE 103Tev-FRB	D103-P104	
FKBP-SopE134Tev-FRB	G134-I135	
FKBP-SopE152Tev-FRB	G152-L153	
FKBP-SopE159Tev-FRB	N159-D160	
FKBP-SopE183Tev-FRB	K183-Y184	
FKBP-SopE189Tev-FRB	I189-N190	
FKBP-SopE215Tev-FRB	E215-C216	
FRB-SopE103Tev-FKBP	D103-P104	
FRB-SopE134Tev-FKBP	G134-I135	
FRB-SopE152Tev-FKBP	G152-L153	
FRB-SopE159Tev-FKBP	N159-D160	This construct was used for mammalian cell experiments.
FRB-SopE183Tev-FKBP	K183-Y184	
FRB-SopE189Tev-FKBP	I189-N190	

FRB-SopE215Tev-FKBP	E215-C216	This construct was used for mammalian cell experiments.

Table 5-2. FKBP-SopE-FRB mutant chart

Cell Culture and transfection

HeLa cells and HEK293T were cultured in Dulbecco's modified Eagle's medium (DMEM) containing 10% FBS and 1mM penicillin/streptomycin (Invitrogen) and 1mM GlutaMAX (Invitrogen). Cells were transfected using Effectene (QIAGEN) and incubated for 24h at 37°C.

Irradiation procedure with live cell imaging

HeLa cells were imaged at 37°C 16 hours after transient transfection. Images from cells irradiated on the whole cell area were acquired on an Applied Precision Deltavision RT Deconvolution microscope. Focal stimulation experiments were conducted on a Zeiss LSM 510 confocal microscope with 100X objective using FRAP setting with 650 nm laser line.

GEF activity assay

FKBP-SopE-FRB or FRB-SopE-FKBP constructs were purified from E. coli in 25mM HEPES pH=7.0, 100mM NaCl were mixed with 2μM GTP, 100nM Rac1 (loaded with mantGDP) for each activity reaction. SopE activities were measured at 10μM concentration. The fluorescence intensity was monitored at 440nm on a Fluorolog-3-11 fluorimeter.

Active Rac pull down assay

HeLa cells were lysed 16 hours after transiently transfected with switchable SopE system with red or far-red stimulation. Cell lysates were incubated at 4°C for 1 hour with

glutathione-Sepharose beads loaded with purified GST-PAK1 (73-113). After washing steps activated Rac1 bound to GST-PAK1 were accessed by western blot with Rac1 antibody.

Phycocyanobilin (PCB) extraction

PCB was purified from *Spirulina* extracts by following standard procedures. (Fu et al, 1979) Pure PCB was stored at -20°C before usage and handled under a safe green light.

Chapter 6

Concluding remarks II

In this study, I demonstrated that the light-mediated heterodimerization between PhyB and Pif3 can modulate subcellular control of proteins in mammalian cells. To test intra-molecular optogenetic control of protein activity using PhyB and Pif3, I chose to engineer SopE, a potent GEF protein from *Salmonella*. (Fig 6-1A) SopE was rationally screened *in vitro* for a specific cleavage site that would enable two individually inactive fragments of SopE to bind via a PhyB-Pif3 interaction. Upon binding, SopE should regain its intrinsic activity and initiate downstream pathways of Rho-GTPases such as Rac and Cdc42. Using our engineered SopE, I show that light-mediated interactions between PhyB- and Pif3-fused SopE fragments by red light stimulation induced ruffle formation. Activity of SopE was ablated by far-red light illumination and the initial membrane morphology was restored. Having successfully engineered a light-controlled intramolecular cellular system, I used PhyB and Pif3 to mediate intermolecular interactions between Wiskott-Aldrich Syndrome protein (WASp) and its upstream activator, Rho GTPase Cdc42 in cells. (Fig 6-1B) Previously, I demonstrated that light-mediated activation of WASp could be achieved when WASp and an inactive form of Cdc42 are fused to PhyB and Pif3 and illuminated with red light *in vitro*. (Leung et al, 2008) In this study, I extended our previous work in cells and demonstrate that optogenetic activation of WASp by Cdc42 can promote actin polymerization and extensive filopodia formation.

Besides its application in SopE and Cdc42-WASp signaling described here, PhyB-Pif3 optogenetic system can also be integrated into the study of multivalency mediated phase separation demonstrated in Chapter 3.

1. PhyB-Pif3 system can replace the heterodimerization system of FKBP and FRB, which will induce phosphorylation of nephrin at the subdomain region of plasma membrane. Locally induced multivalent interactions between proteins may change the pattern of phase separation by altering the nucleation pattern of polymerization.
2. Furthermore, FKBP-FRB and PhyB-Pif3 systems are compatible, which allows us to combine both systems to gain finer control of the phosphorylation state of nephrin. For example, cSrc kinase and PTP1B can be fused to PhyB and FKBP, respectively, which will bring opposing effects on nephrin tethered by Pif3 and FRB. This system may demonstrate how phase separated structure will respond to the dephosphorylation of nephrin.
3. The number of valencies in each protein can be controlled by a light mediated system. For example, if both PhyB and Pif3 are fused to two SH3 domains, irradiation of red light will produce four SH3 domains present in the complex. This experiment will further validate our model of multivalency mediated phase separation.

The role of actin cytoskeletal machinery has been demonstrated by assessing the identity of each protein component in a signaling cascade through numerous biochemical assays. I expect that optogenetic tools along with diverse imaging techniques will answer the

next questions about how spatiotemporal control of protein activity contributes to the specific pattern of actin rearrangement in living cells.

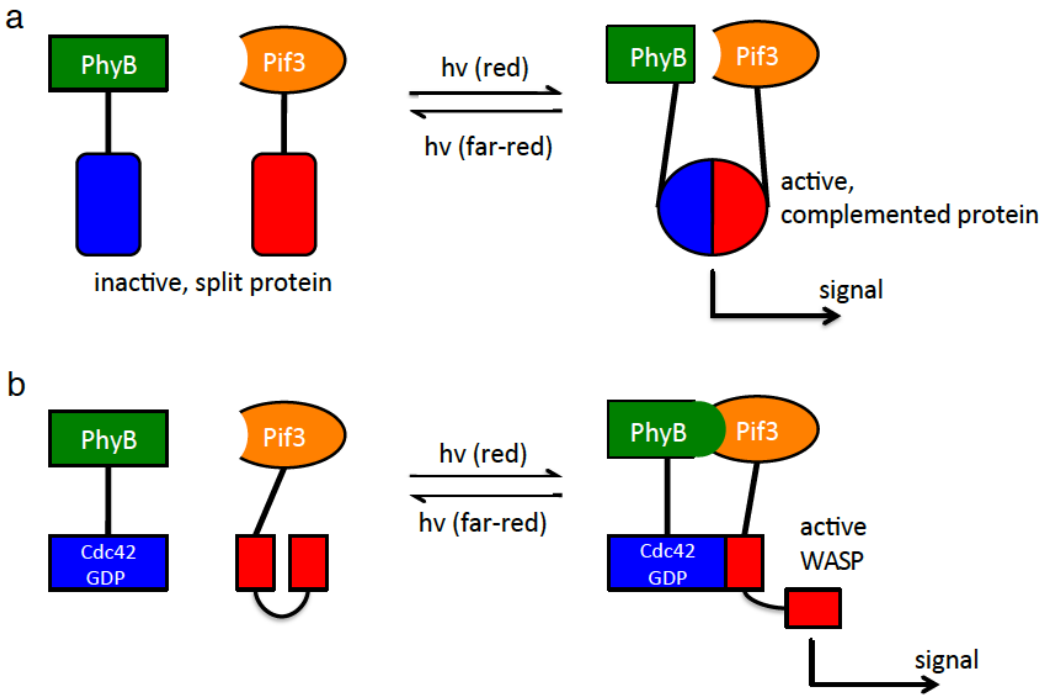

Figure 6-1. Light-mediated regulation over PhyB-Pif3 interaction is used to regulate protein's activity. (A) A single protein is genetically split into two fragments, which can recover its activity when PhyB-Pif3 binding triggers their intra-molecular complementation. (B) PhyB-Pif3 pair is fused with two distinct molecules (here, Cdc42 and WASP, respectively) to control allosteric regulation of a protein.

References

Airan RD, Thompson KR, Fenno LE, Bernstein H, Deisseroth K (2009) Temporally precise in vivo control of intracellular signalling. *Nature* **458:** 1025-1029

Ando R, Mizuno H, Miyawaki A (2004) Regulated fast nucleocytoplasmic shuttling observed by reversible protein highlighting. *Science* **306:** 1370-1373

Arif E, Wagner MC, Johnstone DB, Wong HN, George B, Pruthi PA, Lazzara MJ, Nihalani D (2011) Motor protein Myo1c is a podocyte protein that facilitates the transport of slit diaphragm protein Neph1 to the podocyte membrane. *Mol Cell Biol* **31:** 2134-2150

Astro V, de Curtis I (2015) Plasma membrane-associated platforms: dynamic scaffolds that organize membrane-associated events. *Sci Signal* **8:** re1

Banaszynski LA, Liu CW, Wandless TJ (2005) Characterization of the FKBP.rapamycin.FRB ternary complex. *J Am Chem Soc* **127:** 4715-4721

Banjade S, Rosen MK (2014) Phase transitions of multivalent proteins can promote clustering of membrane receptors. *Elife* **3**

Blasutig IM, New LA, Thanabalasuriar A, Dayarathna TK, Goudreault M, Quaggin SE, Li SS, Gruenheid S, Jones N, Pawson T (2008) Phosphorylated YDXV motifs and Nck SH2/SH3 adaptors act cooperatively to induce actin reorganization. *Mol Cell Biol* **28:** 2035-2046

Brangwynne CP, Eckmann CR, Courson DS, Rybarska A, Hoege C, Gharakhani J, Julicher F, Hyman AA (2009) Germline P granules are liquid droplets that localize by controlled dissolution/condensation. *Science* **324:** 1729-1732

Brangwynne CP, Mitchison TJ, Hyman AA (2011) Active liquid-like behavior of nucleoli determines their size and shape in Xenopus laevis oocytes. *Proc Natl Acad Sci U S A* **108:** 4334-4339

Buchwald G, Friebel A, Galan JE, Hardt WD, Wittinghofer A, Scheffzek K (2002) Structural basis for the reversible activation of a Rho protein by the bacterial toxin SopE. *EMBO J* **21:** 3286-3295

Buday L, Wunderlich L, Tamas P (2002) The Nck family of adapter proteins: regulators of actin cytoskeleton. *Cell Signal* **14:** 723-731

Chen EH, Olson EN (2004) Towards a molecular pathway for myoblast fusion in Drosophila. *Trends Cell Biol* **14:** 452-460

Cheng HC, Skehan BM, Campellone KG, Leong JM, Rosen MK (2008) Structural mechanism of WASP activation by the enterohaemorrhagic E. coli effector EspF(U). *Nature* **454:** 1009-1013

Chinthalapudi K, Rangarajan ES, Patil DN, George EM, Brown DT, Izard T (2014) Lipid binding promotes oligomerization and focal adhesion activity of vinculin. *J Cell Biol* **207:** 643-656

Comer FI, Parent CA (2002) PI 3-kinases and PTEN: how opposites chemoattract. *Cell* **109:** 541-544

Cortesio CL, Perrin BJ, Bennin DA, Huttenlocher A (2010) Actin-binding protein-1 interacts with WASp-interacting protein to regulate growth factor-induced dorsal ruffle formation. *Mol Biol Cell* **21:** 186-197

Cowan CA, Henkemeyer M (2001) The SH2/SH3 adaptor Grb4 transduces B-ephrin reverse signals. *Nature* **413:** 174-179

Coyne CW, Patel K, Heureaux J, Stachowiak J, Fletcher DA, Liu AP (2014) Lipid bilayer vesicle generation using microfluidic jetting. *J Vis Exp***:** e51510

Crosby KC, Postma M, Hink MA, Zeelenberg CH, Adjobo-Hermans MJ, Gadella TW (2013) Quantitative analysis of self-association and mobility of annexin A4 at the plasma membrane. *Biophys J* **104:** 1875-1885

Day CA, Kenworthy AK (2009) Tracking microdomain dynamics in cell membranes. *Biochim Biophys Acta* **1788:** 245-253

Dundr M, Misteli T (2003) Measuring dynamics of nuclear proteins by photobleaching. *Curr Protoc Cell Biol* **Chapter 13:** Unit 13 15

Edidin M (2003) Lipids on the frontier: a century of cell-membrane bilayers. *Nat Rev Mol Cell Biol* **4:** 414-418

Eggeling C, Ringemann C, Medda R, Schwarzmann G, Sandhoff K, Polyakova S, Belov VN, Hein B, von Middendorff C, Schonle A, Hell SW (2009) Direct observation of the nanoscale dynamics of membrane lipids in a living cell. *Nature* **457:** 1159-1162

Erickson JW, Cerione RA (2004) Structural elements, mechanism, and evolutionary convergence of Rho protein-guanine nucleotide exchange factor complexes. *Biochemistry* **43:** 837-842

Faul C, Asanuma K, Yanagida-Asanuma E, Kim K, Mundel P (2007) Actin up: regulation of podocyte structure and function by components of the actin cytoskeleton. *Trends Cell Biol* **17:** 428-437

Feric M, Brangwynne CP (2013) A nuclear F-actin scaffold stabilizes ribonucleoprotein droplets against gravity in large cells. *Nat Cell Biol* **15:** 1253-1259

Forman-Kay JD, Mittag T (2013) From sequence and forces to structure, function, and evolution of intrinsically disordered proteins. *Structure* **21:** 1492-1499

Fu E, Friedman L, Siegelman HW (1979) Mass-spectral identification and purification of phycoerythrobilin and phycocyanobilin. *Biochem J* **179:** 1-6

Garbett D, Bretscher A (2012) PDZ interactions regulate rapid turnover of the scaffolding protein EBP50 in microvilli. *J Cell Biol* **198:** 195-203

Gardel ML, Schneider IC, Aratyn-Schaus Y, Waterman CM (2010) Mechanical integration of actin and adhesion dynamics in cell migration. *Annu Rev Cell Dev Biol* **26:** 315-333

Gerke P (2003) Homodimerization and Heterodimerization of the Glomerular Podocyte Proteins Nephrin and NEPH1. *Journal of the American Society of Nephrology* **14:** 918-926

Goley ED, Welch MD (2006) The ARP2/3 complex: an actin nucleator comes of age. *Nat Rev Mol Cell Biol* **7:** 713-726

Goswami D, Gowrishankar K, Bilgrami S, Ghosh S, Raghupathy R, Chadda R, Vishwakarma R, Rao M, Mayor S (2008) Nanoclusters of GPI-anchored proteins are formed by cortical actin-driven activity. *Cell* **135:** 1085-1097

Gowrishankar K, Ghosh S, Saha S, C R, Mayor S, Rao M (2012) Active remodeling of cortical actin regulates spatiotemporal organization of cell surface molecules. *Cell* **149:** 1353-1367

Grecco HE, Schmick M, Bastiaens PI (2011) Signaling from the living plasma membrane. *Cell* **144:** 897-909

Groves JT, Kuriyan J (2010) Molecular mechanisms in signal transduction at the membrane. *Nat Struct Mol Biol* **17:** 659-665

Hafner C, Schmitz G, Meyer S, Bataille F, Hau P, Langmann T, Dietmaier W, Landthaler M, Vogt T (2004) Differential gene expression of Eph receptors and ephrins in benign human tissues and cancers. *Clin Chem* **50:** 490-499

Hahn KM, Kuhlman B (2010) Hold me tightly LOV. *Nat Methods* **7:** 595, 597

Han TW, Kato M, Xie S, Wu LC, Mirzaei H, Pei J, Chen M, Xie Y, Allen J, Xiao G, McKnight SL (2012) Cell-free formation of RNA granules: bound RNAs identify features and components of cellular assemblies. *Cell* **149:** 768-779

Hancock JF (2006) Lipid rafts: contentious only from simplistic standpoints. *Nat Rev Mol Cell Biol* **7:** 456-462

Hancock JF, Magee AI, Childs JE, Marshall CJ (1989) All ras proteins are polyisoprenylated but only some are palmitoylated. *Cell* **57:** 1167-1177

Handwerger KE, Cordero JA, Gall JG (2005) Cajal bodies, nucleoli, and speckles in the Xenopus oocyte nucleus have a low-density, sponge-like structure. *Mol Biol Cell* **16:** 202-211

Hankins MW, Peirson SN, Foster RG (2008) Melanopsin: an exciting photopigment. *Trends Neurosci* **31:** 27-36

Hardt WD, Chen LM, Schuebel KE, Bustelo XR, Galan JE (1998) S. typhimurium encodes an activator of Rho GTPases that induces membrane ruffling and nuclear responses in host cells. *Cell* **93:** 815-826

Harris TJ, Tepass U (2010) Adherens junctions: from molecules to morphogenesis. *Nat Rev Mol Cell Biol* **11:** 502-514

Henis YI, Hancock JF, Prior IA (2009) Ras acylation, compartmentalization and signaling nanoclusters (Review). *Mol Membr Biol* **26:** 80-92

Himanen JP, Saha N, Nikolov DB (2007) Cell-cell signaling via Eph receptors and ephrins. *Curr Opin Cell Biol* **19:** 534-542

Himanen JP, Yermekbayeva L, Janes PW, Walker JR, Xu K, Atapattu L, Rajashankar KR, Mensinga A, Lackmann M, Nikolov DB, Dhe-Paganon S (2010) Architecture of Eph receptor clusters. *Proc Natl Acad Sci U S A* **107:** 10860-10865

Honerkamp-Smith AR, Veatch SL, Keller SL (2009) An introduction to critical points for biophysicists; observations of compositional heterogeneity in lipid membranes. *Biochim Biophys Acta* **1788:** 53-63

Howes MT, Mayor S, Parton RG (2010) Molecules, mechanisms, and cellular roles of clathrin-independent endocytosis. *Curr Opin Cell Biol* **22:** 519-527

Hyman AA, Weber CA, Julicher F (2014) Liquid-liquid phase separation in biology. *Annu Rev Cell Dev Biol* **30:** 39-58

Imhaus AF, Dumenil G (2014) The number of Neisseria meningitidis type IV pili determines host cell interaction. *EMBO J* **33:** 1767-1783

Janes PW, Nievergall E, Lackmann M (2012) Concepts and consequences of Eph receptor clustering. *Semin Cell Dev Biol* **23:** 43-50

Jaqaman K, Grinstein S (2012) Regulation from within: the cytoskeleton in transmembrane signaling. *Trends Cell Biol* **22:** 515-526

John J, Sohmen R, Feuerstein J, Linke R, Wittinghofer A, Goody RS (1990) Kinetics of interaction of nucleotides with nucleotide-free H-ras p21. *Biochemistry* **29:** 6058-6065

Jones N, Blasutig IM, Eremina V, Ruston JM, Bladt F, Li H, Huang H, Larose L, Li SS, Takano T, Quaggin SE, Pawson T (2006) Nck adaptor proteins link nephrin to the actin cytoskeleton of kidney podocytes. *Nature* **440:** 818-823

Jones N, New LA, Fortino MA, Eremina V, Ruston J, Blasutig IM, Aoudjit L, Zou Y, Liu X, Yu GL, Takano T, Quaggin SE, Pawson T (2009) Nck proteins maintain the adult glomerular filtration barrier. *J Am Soc Nephrol* **20:** 1533-1543

Kato M, Han TW, Xie S, Shi K, Du X, Wu LC, Mirzaei H, Goldsmith EJ, Longgood J, Pei J, Grishin NV, Frantz DE, Schneider JW, Chen S, Li L, Sawaya MR, Eisenberg D, Tycko R, McKnight SL (2012) Cell-free formation of RNA granules: low complexity sequence domains form dynamic fibers within hydrogels. *Cell* **149:** 753-767

Kennedy MJ, Hughes RM, Peteya LA, Schwartz JW, Ehlers MD, Tucker CL (2010) Rapid blue-light-mediated induction of protein interactions in living cells. *Nat Methods* **7:** 973-975

Khanna R, Huq E, Kikis EA, Al-Sady B, Lanzatella C, Quail PH (2004) A novel molecular recognition motif necessary for targeting photoactivated phytochrome signaling to specific basic helix-loop-helix transcription factors. *Plant Cell* **16:** 3033-3044

Kholodenko BN, Hoek JB, Westerhoff HV (2000) Why cytoplasmic signalling proteins should be recruited to cell membranes. *Trends Cell Biol* **10:** 173-178

Konermann S, Brigham MD, Trevino AE, Hsu PD, Heidenreich M, Cong L, Platt RJ, Scott DA, Church GM, Zhang F (2013) Optical control of mammalian endogenous transcription and epigenetic states. *Nature* **500:** 472-476

Kotaja N, Sassone-Corsi P (2007) The chromatoid body: a germ-cell-specific RNA-processing centre. *Nat Rev Mol Cell Biol* **8:** 85-90

Kusumi A, Suzuki KG, Kasai RS, Ritchie K, Fujiwara TK (2011) Hierarchical mesoscale domain organization of the plasma membrane. *Trends Biochem Sci* **36:** 604-615

Lakshminarayan R, Wunder C, Becken U, Howes MT, Benzing C, Arumugam S, Sales S, Ariotti N, Chambon V, Lamaze C, Loew D, Shevchenko A, Gaus K, Parton RG, Johannes L (2014) Galectin-3 drives glycosphingolipid-dependent biogenesis of clathrin-independent carriers. *Nat Cell Biol* **16:** 595-606

Lamaze C, Dujeancourt A, Baba T, Lo CG, Benmerah A, Dautry-Varsat A (2001) Interleukin 2 receptors and detergent-resistant membrane domains define a clathrin-independent endocytic pathway. *Mol Cell* **7:** 661-671

Langeberg LK, Scott JD (2015) Signalling scaffolds and local organization of cellular behaviour. *Nat Rev Mol Cell Biol* **16:** 232-244

Le Roy C, Wrana JL (2005) Clathrin- and non-clathrin-mediated endocytic regulation of cell signalling. *Nat Rev Mol Cell Biol* **6:** 112-126

Lemmon MA (2003) Phosphoinositide recognition domains. *Traffic* **4:** 201-213

Leonard DA, Evans T, Hart M, Cerione RA, Manor D (1994) Investigation of the GTP-binding/GTPase cycle of Cdc42Hs using fluorescence spectroscopy. *Biochemistry* **33:** 12323-12328

Lettau M, Pieper J, Janssen O (2009) Nck adapter proteins: functional versatility in T cells. *Cell Commun Signal* **7:** 1

Leung DW, Otomo C, Chory J, Rosen MK (2008) Genetically encoded photoswitching of actin assembly through the Cdc42-WASP-Arp2/3 complex pathway. *Proc Natl Acad Sci U S A* **105:** 12797-12802

Levskaya A, Chevalier AA, Tabor JJ, Simpson ZB, Lavery LA, Levy M, Davidson EA, Scouras A, Ellington AD, Marcotte EM, Voigt CA (2005) Synthetic biology: engineering Escherichia coli to see light. *Nature* **438:** 441-442

Levskaya A, Weiner OD, Lim WA, Voigt CA (2009) Spatiotemporal control of cell signalling using a light-switchable protein interaction. *Nature* **461:** 997-1001

Li M, Armelloni S, Edefonti A, Messa P, Rastaldi MP (2013) Fifteen years of research on nephrin: what we still need to know. *Nephrol Dial Transplant* **28:** 767-770

Li P, Banjade S, Cheng HC, Kim S, Chen B, Guo L, Llaguno M, Hollingsworth JV, King DS, Banani SF, Russo PS, Jiang QX, Nixon BT, Rosen MK (2012) Phase transitions in the assembly of multivalent signalling proteins. *Nature* **483:** 336-340

Lingwood D, Simons K (2010) Lipid rafts as a membrane-organizing principle. *Science* **327:** 46-50

Liou J, Fivaz M, Inoue T, Meyer T (2007) Live-cell imaging reveals sequential oligomerization and local plasma membrane targeting of stromal interaction molecule 1 after Ca2+ store depletion. *Proc Natl Acad Sci U S A* **104:** 9301-9306

Luby-Phelps K (2013) The physical chemistry of cytoplasm and its influence on cell function: an update. *Mol Biol Cell* **24:** 2593-2596

Martin GS (2001) The hunting of the Src. *Nat Rev Mol Cell Biol* **2:** 467-475

Martinez-Outschoorn UE, Sotgia F, Lisanti MP (2015) Caveolae and signalling in cancer. *Nat Rev Cancer* **15:** 225-237

Mayer BJ (2001) SH3 domains: complexity in moderation. *J Cell Sci* **114:** 1253-1263

McLaughlin S, Wang J, Gambhir A, Murray D (2002) PIP(2) and proteins: interactions, organization, and information flow. *Annu Rev Biophys Biomol Struct* **31:** 151-175

McNally JG (2008) Quantitative FRAP in Analysis of Molecular Binding Dynamics In Vivo. **85:** 329-351

Michaelson D, Silletti J, Murphy G, D'Eustachio P, Rush M, Philips MR (2001) Differential localization of Rho GTPases in live cells: regulation by hypervariable regions and RhoGDI binding. *J Cell Biol* **152:** 111-126

Michelitsch MD, Weissman JS (2000) A census of glutamine/asparagine-rich regions: implications for their conserved function and the prediction of novel prions. *Proc Natl Acad Sci U S A* **97:** 11910-11915

Munro S (2003) Lipid rafts: elusive or illusive? *Cell* **115:** 377-388

New LA, Keyvani Chahi A, Jones N (2013) Direct regulation of nephrin tyrosine phosphorylation by Nck adaptor proteins. *J Biol Chem* **288:** 1500-1510

Ni M, Tepperman JM, Quail PH (1998) PIF3, a phytochrome-interacting factor necessary for normal photoinduced signal transduction, is a novel basic helix-loop-helix protein. *Cell* **95:** 657-667

Ni M, Tepperman JM, Quail PH (1999) Binding of phytochrome B to its nuclear signalling partner PIF3 is reversibly induced by light. *Nature* **400:** 781-784

Nikolov DB, Xu K, Himanen JP (2013) Eph/ephrin recognition and the role of Eph/ephrin clusters in signaling initiation. *Biochim Biophys Acta* **1834:** 2160-2165

Nott TJ, Petsalaki E, Farber P, Jervis D, Fussner E, Plochowietz A, Craggs TD, Bazett-Jones DP, Pawson T, Forman-Kay JD, Baldwin AJ (2015) Phase transition of a disordered nuage protein generates environmentally responsive membraneless organelles. *Mol Cell* **57:** 936-947

Ozkan E, Chia PH, Wang RR, Goriatcheva N, Borek D, Otwinowski Z, Walz T, Shen K, Garcia KC (2014) Extracellular architecture of the SYG-1/SYG-2 adhesion complex instructs synaptogenesis. *Cell* **156:** 482-494

Padrick SB, Rosen MK (2010) Physical mechanisms of signal integration by WASP family proteins. *Annu Rev Biochem* **79:** 707-735

Paladino S, Lebreton S, Tivodar S, Formiggini F, Ossato G, Gratton E, Tramier M, Coppey-Moisan M, Zurzolo C (2014) Golgi sorting regulates organization and activity of GPI proteins at apical membranes. *Nat Chem Biol* **10:** 350-357

Palmer A, Zimmer M, Erdmann KS, Eulenburg V, Porthin A, Heumann R, Deutsch U, Klein R (2002) EphrinB phosphorylation and reverse signaling: regulation by Src kinases and PTP-BL phosphatase. *Mol Cell* **9:** 725-737

Paluch E, Sykes C, Prost J, Bornens M (2006) Dynamic modes of the cortical actomyosin gel during cell locomotion and division. *Trends Cell Biol* **16:** 5-10

Pani B, Ong HL, Liu X, Rauser K, Ambudkar IS, Singh BB (2008) Lipid rafts determine clustering of STIM1 in endoplasmic reticulum-plasma membrane junctions and regulation of store-operated Ca2+ entry (SOCE). *J Biol Chem* **283:** 17333-17340

Papayannopoulos V, Co C, Prehoda KE, Snapper S, Taunton J, Lim WA (2005) A polybasic motif allows N-WASP to act as a sensor of PIP(2) density. *Mol Cell* **17:** 181-191

Parsons JT, Horwitz AR, Schwartz MA (2010) Cell adhesion: integrating cytoskeletal dynamics and cellular tension. *Nat Rev Mol Cell Biol* **11:** 633-643

Patel JC, Galan JE (2005) Manipulation of the host actin cytoskeleton by Salmonella--all in the name of entry. *Curr Opin Microbiol* **8:** 10-15

Petrovska I, Nuske E, Munder MC, Kulasegaran G, Malinovska L, Kroschwald S, Richter D, Fahmy K, Gibson K, Verbavatz JM, Alberti S (2014) Filament formation by metabolic enzymes is a specific adaptation to an advanced state of cellular starvation. *Elife*

Pollard TD (2007) Regulation of actin filament assembly by Arp2/3 complex and formins. *Annu Rev Biophys Biomol Struct* **36:** 451-477

Pollard TD, Cooper JA (2009) Actin, a central player in cell shape and movement. *Science* **326:** 1208-1212

Pucadyil TJ, Schmid SL (2009) Conserved functions of membrane active GTPases in coated vesicle formation. *Science* **325:** 1217-1220

Qin XS, Tsukaguchi H, Shono A, Yamamoto A, Kurihara H, Doi T (2009) Phosphorylation of nephrin triggers its internalization by raft-mediated endocytosis. *J Am Soc Nephrol* **20:** 2534-2545

Quack I, Rump LC, Gerke P, Walther I, Vinke T, Vonend O, Grunwald T, Sellin L (2006) beta-Arrestin2 mediates nephrin endocytosis and impairs slit diaphragm integrity. *Proc Natl Acad Sci U S A* **103:** 14110-14115

Rafelski SM, Theriot JA (2004) Crawling toward a unified model of cell mobility: spatial and temporal regulation of actin dynamics. *Annu Rev Biochem* **73:** 209-239

Rana A, Dolmetsch RE (2010) Using light to control signaling cascades in live neurons. *Curr Opin Neurobiol* **20:** 617-622

Rao M, Mayor S (2014) Active organization of membrane constituents in living cells. *Curr Opin Cell Biol* **29:** 126-132

Rivera GM, Briceño CA, Takeshima F, Snapper SB, Mayer BJ (2004) Inducible Clustering of Membrane-Targeted SH3 Domains of the Adaptor Protein Nck Triggers Localized Actin Polymerization. *Current Biology* **14:** 11-22

Rockwell NC, Su YS, Lagarias JC (2006) Phytochrome structure and signaling mechanisms. *Annu Rev Plant Biol* **57:** 837-858

Ruotsalainen V, Ljungberg P, Wartiovaara J, Lenkkeri U, Kestila M, Jalanko H, Holmberg C, Tryggvason K (1999) Nephrin is specifically located at the slit diaphragm of glomerular podocytes. *Proc Natl Acad Sci U S A* **96:** 7962-7967

Sabharanjak S, Sharma P, Parton RG, Mayor S (2002) GPI-anchored proteins are delivered to recycling endosomes via a distinct cdc42-regulated, clathrin-independent pinocytic pathway. *Dev Cell* **2:** 411-423

Saleem MA, Ni L, Witherden I, Tryggvason K, Ruotsalainen V, Mundel P, Mathieson PW (2002) Co-localization of nephrin, podocin, and the actin cytoskeleton: evidence for a role in podocyte foot process formation. *Am J Pathol* **161:** 1459-1466

Schepens I, Duek P, Fankhauser C (2004) Phytochrome-mediated light signalling in Arabidopsis. *Curr Opin Plant Biol* **7:** 564-569

Schleich K, Warnken U, Fricker N, Ozturk S, Richter P, Kammerer K, Schnolzer M, Krammer PH, Lavrik IN (2012) Stoichiometry of the CD95 death-inducing signaling complex: experimental and modeling evidence for a death effector domain chain model. *Mol Cell* **47:** 306-319

Seiradake E, Schaupp A, del Toro Ruiz D, Kaufmann R, Mitakidis N, Harlos K, Aricescu AR, Klein R, Jones EY (2013) Structurally encoded intraclass differences in EphA clusters drive distinct cell responses. *Nat Struct Mol Biol* **20:** 958-964

Sens KL, Zhang S, Jin P, Duan R, Zhang G, Luo F, Parachini L, Chen EH (2010) An invasive podosome-like structure promotes fusion pore formation during myoblast fusion. *J Cell Biol* **191:** 1013-1027

Shaner NC, Steinbach PA, Tsien RY (2005) A guide to choosing fluorescent proteins. *Nat Methods* **2:** 905-909

Sharma P, Varma R, Sarasij RC, Ira, Gousset K, Krishnamoorthy G, Rao M, Mayor S (2004) Nanoscale organization of multiple GPI-anchored proteins in living cell membranes. *Cell* **116:** 577-589

Sharrock RA (2008) The phytochrome red/far-red photoreceptor superfamily. *Genome Biol* **9:** 230

Sherman E, Barr V, Manley S, Patterson G, Balagopalan L, Akpan I, Regan CK, Merrill RK, Sommers CL, Lippincott-Schwartz J, Samelson LE (2011) Functional nanoscale organization of signaling molecules downstream of the T cell antigen receptor. *Immunity* **35:** 705-720

Shilagardi K, Li S, Luo F, Marikar F, Duan R, Jin P, Kim JH, Murnen K, Chen EH (2013) Actin-propelled invasive membrane protrusions promote fusogenic protein engagement during cell-cell fusion. *Science* **340:** 359-363

Shimizu-Sato S, Huq E, Tepperman JM, Quail PH (2002) A light-switchable gene promoter system. *Nat Biotechnol* **20:** 1041-1044

Shono A, Tsukaguchi H, Kitamura A, Hiramoto R, Qin XS, Doi T, Iijima K (2009) Predisposition to relapsing nephrotic syndrome by a nephrin mutation that interferes with assembly of functioning microdomains. *Hum Mol Genet* **18:** 2943-2956

Sohn RL, Huang P, Kawahara G, Mitchell M, Guyon J, Kalluri R, Kunkel LM, Gussoni E (2009) A role for nephrin, a renal protein, in vertebrate skeletal muscle cell fusion. *Proc Natl Acad Sci U S A* **106:** 9274-9279

Spector DL (2006) SnapShot: Cellular bodies. *Cell* **127:** 1071

Strickland D, Yao X, Gawlak G, Rosen MK, Gardner KH, Sosnick TR (2010) Rationally improving LOV domain-based photoswitches. *Nat Methods* **7:** 623-626

Takenawa T, Miki H (2001) WASP and WAVE family proteins: key molecules for rapid rearrangement of cortical actin filaments and cell movement. *J Cell Sci* **114:** 1801-1809

Takenawa T, Suetsugu S (2007) The WASP-WAVE protein network: connecting the membrane to the cytoskeleton. *Nat Rev Mol Cell Biol* **8:** 37-48

Toulmay A, Prinz WA (2013) Direct imaging reveals stable, micrometer-scale lipid domains that segregate proteins in live cells. *J Cell Biol* **202:** 35-44

Tryggvason K, Pikkarainen T, Patrakka J (2006) Nck links nephrin to actin in kidney podocytes. *Cell* **125:** 221-224

van den Bogaart G, Meyenberg K, Risselada HJ, Amin H, Willig KI, Hubrich BE, Dier M, Hell SW, Grubmuller H, Diederichsen U, Jahn R (2011) Membrane protein sequestering by ionic protein-lipid interactions. *Nature* **479:** 552-555

Varma R, Mayor S (1998) GPI-anchored proteins are organized in submicron domains at the cell surface. *Nature* **394:** 798-801

Veatch SL, Cicuta P, Sengupta P, Honerkamp-Smith A, Holowka D, Baird B (2008) Critical fluctuations in plasma membrane vesicles. *ACS Chem Biol* **3:** 287-293

Wang JT, Smith J, Chen BC, Schmidt H, Rasoloson D, Paix A, Lambrus BG, Calidas D, Betzig E, Seydoux G (2014) Regulation of RNA granule dynamics by phosphorylation of serine-rich, intrinsically disordered proteins in C. elegans. *Elife* **3:** e04591

Weisswange I, Newsome TP, Schleich S, Way M (2009) The rate of N-WASP exchange limits the extent of ARP2/3-complex-dependent actin-based motility. *Nature* **458:** 87-91

Welsh GI, Saleem MA (2010) Nephrin-signature molecule of the glomerular podocyte? *J Pathol* **220:** 328-337

Wu H (2013) Higher-order assemblies in a new paradigm of signal transduction. *Cell* **153:** 287-292

Wu L, Pan L, Zhang C, Zhang M (2012) Large protein assemblies formed by multivalent interactions between cadherin23 and harmonin suggest a stable anchorage structure at the tip link of stereocilia. *J Biol Chem* **287:** 33460-33471

Wu MM, Buchanan J, Luik RM, Lewis RS (2006) Ca2+ store depletion causes STIM1 to accumulate in ER regions closely associated with the plasma membrane. *J Cell Biol* **174:** 803-813

Wu Y, Vendome J, Shapiro L, Ben-Shaul A, Honig B (2011) Transforming binding affinities from three dimensions to two with application to cadherin clustering. *Nature* **475:** 510-513

Wu YI, Frey D, Lungu OI, Jaehrig A, Schlichting I, Kuhlman B, Hahn KM (2009) A genetically encoded photoactivatable Rac controls the motility of living cells. *Nature* **461:** 104-108

Yao X, Rosen MK, Gardner KH (2008) Estimation of the available free energy in a LOV2-J alpha photoswitch. *Nat Chem Biol* **4:** 491-497

Yap AS, Brieher WM, Gumbiner BM (1997) Molecular and functional analysis of cadherin-based adherens junctions. *Annu Rev Cell Dev Biol* **13:** 119-146

Yazawa M, Sadaghiani AM, Hsueh B, Dolmetsch RE (2009) Induction of protein-protein interactions in live cells using light. *Nat Biotechnol* **27:** 941-945

Ye H, Daoud-El Baba M, Peng RW, Fussenegger M (2011) A synthetic optogenetic transcription device enhances blood-glucose homeostasis in mice. *Science* **332:** 1565-1568

Yi J, Wu XS, Crites T, Hammer JA, 3rd (2012) Actin retrograde flow and actomyosin II arc contraction drive receptor cluster dynamics at the immunological synapse in Jurkat T cells. *Mol Biol Cell* **23:** 834-852

Yoneda Y (1997) How proteins are transported from cytoplasm to the nucleus. *J Biochem* **121:** 811-817

Yu Y, Smoligovets AA, Groves JT (2013) Modulation of T cell signaling by the actin cytoskeleton. *J Cell Sci* **126:** 1049-1058

Zeke A, Lukacs M, Lim WA, Remenyi A (2009) Scaffolds: interaction platforms for cellular signalling circuits. *Trends Cell Biol* **19:** 364-374

Zhang F, Wang LP, Brauner M, Liewald JF, Kay K, Watzke N, Wood PG, Bamberg E, Nagel G, Gottschalk A, Deisseroth K (2007) Multimodal fast optical interrogation of neural circuitry. *Nature* **446:** 633-639

Zhou D, Galan J (2001) Salmonella entry into host cells: the work in concert of type III secreted effector proteins. *Microbes Infect* **3:** 1293-1298

Zhou XX, Chung HK, Lam AJ, Lin MZ (2012) Optical control of protein activity by fluorescent protein domains. *Science* **338:** 810-814

Zhou Y, Liang H, Rodkey T, Ariotti N, Parton RG, Hancock JF (2014) Signal integration by lipid-mediated spatial cross talk between Ras nanoclusters. *Mol Cell Biol* **34:** 862-876

Ziegler WH, Liddington RC, Critchley DR (2006) The structure and regulation of vinculin. *Trends Cell Biol* **16:** 453-460